CFD ANALYSIS OF TWO-DIMENSIONAL LINEAR COMPRESSOR CASCADE FLOWS

By

Javier García Unzue

Computational Fluid Dynamics Laboratory
Advisor: Professor Yun-Ho Choi

Ajou School of Engineering

Fall semester of 2010

CONTENTS

1. INTRODUCTION

1.1 Introduction to the project

This project analyzes two-dimensional linear cascade flows of an axial compressor on the stator vanes. It analyzes the influence of the angle of attack in the leading edge for different pressure ratios. The problem studied is a compressible, viscous and steady flow. A test case of an inviscid model flow has been carried out as well. Two types of grid are also being analyzed, the unstructured grid, with only triangular mesh elements, and a structured grid with only quadrilateral mesh elements. The modeling has been done with Gambit while the processing has been done with the Fluent code.

To assure the validity of the results, this project is being compared with *experimental results for two-dimensional experimental cascade performance for controlled diffusion compressor stator blading* done by Sanger and Shreeve and with the work done by Jong-Uk Lee and Yun-ho Choi in the *Numerical analysis of two-dimensional linear cascade flows* paper.

1.2 History of fluid mechanics

The fundamental discoveries of fluids mechanics were done in the eighteenth and nineteenth centuries.

Ancient civilizations had enough knowledge to solve certain flow problems. For example, sailing ships with oars and irrigation systems were both known in prehistoric times. The Greeks produced quantitative information. Archimedes and Hero of Alexandria postulated the parallelogram law for vector addition in the third century B.C.. Archimedes (287-212 B.C.) was a Greek mathematician, physicist, engineer, inventor, and astronomer, and he was the one who formulated the laws of buoyancy and applied them to floating and submerged bodies, by deriving a form of the differential calculus as part of the analysis.

Up to the Renaissance, there was a steady improvement in the design of such flow systems as ships, canals, and water conduits, but not recorder evidence of fundamental improvements in flow analysis. Then Leonardo da Vinci (1452-1519) who was a painter, sculptor, architect, musician, scientist, mathematician, engineer, inventor, anatomist etc, he derived the equation of the mass conservation in one dimensional steady flow. Leonardo was a an excellent experimentalist, and his notes contain accurate descriptions of the waves, jets,

hydraulic jumps, eddy formation, and both low-drag (streamlined) and high-drag (parachutes) design. A Frenchman, Edme Mariotte (1620-1684) built the first wind tunnel and tested models in it. Edme postulated the Boyle's law which describes the inversely proportional relationship between the absolute pressure and volume of an ideal gas, if the temperature is kept constant within a closed system.

In 1687, Isaac Newton (1642-1727) who was a physicist, mathematician, astronomer, natural philosopher, alchemist and theologian, is consider to be one of the most influential people in human history. Isaac postulated the law of motion and the law of viscosity of the linear fluids nowadays called newtonian. The theory first yielded to the assumption of a "perfect" or frictionless fluid,and eighteenth-century mathematicians such as Daniel Bernoulli, Leonhard Euler, Jean D'Alambert, Lagrange, and Laplace, produced many beautiful solutions of frictionless- flow problems. Euler developed both the differential equation of motion and their integrated form, now called the Bernoulli equation. D'Alambert used them to show his famous paradox: that a body immersed in a frictionless fluid has zero drag. These beautiful results amounted to overkill, since perfect-fluid assumptions have very limited applications in practice and most engineers flows are dominated by the effect of viscosity. Engineers began to reject what they regarded as a totally unrealistic theory and developed the science of hydraulics, relying almost entirely on experiment. Such experimentalist as Chezy, Pitot, Borda, Weber, Francis, Hagen, Poiseuille, Darcy, Manning, Bazing and Weisbach produced data on a variety of flows such as open channels, ships resistance, pipe flows, waves, and turbines.

At the end of the nineteenth century, unification between experimental hydraulics and theoretical hydrodynamics finally began. William Froude (1810-1879) and his son Robert (1846-1924) developed laws of model testing, Lord Rayleigh (1842-1919) proposed the technique of dimensional analysis, and Osborne Reynolds (1842-1912) published the classic pipe experiment in 1883 which showed the importance of the dimensionless Reynolds number named after him. Meanwhile, viscous-flow theory was available but unexploited since Navier (1785-1836) and Stokes (1819-1903) had successfully added the Newtonian viscous term in the governing equations of motion. Unfortunately, the resulting Navier-Stokes equations were too difficult to analyze for arbitrary flows.

In 1904, a German engineer, Ludwig Prandtl (1875-1953), published perhaps the most important paper ever written on fluids mechanics. Prandtl pointed out that fluids flows with small viscosity (water and air flows) can be divided into a thin viscous layer, or boundary layer, near solid surfaces, and interfaces, patched onto a nearby inviscid outer layer, where the Euler and Bernoulli equations apply. Boundary-layer theory has proven to be the single most important tool in the modern flow analysis. The twentieth-century foundations for the present state of the art in fluid mechanics were laid in a series of broad-based experiments by Prandtl and his two chief friendly competitors, Theodore von Karman (1881-1963) and Sir Geoffrey I.Taylor (1886-1975).

1.3 History of Computational Fluid Dynamics.

In the eighteenth and nineteenth century, significant work was done trying to mathematically describe the motion of fluids. Daniel Bernoulli derived the famous Bernoulli's equation, and Leonhard Euler proposed the Euler equations which describes the conservation of momentum for an inviscid fluid, and conservation of mass. He also proposed the velocity potential theory. Two other important contributors to this field emerged at this time, Claude Louis Marie Henry Navier and the Irishman, George Gabriel Stokes who introduced viscous transport into the Euler equations, which resulted in the now famous Navier-Stokes equations. These forms of the differential mathematical equations that they proposed nearly 200 years ago are the basis of the modern day computational fluid dynamics (CFD) industry, and they include expressions for the conservation of mass, momentum, pressure, species and turbulence. Indeed, the equations are so closely coupled and difficult to solve that it was not until the advent of modern digital computers in the 1960s and 1970s that they could be resolved for real flow problems within reasonable timescales.

In the early 20th Century, much work was done on refining theories of boundary layers and turbulence in fluid flow.

It is debatable as to who did the earliest CFD calculations (in a modern sense) although Lewis Fry Richardson in England (1881-1953) developed the first numerical weather prediction system when he divided physical space into grid cells and used the finite difference approximations of Bjerknes's "primitive differential equations". His own attempt to calculate weather for a single eight-hour period took six weeks of real time and ended in failure! His model's enormous calculation requirements led Richardson to propose a solution he called the "forecast-factory". The "factory" would have involved filling a vast stadium with 64,000 people. Each one, armed with a mechanical calculator, would perform part of the flow calculation. A leader in the center, using colored signal lights and telegraph communication, would coordinate the forecast. What he was proposing would have been a very rudimentary CFD calculation. The earliest numerical solution for flow past a cylinder was carried out in 1933 by Thom and reported in England.

It was in the early 1980s that commercial CFD codes came into the open market place in a big way. The use of commercial CFD software started to become accepted by major companies around the world rather than their continuing to develop in-house CFD codes. Commercial CFD software is therefore based on sets of very complex non-linear mathematical expressions that define the fundamental equations of fluid flow, heat and materials transport. These equations are solved iteratively using complex computer algorithms embedded within CFD software. The net effect of such software is to allow the user to computationally model any flow field provided the geometry of the object being modeled is known, the physics and chemistry are identified, and

some initial flow conditions are prescribed. Outputs from CFD software can be viewed graphically in color plots of velocity vectors, contours of pressure, lines of constant flow field properties, or as "hard" numerical data and X-Y plots.

CFD is now recognized to be a part of the computer-aided engineering (CAE) spectrum of tools used extensively today in all industries, and its approach to modeling fluid flow phenomena allows equipment designers and technical analysts to have the power of a virtual wind tunnel on their desktop computer. CFD software has evolved far beyond what Navier, Stokes or Da Vinci could ever have imagined. CFD has become an indispensable part of the aerodynamic and hydrodynamic design process for planes, trains, automobiles, rockets, ships, submarines; and indeed any moving craft or manufacturing process that mankind has devised.

1.4 Navier-Stokes equations

This equations describes the motion of compressible viscous fluid substances. For the general case of a three-dimensional motion, the flow field is determined by the velocity vector,

$$\vec{v} = u\vec{i} + v\vec{j} + w\vec{k}$$

with the three rectangular components *u*,*v*,*w*, the pressure *p* and density ρ. To determine these five magnitudes, we have the mass conservation equation (continuity equation), the *x*-.*y*- and *z*- momentum equations, and the energy equation and//or the equation of state,

$$p = p(\rho, T) \text{ and } i = i(\rho, T)$$

Continuity equation or mass conservation equation

The continuity equation states the mass balance for the fluid element:

Rate of increase of mass in fluid element	=	*Net rate of flow of mass into fluid element*

$$\frac{\partial \rho}{\partial t} + \frac{\partial (\rho u)}{\partial x} + \frac{\partial (\rho v)}{\partial y} + \frac{\partial (\rho w)}{\partial z} = 0$$

Or

$$\frac{\partial \rho}{\partial t} + div(\rho \vec{u}) = 0$$

If the flow is incompressible, density does not vary along the time and therefore, the equations simplifies:

$$div(\rho \vec{u}) = 0$$

Momentum equations:

We start with the Newton's second law which states that the rate of change of momentum of a fluid particle equals the sum of the forces on the particle:

Rate of increase of momentum of fluid particle	=	*Sum of forces on fluid particle*

The rates of increase of x-,y-, and z- momentum per unit volume of a fluid particle are given by:

$$\rho \frac{Du}{Dt} \qquad \rho \frac{Dv}{Dt} \qquad \rho \frac{Dw}{Dt}$$

The forces that interact are surface forces (pressure, viscous, and gravity) and body forces (centrifugal, coriolis, and electromagnetic). It is common practice to highlight the contributions due to the surface forces as separate terms in the momentum equation and to include the effects of body forces as source terms.

The state of stress of a fluid element is defined in terms of the pressure and the nine viscous stress components. The pressure, a normal stress, is denoted by *p* and the viscous stress by τ. The notation for the suffix $\tau_{i,j}$ indicated the direction of the viscous stresses. The suffice *i* indicates that the stress component acts in the surface normal to the i-direction and the suffice *j* indicate that the stress component acts in the j-direction.

If we combine these nine components we can form a stress tensor. This group of the nine components are also called matrix of stress tensor

$$\Pi = \begin{pmatrix} \tau_x & \tau_{xy} & \tau_{xz} \\ \tau_{yx} & \tau_y & \tau_{yz} \\ \tau_{zx} & \tau_{zy} & \tau_z \end{pmatrix}$$

Due to the symmetry of the stress tensor, we have $\tau_{xy} = \tau_{yx}$; $\tau_{xz} = \tau_{zx}$; $\tau_{yz} = \tau_{zy}$ hence we decrease the number of components to six

$$\Pi = \begin{pmatrix} \tau_x & \tau_{xy} & \tau_{xz} \\ \tau_{xy} & \tau_y & \tau_{yz} \\ \tau_{xz} & \tau_{yz} & \tau_z \end{pmatrix}$$

The total force per unit volume in the *x*-direction on the fluid due to these surfaces stresses is equal to the sum of the net force in the *x*-direction, divided by the volume $\delta x \delta y \delta z$:

$$\frac{\partial(-p + \tau_{xx})}{\partial_x} + \frac{\partial \tau_{yx}}{\partial y} + \frac{\partial \tau_{zx}}{\partial z}$$

We can do the same for the *y*-, and *z*-direction.

In this equation we don't include the effect of the body forces as we introduced them in the momentum equation as sources (S_{Mx} , S_{My} , S_{Mz}). The *x*-,*y*-, and *z*-component of the momentum equation is found by setting the rate of change of *x*-,*y*-, and *z*-momentum of the fluid particle equal to the total force in the *x*-,*y*-, and *z*-direction respectively on the element due to surface stresses plus the rate of increase of *x*-,*y*-, and *z*-momentum due to sources:

x-momentum:

$$\rho \frac{Du}{Dt} = \frac{\partial(-p + \tau_{xx})}{\partial_x} + \frac{\partial \tau_{yx}}{\partial y} + \frac{\partial \tau_{zx}}{\partial z} + S_{Mx}$$

y-momentum:

$$\rho \frac{Dv}{Dt} = \frac{\partial \tau_{xy}}{\partial_x} + \frac{\partial\left(-p + \tau_{yy}\right)}{\partial y} + \frac{\partial \tau_{zy}}{\partial z} + S_{My}$$

z-momentum:

$$\rho \frac{Dw}{Dt} = \frac{\partial \tau_{xz}}{\partial_x} + \frac{\partial \tau_{yz}}{\partial y} + \frac{\partial(-p + \tau_{zz})}{\partial z} + S_{Mz}$$

If we remember the total or substantial derivative definition of a random property ϕ

$$\frac{D\phi}{Dt} = \frac{\partial \phi}{\partial t} + \vec{u} grad \phi$$

we can rewrite the momentum equations as follow:

$$\frac{\partial(\rho u)}{\partial t} + div(\rho u \vec{u}) = -\frac{\partial p}{\partial x} + div(\mu \, grad \, u) + S_{Mx}$$

$$\frac{\partial(\rho v)}{\partial t} + div(\rho v \vec{u}) = -\frac{\partial p}{\partial y} + div(\mu \, grad \, u) + S_{My}$$

$$\frac{\partial(\rho w)}{\partial t} + div(\rho w \vec{u}) = -\frac{\partial p}{\partial z} + div(\mu \, grad \, u) + S_{Mz}$$

Where μ is the dynamic viscosity, a constant of proportionality in the Newton's law of viscosity for compressible flows.

Energy equation:

The energy equation is derived from the first law of thermodynamics, which states that the rate of change of energy of a fluid particle is equal to the rate of heat addition to the fluid particle plus the rate of work done on the particle:

Rate of increase of energy of fluid particle	=	Net rate of heat added to fluid particle	+	Net rate of work done on fluid particle

Same as before, we are going to be deriving an equation for the rate of increase of energy of a fluid particle per unit volume, which is given by

$$\rho \frac{DE}{Dt}$$

- Work done by surface forces:

The rate of work done on the fluid particle in the element by a surface force is equal to the product of the force and velocity component in the direction of the force.

The net rate of work done by these surface forces acting in the *x*-direction is given by

$$\left[\frac{\partial\left(u(-p+\tau_{xx})\right)}{\partial x}+\frac{\partial\left(u\tau_{yx}\right)}{\partial y}+\frac{\partial(u\tau_{zx})}{\partial z}\right]\delta x\delta y\delta z$$

The same for the *y*-, and *z*-direction.

The total rate of work done per unit volume on the fluid particle by all the surface forces is given by the sum of the net rate work done in all surfaces divided by the volume $\delta x\delta y\delta z$. We can collect the terms containing the pressure as

$$-\frac{\partial(up)}{\partial x}-\frac{\partial(vp)}{\partial y}-\frac{\partial(wp)}{\partial z}=-div(p\vec{u})$$

And therefore, the total rate of work done on the fluid particle by surface stresses is:

$$\begin{aligned}&-div(p\vec{u})\\&+\left[\frac{\partial(u\tau_{xx})}{\partial x}+\frac{\partial\left(u\tau_{yx}\right)}{\partial y}+\frac{\partial(u\tau_{zx})}{\partial z}+\frac{\partial\left(v\tau_{xy}\right)}{\partial x}+\frac{\partial\left(v\tau_{yy}\right)}{\partial y}+\frac{\partial\left(v\tau_{zy}\right)}{\partial z}\right.\\&\left.+\frac{\partial(w\tau_{xz})}{\partial x}+\frac{\partial\left(w\tau_{yz}\right)}{\partial y}+\frac{\partial(w\tau_{zz})}{\partial z}\right]\end{aligned}$$

- Energy flux due to heat conduction:

The heat flux vector $\vec{q}$ has three components: q_x, q_y, and q_z.

The total rate of heat added to the fluid particle per unit volume due to heat flow across its boundaries is:

$$-\frac{\partial q_x}{\partial x}-\frac{\partial q_y}{\partial y}-\frac{\partial q_z}{\partial z}=-div\,\vec{q}$$

Remembering the Fourier's law of heat conductions relates the heat flux to the local temperature gradient. Thus

$$q_x=-k\frac{\partial T}{\partial x}\qquad q_y=-k\frac{\partial T}{\partial y}\qquad q_z=-k\frac{\partial T}{\partial z}$$

In vector form:

$$\vec{q}=div(k\ grad\ T)$$

Combining this two equations yields the final form of the rate of heat addition to the fluid particle due to heat conduction across element boundaries:

$$-div\ \vec{q} = div(k\ grad\ T)$$

The effect of potential energy is included in the source term.

Finally the energy equation is:

$$\rho\frac{DE}{Dt} = -div(p\vec{u}) + \left[\frac{\partial(u\tau_{xx})}{\partial x} + \frac{\partial(u\tau_{yx})}{\partial y} + \frac{\partial(u\tau_{zx})}{\partial z} + \frac{\partial(v\tau_{xy})}{\partial x} + \frac{\partial(v\tau_{yy})}{\partial y} + \frac{\partial(v\tau_{zy})}{\partial z} + \frac{\partial(w\tau_{xz})}{\partial x} + \frac{\partial(w\tau_{yz})}{\partial y} + \frac{\partial(w\tau_{zz})}{\partial z}\right] + div(k\ grad\ T) + S_E$$

Where E equals the internal energy (i) plus the kinetic energy ($0.5(u^2 + v^2 + w^2)$).

The Navier-Stokes equation for a Newtonian fluid:

The governing equations contains as further unknowns the viscous stress components τ_{ij}. The most useful forms of the conservation equations for fluid flows are obtained by introducing a suitable model for the viscous stresses τ_{ij}.

In many fluid flows the viscous stresses can be expressed as functions of the local deformation rate or strain rate. In three-dimensional flows the local rate of deformation is composed of the linear deformation rate and the volumetric deformation rate. We assume that the fluids are isotropic.

The rate of linear deformation of a fluid element has nine components in three dimensions, six of which are independent in isotropic fluids. We denote them by the symbol s_{ij}.

There are three linear elongating deformation components:

$$s_{xx} = \frac{\partial u}{\partial x} \qquad s_{yy} = \frac{\partial v}{\partial y} \qquad s_{zz} = \frac{\partial w}{\partial z}$$

There are also six shearing linear deformation components:

$$s_{xy} = s_{yx} = \frac{1}{2}\left(\frac{\partial u}{\partial y} + \frac{\partial v}{\partial x}\right)$$

$$s_{xz} = s_{zx} = \frac{1}{2}\left(\frac{\partial u}{\partial z} + \frac{\partial w}{\partial x}\right)$$

$$s_{yz} = s_{zy} = \frac{1}{2}\left(\frac{\partial v}{\partial z} + \frac{\partial w}{\partial y}\right)$$

The volumetric deformation is given by:

$$\frac{\partial u}{\partial x}+\frac{\partial v}{\partial y}+\frac{\partial w}{\partial z}=div\,\vec{u}$$

In a Newtonian fluid the viscous stresses are proportional to the rates of deformation. The three-dimensional form of the Newton's law of viscosity for compressible flows involves two constants of proportionality: the dynamic viscosity μ to relate stresses to linear deformations, and the second viscosity λ, to relate stresses to the volumetric deformation. Thus, the nine viscous stress components, of which six are independent, are

$$\tau_{xx}=2\,\mu\frac{\partial u}{\partial x}+\,\lambda\,div\,\vec{u}\;\;;\;\;\tau_{yy}=2\,\mu\frac{\partial v}{\partial y}+\,\lambda\,div\,\vec{u}\;\;;\;\;\tau_{zz}=2\,\mu\frac{\partial w}{\partial z}+\,\lambda\,div\,\vec{u}$$

$$\tau_{xy}=\tau_{yx}=\mu\left(\frac{\partial u}{\partial y}+\frac{\partial v}{\partial x}\right)$$

$$\tau_{xy}=\tau_{yx}=\mu\left(\frac{\partial u}{\partial z}+\frac{\partial w}{\partial x}\right)$$

$$\tau_{xy}=\tau_{yx}=\mu\left(\frac{\partial v}{\partial z}+\frac{\partial w}{\partial y}\right)$$

If we substitute this shear stresses into the momentum equation we obtain the so-called Navier-Stokes equations:

$$\rho\frac{Du}{Dt}=-\frac{\partial p}{\partial x}+\frac{\partial}{\partial x}\left[2\,\mu\frac{\partial u}{\partial x}+\lambda\,div\,\vec{u}\right]+\frac{\partial}{\partial y}\left[\mu\left(\frac{\partial u}{\partial y}+\frac{\partial v}{\partial x}\right)\right]+\frac{\partial}{\partial z}\left[\mu\left(\frac{\partial u}{\partial z}+\frac{\partial w}{\partial x}\right)\right]+S_{Mx}$$

$$\rho\frac{Dv}{Dt}=-\frac{\partial p}{\partial y}+\frac{\partial}{\partial x}\left[\mu\left(\frac{\partial u}{\partial y}+\frac{\partial v}{\partial x}\right)\right]+\frac{\partial}{\partial y}\left[2\,\mu\frac{\partial v}{\partial y}+\,\lambda\,div\,\vec{u}\right]+\frac{\partial}{\partial z}\left[\mu\left(\frac{\partial v}{\partial z}+\frac{\partial w}{\partial y}\right)\right]+S_{My}$$

$$\rho\frac{Dw}{Dt}=-\frac{\partial p}{\partial z}+\frac{\partial}{\partial x}\left[\mu\left(\frac{\partial u}{\partial z}+\frac{\partial w}{\partial x}\right)\right]+\frac{\partial}{\partial y}\left[\mu\left(\frac{\partial v}{\partial z}+\frac{\partial w}{\partial y}\right)\right]+\frac{\partial}{\partial z}\left[2\,\mu\frac{\partial w}{\partial z}+\,\lambda\,div\,\vec{u}\right]+S_{Mz}$$

Often it is useful to rearrange the viscous stress terms as follows:

$$\frac{\partial}{\partial x}\left[2\,\mu\frac{\partial u}{\partial x}+\lambda\,div\,\vec{u}\right]+\frac{\partial}{\partial y}\left[\mu\left(\frac{\partial u}{\partial y}+\frac{\partial v}{\partial x}\right)\right]+\frac{\partial}{\partial z}\left[\mu\left(\frac{\partial u}{\partial z}+\frac{\partial w}{\partial x}\right)\right]$$
$$=\frac{\partial}{\partial x}\left(\mu\frac{\partial u}{\partial x}\right)+\frac{\partial}{\partial y}\left(\mu\frac{\partial u}{\partial y}\right)+\frac{\partial}{\partial z}\left(\mu\frac{\partial u}{\partial z}\right)$$
$$+\left[\frac{\partial}{\partial x}\left(\mu\frac{\partial u}{\partial x}\right)+\frac{\partial}{\partial y}\left(\mu\frac{\partial v}{\partial x}\right)+\frac{\partial}{\partial z}\left(\mu\frac{\partial w}{\partial x}\right)+\frac{\partial}{\partial x}(\lambda\,div\,\vec{u})\right]$$
$$=div(\mu\,grad\,u)+[S_{Mx}]$$

The viscous stresses in the *y*-, and *z*-component equation can be recast in a similar manner. If we try to simplify the momentum equation by "hiding" the bracketed smaller contribution to the viscous stress terms in the momentum source, we can define a new source by

$$S_M = S_M + [s_M]$$

We can rewrite the Navier-Stokes equations in the most useful form for the development of the finite volume method:

$$\rho\frac{Du}{Dt}=-\frac{\partial p}{\partial x}+div(\mu\,grad\,u)+S_{Mx}$$

$$\rho\frac{Dv}{Dt}=-\frac{\partial p}{\partial y}+div(\mu\,grad\,v)+S_{My}$$

$$\rho\frac{Du}{Dt}=-\frac{\partial p}{\partial z}+div(\mu\,grad\,w)+S_{Mz}$$

1.5 No-slip condition.

The no-slip condition is a property of the viscous flow which requires the fluid in contact with a container's wall to be at rest. This means that the tangencial motion of the flow in contact with the wall must be zero. This is because particles close to a surface do not move along with a flow when adhesion is stronger than cohesion but as with many engineering approximations, the no-slip condition does not always hold in reality. For example, at a very low pressure, even when the continuum approximation still holds there may be so few molecules near the surface that they "bounce along" down the surface.

As a fluid flows along a solid surface, it tends to "stick" to the surface. That is, the velocity of the fluid that is at the solid surface matches the velocity of the solid surface. So, for water in a pipe, the velocity of the water at the surface of the wall of the pipe will be equal to the velocity of the pipe wall surface. This is the "no-slip" condition and is a very important condition that must be satisfied in any accurate analysis of fluid flow phenomena. At a solid boundary, the fluid will have zero velocity relative to the boundary. In other words, the fluid velocity at all fluid–solid boundaries is equal to that of the solid boundary.

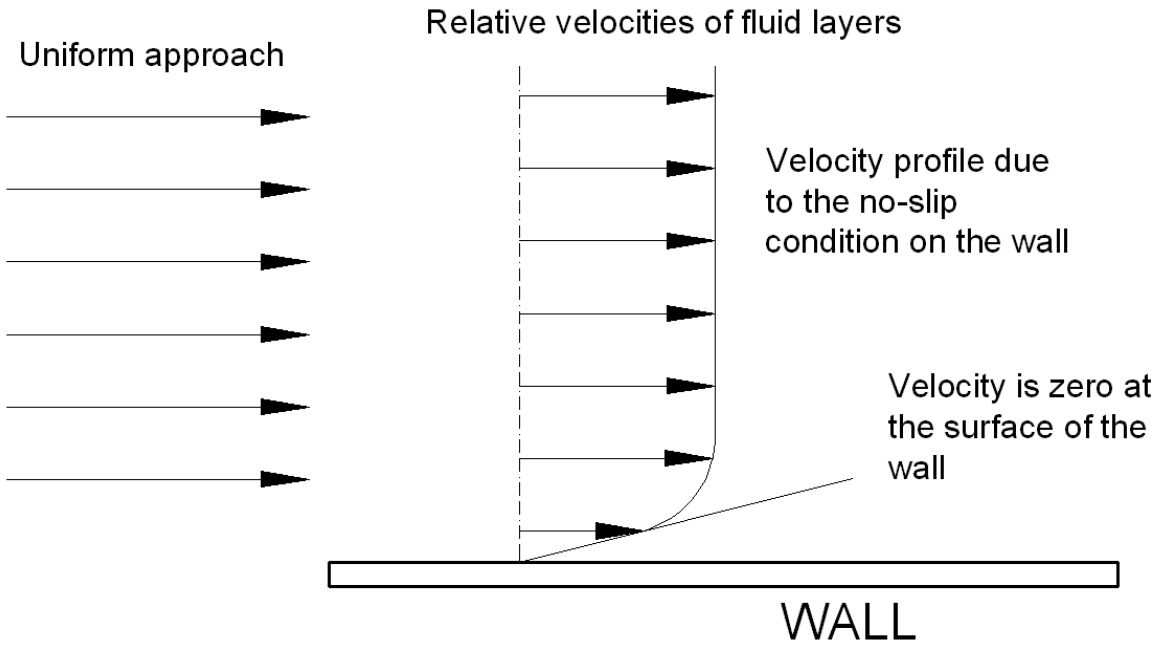

The flow region adjacent to the wall in which the viscous effects (and thus the velocity gradients) are significant is called boundary layer.

While the no-slip condition is used almost universally in modeling of viscous flows, it is sometimes neglected in favor of the ‘no-penetration condition’ (where the fluid velocity normal to the wall is set to the wall velocity in this direction, but the fluid velocity parallel to the wall is unrestricted) in elementary analysis of inviscid flow, where the effect of boundary layer is neglected.

The no-slip condition poses a problem in viscous flow theory at contact lines: places where an interface between two fluids meets a solid boundary. Here, the no-slip boundary condition implies that the position of the contact line does not move, which is not observed in reality. Analysis of a moving contact line with the no slip condition results in infinite stresses that can't be integrated over. The rate of movement of the contact line is believed to be dependent

on the angle the contact line makes with the solid boundary, but the mechanism behind this is not yet fully understood.

The fluid property responsible for the no-slip condition and the development of the boundary layer is the viscosity.

The layer of fluid at a moving surface has the same velocity as the surface itself. A consequence of the no-slip condition is that all velocity profiles must have zero values with respect to the surface at the points of contact between a fluid and a solid surface. Another consequence of the no-slip condition is the surface drag, which is the force a fluid exerts on a surface in the flow direction.

Fluid flow is often confined by solid surfaces, and it is important to understand how the presence of solid surfaces affects fluid flow. Water in a river cannot flow through large rocks, and goes around them. That is, the water velocity normal to the rock surface must be zero, and water approaching the surface normally comes to a complete stop at the surface. What is not so obvious is that water approaching the rock at any angle also comes to a complete stop at the rock surface, and thus the tangential velocity of water at the surface is also zero.

1.6 Introduction to turbulence.

In fluid dynamics, turbulence or turbulent flow is a fluid regime characterized by chaotic, stochastic property changes. This includes low momentum diffusion, high momentum convection, and rapid variation of pressure and velocity in space and time. Nobel Laureate Richard Feynman describes turbulence as "the most important unsolved problem of classical physics.

The Reynolds number of a flow gives a measure of the relative importance of inertia forces (associated with convective effects) and viscous forces. In experiments on fluid systems it is observed that at values below the so-called critical Reynolds number Re_{crit} the flow is smooth and adjacent layers of fluid slide past each other in an orderly fashion. If the applied boundary conditions do not change with time the flow is steady. This regime is called laminar flow.

The Reynolds number is defined as follows:

$$Re = \frac{\rho V L}{\mu} = \frac{V L}{\nu}$$

Where:

V is the mean fluid velocity
L is a characteristic linear dimension
μ is the dynamic viscosity of the fluid

ν is the kinematic viscosity
ρ is the density

At values of Reynolds number above Re_{crit} a complicated series of events takes place which eventually leads to a radical change of the flow character. In the final state the flow behavior is random and chaotic. The motion becomes intrinsically unsteady even with constant imposed boundary conditions. The velocity and all other flow properties vary in a random and chaotic way. This regime is called turbulent flow. A typical point velocity measurement might exhibit the form shown in the next illustration.

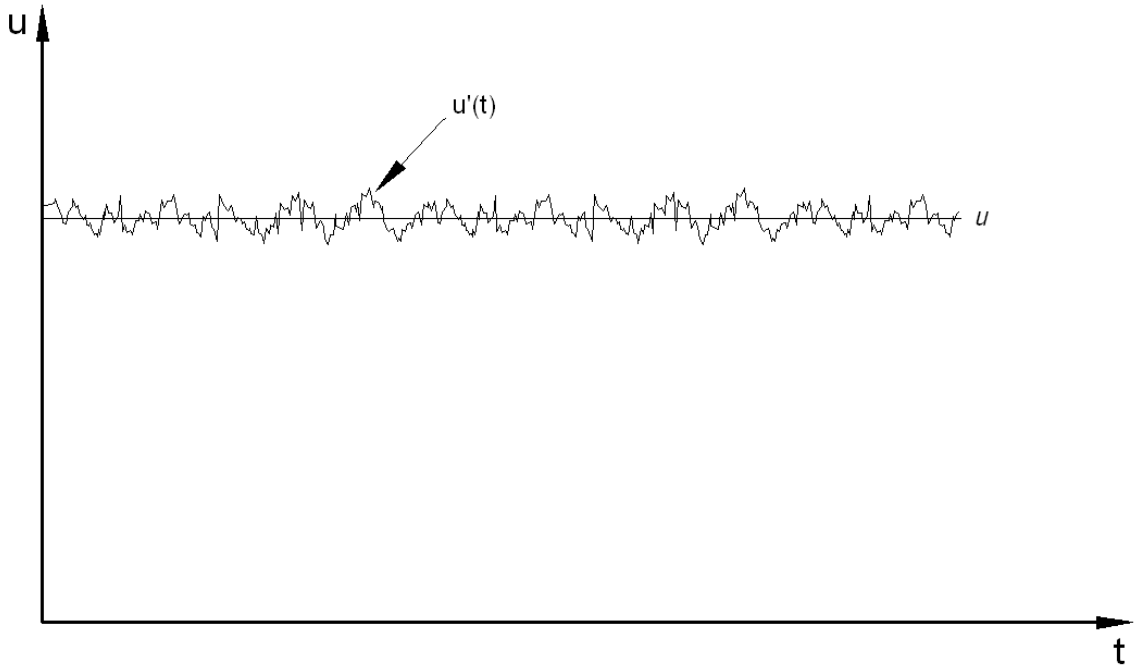

The random nature of a turbulent flow precludes an economical description of the motion of all the fluid particles. To make this easier, the velocity is decomposed into a steady mean value *U* with a fluctuating component *u'(t)* superimposed on it:

$$u(t) = U + u'(t)$$

This is called the Reynolds decomposition. A turbulent flow can now be characterized in terms of the mean values of flow properties and some statistical properties of their fluctuations.

Turbulence causes the formation of eddies of many different length scales. Most of the kinetic energy of the turbulent motion is contained in the large scale structures. The energy goes

down from these large scale structures to smaller scale structures by an inertial and essentially inviscid mechanism. This process continues, creating smaller and smaller structures which produces a hierarchy of eddies. Eventually this process creates structures that are small enough that molecular diffusion becomes important and viscous dissipation of energy finally takes place. The scale at which this happens is the Kolmogorov length scale.

Turbulent diffusion is usually described by a turbulent diffusion coefficient. This turbulent diffusion coefficient is defined in a phenomenological sense, by analogy with the molecular diffusivities, but it does not have a true physical meaning, being dependent on the flow conditions, and not a property of the fluid itself. In addition, the turbulent diffusivity concept assumes a constitutive relation between a turbulent flux and the gradient of a mean variable similar to the relation between flux and gradient that exists for molecular transport. In the best case, this assumption is only an approximation. Nevertheless, the turbulent diffusivity is the simplest approach for quantitative analysis of turbulent flows, and many models have been postulated to calculate it. For instance, in large bodies of water like oceans this coefficient can be found using Richardson's four-third power law and is governed by the random walk principle. In rivers and large ocean currents, the diffusion coefficient is given by variations of Elder's formula.

Although it is possible to find some particular solutions of the Navier-Stokes equations governing fluid motion, all such solutions are unstable at large Reynolds numbers. Sensitive dependence on the initial and boundary conditions makes fluid flow irregular both in time and in space so that a statistical description is needed. Russian mathematician Andrey Kolmogorov proposed the first statistical theory of turbulence, based on the aforementioned notion of the energy cascade (an idea originally introduced by Richardson) and the concept of self-similarity. As a result, the Kolmogorov microscales were named after him. Still, the complete description of turbulence remains one of the unsolved problems in physics

1.7 Pressure coefficient.

The pressure coefficient is a dimensionless number which describes the relative pressures throughout a flow field in fluid dynamics. The pressure coefficient is used in aerodynamics and hydrodynamics. Every point in a fluid flow has its own unique pressure coefficient, C_p.

In many situations in aerodynamics and hydrodynamics, the pressure coefficient at a point near a body is independent of body size. Consequently an engineering model can be tested in a wind tunnel or water tunnel, pressure coefficients can be determined at critical locations around the model, and these pressure coefficients can be used with confidence to predict the fluid pressure at those critical locations around a full-size aircraft or boat for example.

For incompressible flows:

The pressure coefficient is a very useful parameter for studying the flow of incompressible fluids such as water, and also the low-speed flow of compressible fluids such as air. The relationship between the dimensionless coefficient and the dimensional numbers is:

$$C_p = \frac{p - p_\infty}{\frac{1}{2}\rho_\infty V_\infty^2}$$

where:

p is the pressure at the point for which pressure coefficient is being evaluated
p_∞ is the pressure in the freestream (remote from any disturbance)
ρ_∞ is the density in the freestream
V_∞ is the velocity in the freestream
The denominator is the dynamic pressure

"We will discuss these parameters for our current problem of study further in this project."

The pressure coefficient can be further simplified for incompressible, lossless, and steady flow by using the the Bernoulli's equation.

$$C_p = 1 - \left(\frac{V}{V_\infty}\right)^2$$

This relationship is also valid for the flow of compressible fluids where variations in speed and pressure are sufficiently small that variations in fluid density can be ignored. This is a reasonable assumption when the Mach Number is less than about 0.3.

The pressure coefficient range of values vary from a -1 to 1. Nevertheless, for compressible flows the pressure coefficient can be slightly bigger/smaller than ± 1.

C_p	Conclusion
0	The pressure is the same as the free stream pressure
1	The pressure is stagnation pressure and the point is a stagnation point
-1	Indicates the perfect location for a "total energy" port for supply of signal pressure to the Variometer. (Significant for the design of gliders)

In the fluid flow field around a body there will be points having positive pressure coefficients up to one, and negative pressure coefficients including coefficients less than minus one, but nowhere will the coefficient exceed plus one (unless for compressible flows) because the highest pressure that can be achieved is the stagnation pressure. The only time the coefficient will exceed plus one is when advanced boundary layer control techniques, such as blowing, is used.

For compressible flow:

In the flow of compressible fluids such as air, and particularly the high-speed flow of compressible fluids, $\rho v^2 / 2$ (the dynamic pressure) is no longer an accurate measure of the difference between stagnation pressure and static pressure. Also, the familiar relationship that stagnation pressure is equal to total pressure does not always hold true. (It is always true in isentropic flow but the presence of shock waves can cause the flow to depart from isentropic.) As a result, pressure coefficients can be greater than one in compressible flow.

A pressure coefficient greater than one indicates the free stream flow is compressible.

$$C_p = \frac{2}{\gamma p_\infty M_\infty^2}\left(\frac{p}{p_\infty} - 1\right)$$

where:

γ is the coefficient between the heat capacity at constant pressure and the heat capacity at constant volume
M_∞ is the Mach number in the free stream

The equation for both, the incompressible and compressible flow is the same. If we start with the compressible flow equation, we can arrive by rewriting the equation to the equation of the uncompressible flow.

Rewriting the formula:

$$C_p = \frac{p - p_\infty}{\frac{1}{2}\gamma p_\infty M_\infty^2}$$

The Mach number by definition is:

$$M = \frac{V}{a}$$

where:

V is the velocity of the flow
a is the velocity of the sound

If we use the ideal gas law, we can define the speed of sound *a* as:

$$a_{ideal} = \sqrt{\gamma \frac{RT}{m}} = \sqrt{\gamma \frac{p_\infty}{\rho_\infty}}$$

Assuming the number of mols equals 1 (n=1)

m is the mass of a single molecule in Kg.

Replacing the term M in the equation:

$$C_p = \frac{p - p_\infty}{\frac{1}{2}\gamma p_\infty \frac{V^2}{\gamma \frac{p_\infty}{\rho_\infty}}}$$

Simplifying:

$$C_p = \frac{p - p_\infty}{\frac{1}{2} p_\infty \frac{V^2}{\frac{p_\infty}{\rho_\infty}}}$$

$$C_p = \frac{p - p_\infty}{\frac{1}{2}\rho_\infty V_\infty^2}$$

Pressure distribution:

An airfoil at a given angle of attack will have what is called a pressure distribution. This pressure distribution is simply the pressure at all points around an airfoil. Typically, graphs of these distributions are drawn so that negative numbers are higher on the graph, as the C_p for the upper surface of the airfoil will usually be farther below zero and will hence be the top line on the graph. This graphics will be shown later on in this project.

2. PRELIMINARIES OF THE NUMERICAL SIMULATION

2.1 Importance of the hardware.

It is important to have a good CPU in order to be efficient in our work. CFD solves the well-known Partial Differential Equations of Navier-Stokes, and sometimes a high number of iterations are required. The better the CPU is, the fastest the computation would be and therefore, the more efficient we would be.

Nowadays we have different and better computer processors than the traditional one core per chip. We have the Dual core, Tripe core, or Quad core processors. Cluster computers are commonly used when it is needed to improve performance and availability over that a single computer, while typically being much more cost-effective than single computers of comparable speed or availability.

2.1.1 Computer characteristics.

The computer used for this project has the following characteristics:

CPU	Intel Core 2 CPU 6400 2.13GHz 1.61GHz
MEMORY	2,00 GB of RAM
Mass storage service	280 GB
Operating System	Microsoft Windows XP 64 bits SP2

2.1.2 Cluster.

A computer cluster is a group of linked computers, working together closely thus in many respects forming a single computer. The components of a cluster are commonly, but not always, connected to each other through fast local area networks. Clusters are usually deployed to improve performance and availability over that of a single computer, while typically being much more cost-effective than single computers of comparable speed or availability.

There are several types of clusters,

- High-availability clusters (also known as Failover Clusters) are implemented primarily for the purpose of improving the availability of services that the cluster provides. They operate by having redundant nodes, which are then used to provide service when system components fail. The most common size for an HA cluster is

two nodes, which is the minimum requirement to provide redundancy. HA cluster implementations attempt to use redundancy of cluster components to eliminate single points of failure.

- Load-balancing is when multiple computers are linked together to share computational workload or function as a single virtual computer. Logically, from the user side, they are multiple machines, but function as a single virtual machine. Requests initiated from the user are managed by, and distributed among, all the standalone computers to form a cluster. This results in balanced computational work among different machines, improving the performance of the cluster systems.

- Compute clusters. Often clusters are used primarily for computational purposes, rather than handling IO-oriented operations such as web service or databases. For instance, a cluster might support computational simulations of weather or vehicle crashes. The primary distinction within computer clusters is how tightly-coupled the individual nodes are. For instance, a single computer job may require frequent communication among nodes - this implies that the cluster shares a dedicated network, is densely located, and probably has homogenous nodes. This cluster design is usually referred to as Beowulf Cluster. The other extreme is where a computer job uses one or few nodes, and needs little or no inter-node communication. This latter category is sometimes called "Grid" computing. Tightly-coupled compute clusters are designed for work that might traditionally have been called "supercomputing".

The cluster computer in this CFD laboratory has the following characteristics:

CPU	Quad-Core Intel Nehalem 5520 2.26 GHz / 4MB (5.86 GT/s)
MEMORY	2,00 GB DDR3 ECC Registered DIMM Memory
Mass storage service	1 TB (7,200 RPM)
Operating System	Linux

2.1.3 Computational time.

To highlight the importance of the CPU, this project compares the time taken by Fluent on completing 5000 iterations for both, the dual core, and the cluster.

5000 Iterations		
	Unstructured Grid	Structured Grid
Dual Core (PC used in this project)	29 min, 30 sec	14 min, 37 sec
Cluster	14 min, 55 sec	6 min, 22 sec

It is important to know that the big difference between the unstructured and the structured grid is because of the number of mesh element (24939 mesh elements for the unstructured, and 13200 mesh elements for the structured) and not because the type of grid. This proves the importance of a good CPU when working with CFD.

2.2 Selection of the software.

There are different programs for the pre processing, the processing and the post processing. Here we name some of the most important programs and describe the main functions of them.

2.2.1 Pre-processing.

Pre-processing refers to the first steps of our study in where we model our geometry, generate the mesh, define the fluid properties and the flow physics as well as the specification of the boundary conditions etc.

It is also possible to read some data files containing the geometry of study or input some CAD drawing directly into the pre-processing software. Each software has their characteristics and the suitability of it relies on the purpose of study.

Some preprocessor commonly used are; Gambit, Ansa, Icem CFD, GridGen, Harpoon. Gambit is the one chosen for this project

2.2.2 Solver (processing).

The solver allows inputting files (created by the pre-processor) run some calculations, and monitor the calculation progress.

There are different types of solvers. We can find commercial codes such as CFX, Fluent, Phoenix etc. and also free codes, such as Elmer, OpenFOAM and many others. Probably the most popular is Fluent, which is the software chosen for this project.

2.2.3 Post-processing.

With the post processor it is possible to manipulate and display the results, do any further analysis or report some findings.

The post processor is the last phase of the CFD process which involves results analysis of the CFD work and data visualization. This phase uses the versatile data visualization tools of the CFD solver to observe the following results of the simulation.

- Domain geometry and grid display
- Vector plots
- Contour plots (filled or not)
- 2D and 3D surface plots
- Particle tracking
- XY plots and graphs
- Report results

Fluent works also as a post processor and it has been used for this project as well as TecPlot.

3. Pre processing with Gambit.

3.1 Basics.

Gambit is an integrated preprocessor for CFD analysis. Users use Gambit for modeling the geometry of study and building the grid for it, or for importing a geometry created by a drawing package 3D CAD/CAE, made some proper modification, and finally generate the grid.

The grid options that we can find in Gambit, offer many flexibilities and possibilities. We can select different geometries for the grids or we can use the default option as well, with the unstructured grid. We can also generate high quality meshes with triangular and quadratics elements as well as meshes containing pyramids and prism elements.

Gambit allows users to check the quality of the mesh with some of the tools that it provides.

3.2 Building the linear cascade geometry.

A data file with all the information about the two-dimensional compressor stator blade profile was provided. This file contained all the blade dimensions as well as the *x*, and *y*-coordinates of all the points of the blade so it can be read by Gambit.

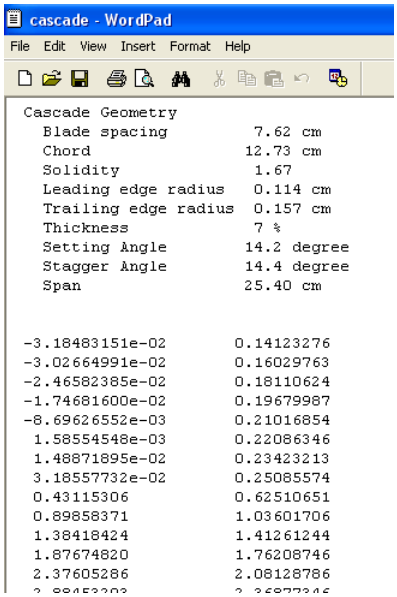

The first column indicates the x-coordinates of each point while the second column indicates the y-coordinate of each point given

As default, Gambit reads all the data files as three dimensional so in order to make it properly read, another column was needed to be written with all the *z*-coordinates. All the information above the coordinates was required to be deleted.

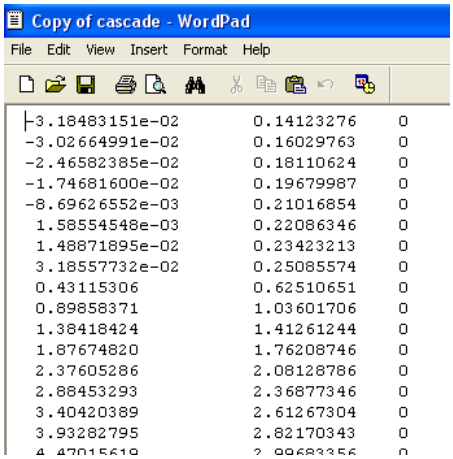

Finally, all the points read by Gambit are shown below

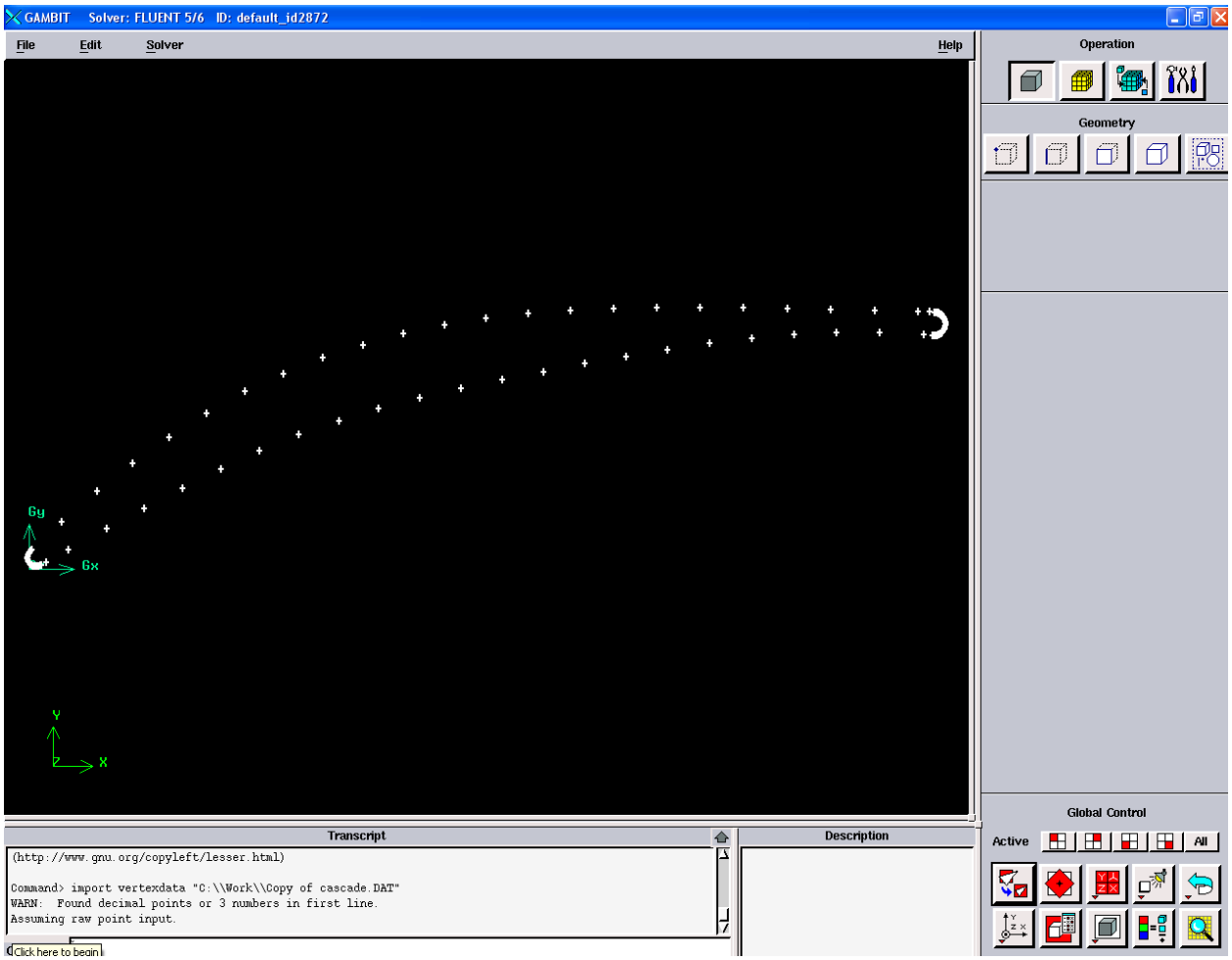

Once with the geometry of the blade built, we could start drawing the geometry of the cascade by first, connecting all the points,

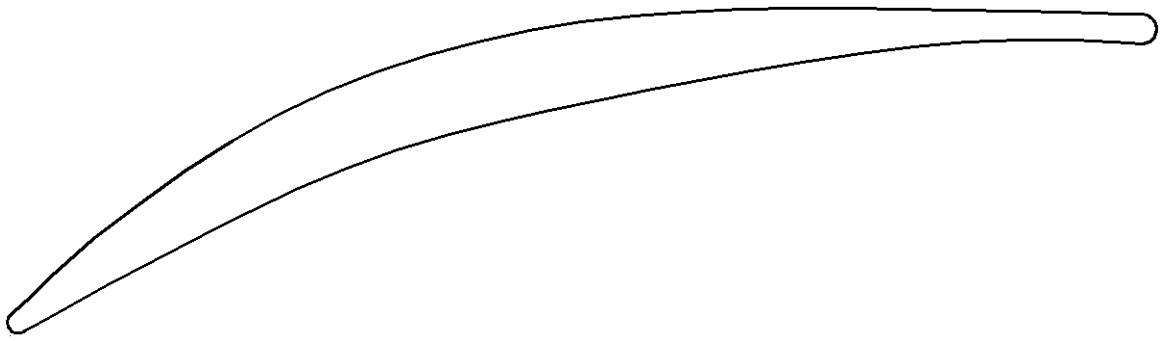

and then, according to the information provided about the cascade geometry, building the rest:

Blade spacing	7.62 cm
Chord	12.73 cm
Solidity	1.67 cm
Leading edge radius	0.114 cm
Trailing edge radius	0.157 cm
Thickness	7%
Setting angle	14.2 degrees
Stagger angle	14.4 degrees
Span	25.40 cm

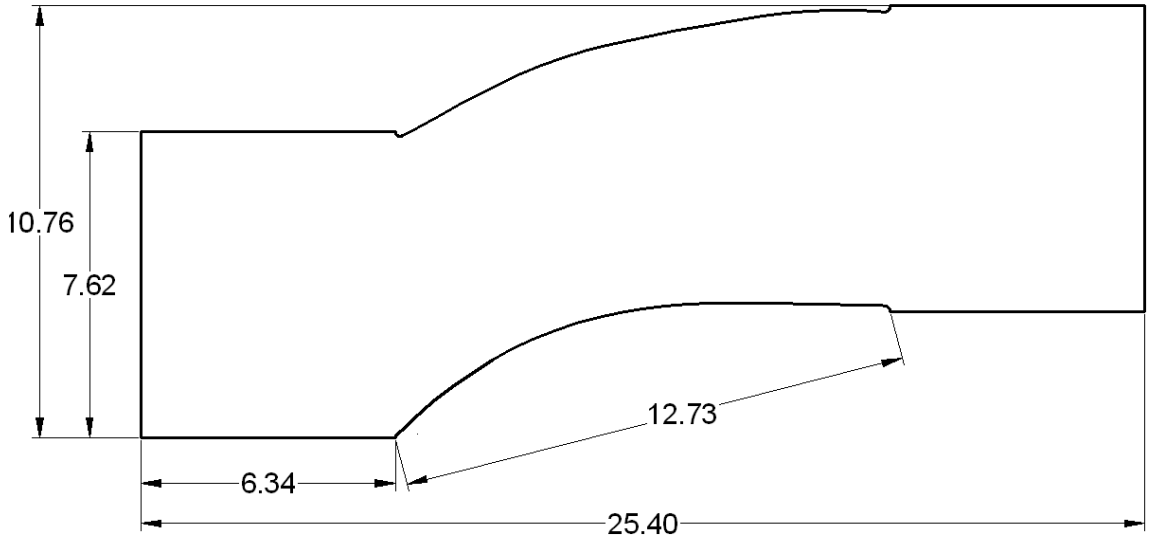

Figure 1 Dimensions of the cascade

This is our geometry of study due to the periodic characteristic of the cascade. The study of just one blade spacing is valid for all the cascade geometry, as all of them are similar.

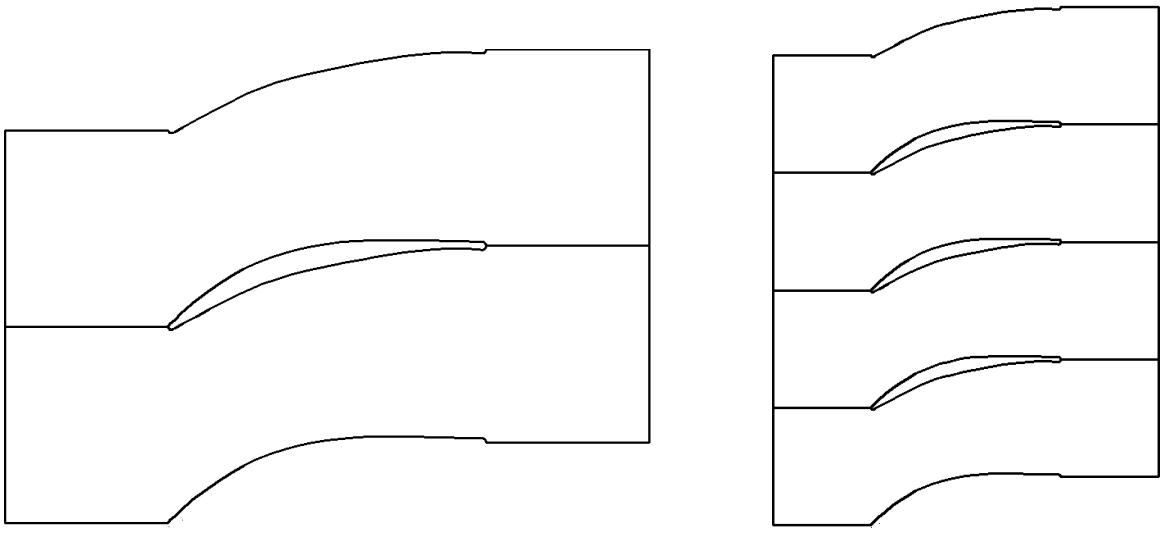

3.3 The quality of the mesh

Gambit offers a tool to analyze the quality of the mesh. We can analyze the quality of the mesh in terms of the skewness of the element (size and angle), and also in terms of the aspect ratio, edge ratio, area, and size change.

- Area: The Area specification applies only to 2-D elements and represents mesh quality on the basis of element area.
- Aspect ratio: The Aspect Ratio applies to triangular, tetrahedral, quadrilateral, and hexahedral elements and is defined differently for each element type. The definitions are as follows.

For triangular and tetrahedral elements:

$$Q_{AE} = f.\left(\frac{R}{r}\right)$$

where f is a scaling factor, and r and R represent the radius of the circles (or spheres for tetrahedral) that inscribe and circumscribe the mesh element. For triangular elements, *f*=1/2; for tetrahedral elements, *f*=1/3. Q=1 describes an equilateral element.

For quadrilateral and hexahedral elements:

$$Q_{AR} = \frac{max[e_1, e_2, \dots, e_n]}{min[e_1, e_2, \dots, e_n]}$$

where e_i is the average length of the edges in a coordinate direction (i) local to the element (see Figure 3-25) and n is the total number of coordinate directions associated with the element. For quadrilateral elements, n = 2; for hexahedral elements, n = 3.

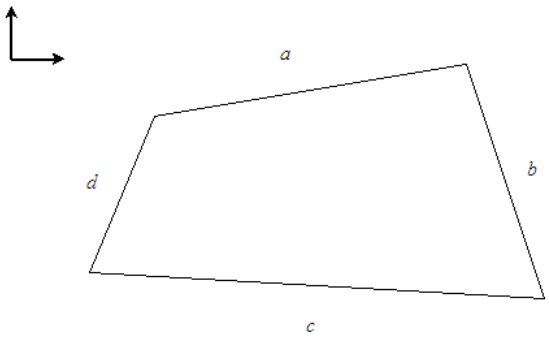

$$e_1 = \frac{a+c}{2} \qquad e_2 = \frac{b+d}{2}$$

- Diagonal ratio: The Diagonal Ratio applies only to quadrilateral and hexahedral elements and is defined as follows:

$$Q_{DR} = \frac{max[d_1, d_2, \dots, d_n]}{min[d_1, d_2, \dots, d_n]}$$

where the d_i are the lengths of the element diagonals. For quadrilateral elements, n = 2; for hexahedral elements, n = 4.

- Edge ratio: The edge ratio is defined as follows:

$$Q_{ER} = \frac{max[s_1, s_2, \dots, s_n]}{min[s_1, s_2, \dots, s_n]}$$

where s_i represents the length of the element edge i, and n is the total number of edges associated with the element.

- EquiAngle Skew: The EquiAngle Skew is a normalized measure of skewness that is defined as follows:

$$Q_{EAS} = \left\{ \frac{\theta_{max} - \theta_{eq}}{180 - \theta_{eq}}, \frac{\theta_{eq} - \theta_{min}}{\theta_{min}} \right\}$$

where θ_{max} and θ_{min} are the maximum and minimum angles (in degrees) between the edges of the element, and θ_{eq} is the characteristic angle corresponding to an equilateral cell of similar form. For triangular and tetrahedral elements, θ_{eq} = 60. For quadrilateral and hexahedral elements, θ_{eq} = 90.

The next table outlines the overall relationship between Q_{EAS} and element quality:

Q_{EAS}	Quality
$Q_{EAS} = 0$	Equilateral (Perfect)
$0 < Q_{EAS} \leq 0.25$	Excellent
$0.25 < Q_{EAS} \leq 0.5$	Good
$0.5 < Q_{EAS} \leq 0.75$	Fair
$0.75 < Q_{EAS} \leq 0.9$	Poor
$0.9 < Q_{EAS} \leq 1$	Very poor
$Q_{EAS} = 1$	Degenerate

- EquiSize Skew: The EquiSize Skew is a measure of skewness that is defined as follows:

$$Q_{EVS} = \frac{(S_{eq} - S)}{S_{eq}}$$

where *S* is the area (2-D) or volume (3-D) of the mesh element, and S_{eq} is the maximum area (2-D) or volume (3-D) of an equilateral cell the circumscribing radius of which is identical to that of the mesh element.

The next table outlines the overall relationship between Q_{EVS} and element quality:

Q_{EVS}	Quality
$Q_{EVS} = 0$	Equilateral (Perfect)
$0 < Q_{EVS} \leq 0.25$	Excellent
$0.25 < Q_{EVS} \leq 0.5$	Good
$0.5 < Q_{EVS} \leq 0.75$	Fair
$0.75 < Q_{EVS} \leq 0.9$	Poor
$0.9 < Q_{EVS} \leq 1$	Very poor
$Q_{EVS} = 1$	Degenerate

3.4 The unstructured grid.

3.4.1 Basics.

The unstructured grid is characterized by having only simple shapes such as triangular or tetrahedral mesh element in an irregular pattern. Grids of this type may be used in finite elements analysis when the input to be analyzed has an irregular shape. Unlike structured grids, unstructured grids require a list of the connectivity which specifies the way a given set of vertices make up individual elements.

Many modeling problems involve objects with irregular geometric definitions. The dataset is typically defined as a mesh covering the surfaces or volumes of these objects, and mesh granularity depends on local properties of the problem domain. Entities in the mesh (i.e., points, edges, faces, and/or volumes) must be explicitly represented, usually using multiple tables, one for each entity type, linked by pointers or integer offsets. Computations frequently involve the numerical solution of differential equations. Applications typically require the modeling of quantities such as tension, temperature, or pressure at each point in the grid, evolving over time. Computation proceeds as a sequence of mesh update steps. At each step, values associated with each entity are updated in parallel, based on values retrieved from neighboring entities. The general form of the computation accesses neighboring elements, as in the structured grid, but the neighbors could be either points, or edges, or faces, or volumes. Datasets can be very large, involving millions of grid points, at each of which the application must perform time-stepped updates based on nearest-neighbor values.

The mesh of data can be represented as a graph whose edges represent the geometric nearest-neighbor relationship between mesh points. Typically, the communication patterns in mesh problems follows this nearest-neighbor relationship. That is, the value of a mesh point in the future will depend on its own value and the values of its geometric neighborhood. Partitioning such a nearest-neighbor graph to minimize the number of cross-partition edges (total edge cut) is equivalent to finding a communication-minimizing data distribution. The updates to a processor's sub-mesh will depend on the sub-meshes of processors containing its nearest-neighbors. Since the size of sub-meshes (i.e. the number of grid-points per sub-mesh) determines the amount of work each processor is assigned, and thus the load balance of the computation, it is important for each processor's sub-domain to be of approximately equal size.

For example, the design of airfoils for airplanes requires modeling the fluid dynamics of a wing in air. In this instance, the surface of the airfoil forms is defined as a mesh of points, whose geometric properties are of import to the problem. In large, flat surfaces of the wing, the mesh can be coarse, as the dynamics on these regions will tend to be low-magnitude. At the wing-tips, however, where the surface has high curvature, a finer-granularity mesh is necessary to effectively capture the system's properties.

3.4.2 Building the unstructured grid

In order to achieve precision in our results, the mesh need to be smaller near the wall of the blade, where the no-slip condition characterize the motion of the flow, and need to be bigger in the areas away from the wall, where the flow is predictable and uncomplicated in order to speed up the computation time while solving the PDEs (Partial Differential Equations).

To be able to do that, the geometry of the cascade was divided in several parts

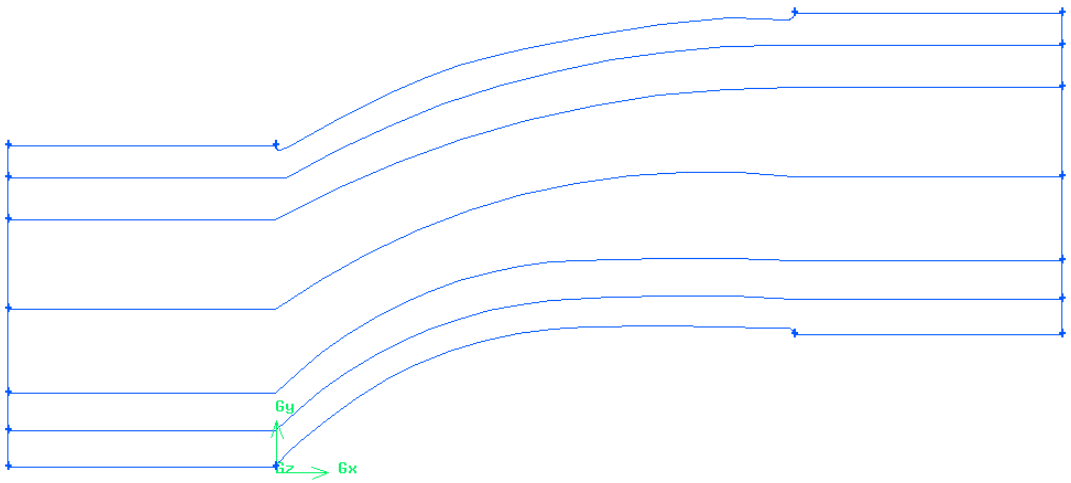

Then, each edge was meshed with different grading ratios. In the next picture we name the different zones of the cascade

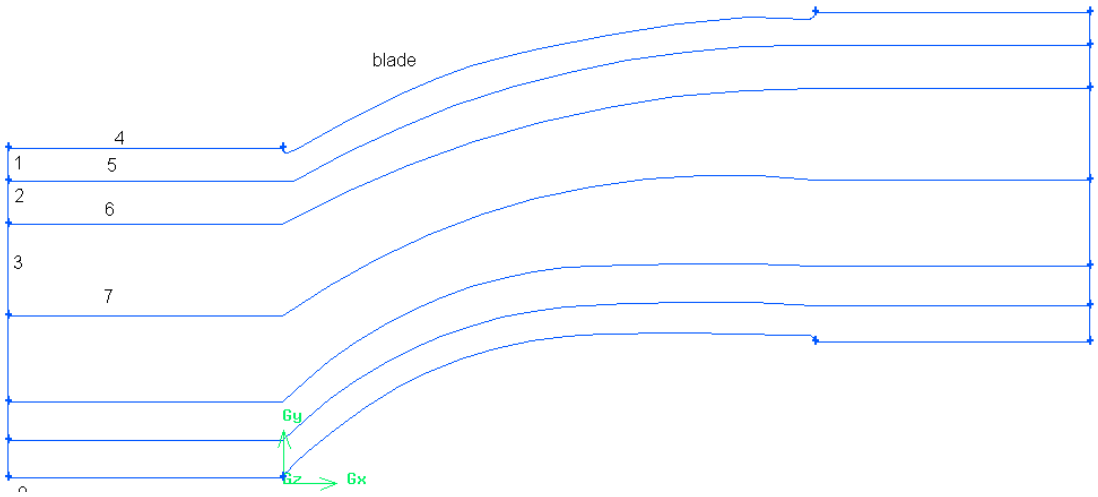

The next table provides all the information about the mesh properties:

Element meshed	Grading Ratio	Interval count
1 vertical	1.05	7
2 vertical	1.07	9
3 vertical	1.1	8
4 horizontal	1.015	100
5 horizontal	1	165
6 horizontal	1	105
7 horizontal	1	75
blade	1.005	326

EquiSize Skew: 0.684078 (worst element)
EquiAngle Skew: 0.597501 (worst element)
Total number of mesh elements: 24939

Figure 2Unstructured mesh properties

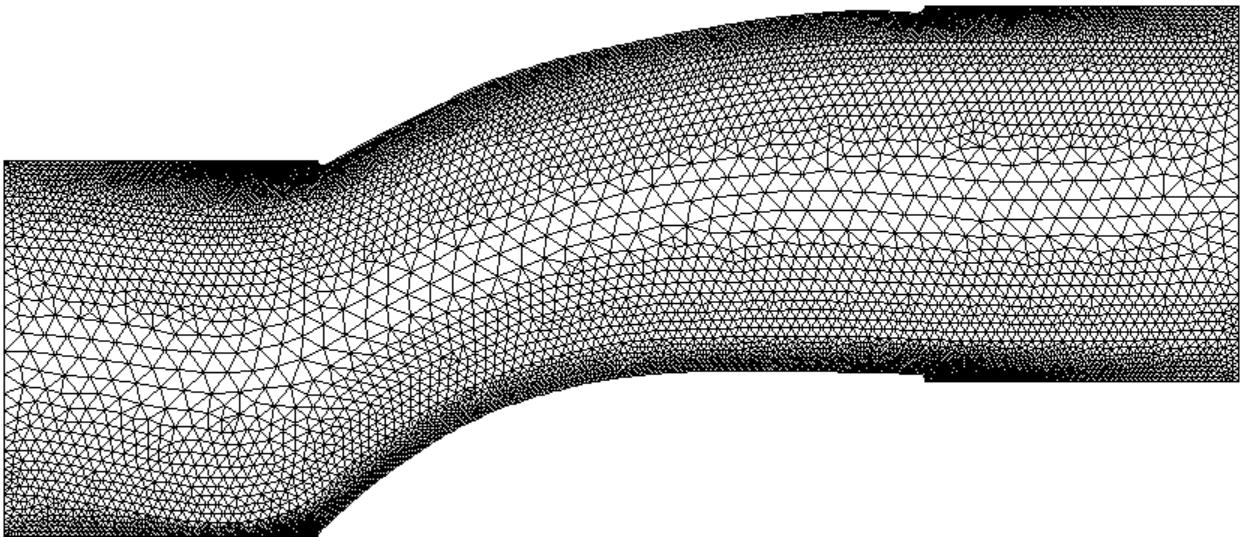

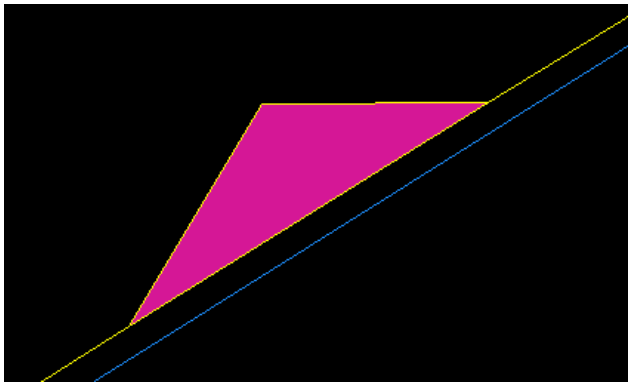

EquiSize Skew unstructured (worst element)

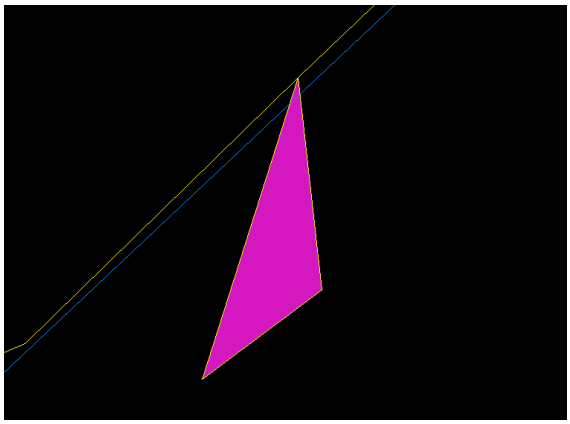

EquiAngle Skew unstructured (worst element)

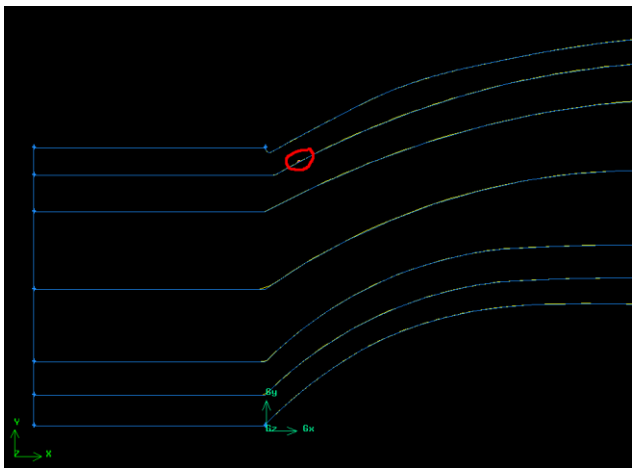

Worst element location. EquiSize Skew

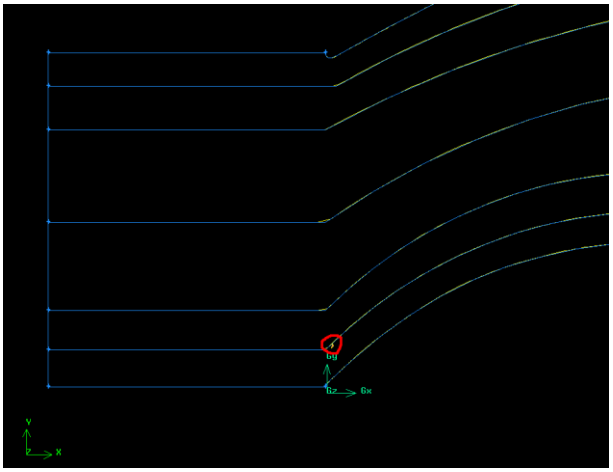

Worst element location. EquiAngle Skew

3.5 The structured grid.

3.4.1 Basics.

The structured grid is characterized by having only quadrilateral or hexahedral mesh element in a regular pattern. This type of grid may be used in finite element analysis as well as finite volume methods and finite difference methods. Since the derivatives of field variables can be conveniently expressed as finite differences, structured grids mainly appear in finite difference methods. Unstructured grids offer more flexibility than structured grids and hence are very useful in finite element and finite volume methods.

Computation proceeds as a sequence of grid update steps. At each step, all points are updated using values from a small neighborhood around each point.

The structured grid concept allows one to define the grid characteristics through coordinate transformation as features of the coordinate curves, coordinate surfaces, coordinate volumes etc. In general these features are determined through the elements of the metric tensor and their derivatives. In particular, some grid properties can be described in terms of the invariants of the covariant metric tensor.

A structured grid is organized in rows and columns of cells (for two-dimensions) so that a program sweeping over the entire mesh can directly address the neighboring cells to evaluate differencing expressions. There is a direct relationship between a cell's location in its row and column and the location in the CFD program's arrays used to store physical variables associated with the cell.

With structured grids, the program is less complex than the unstructured grid, because it addresses your data (values for the variables in each cell) directly with subscripts that exploit the fact that the cells are in rows and columns. The down side is that, in order to bend the structured mesh to the physical space being modeled, cells can take on an odd shape or undesirable size.

In structured meshes, one important characteristic is that the direction of the flow matches the main direction of the mesh. If we respect this, the flow that goes out from the element and enter to the next one, has its properties. If this is not respected and the flow does not follow the direction of the mesh, the flow goes away from one element and enters to another one, then if there is a variation in one or more variables, the mesh cannot take all the information and loses part of it. This is why convergence was getting harder as we were increasing the angle of attack in our project.

3.4.2 Building the structured grid.

In order to achieve precision in our results, the mesh need to be smaller near the wall of the blade, where the no-slip condition characterize the motion of the flow, and need to be bigger in the areas away from the wall, where the flow is predictable and uncomplicated in order to speed up the computation time while solving the PDEs (Partial Differential Equations).

To be able to do that, the geometry of the cascade was divided in several parts

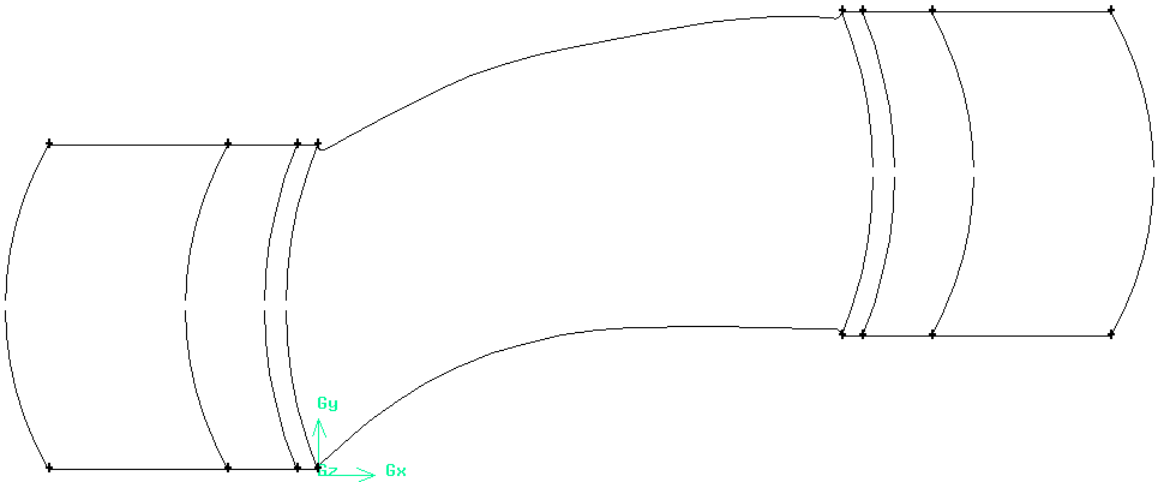

Then, each edge was meshed with different grading ratios. In the next picture we name the different zones of the cascade. In the next picture we name the different edges of the cascade:

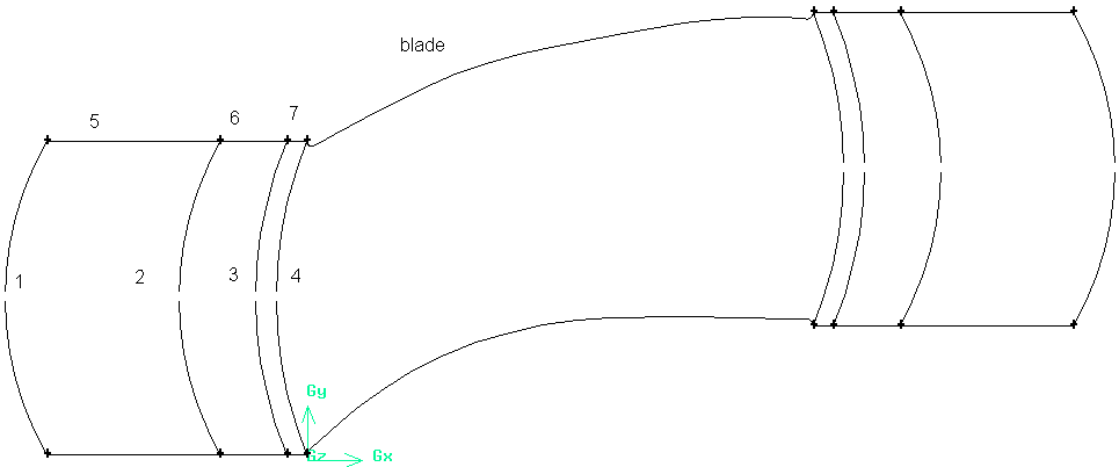

The next table provides all the information about the mesh properties:

Element meshed	Grading Ratio	Interval count
Edge 1	1.15	60
Edge 2	1.15	60
Edge 3	1.15	60
Edge 4	1.15	60
Edge 5	1.05	15
Edge 6	1.10	20
Edge 7	1.035	25
blade	1.08	100
EquiSize Skew: 0.74569 (worst element)		
EquiAngle Skew: 0.74569 (worst element)		
Total number of mesh elements: 13200		

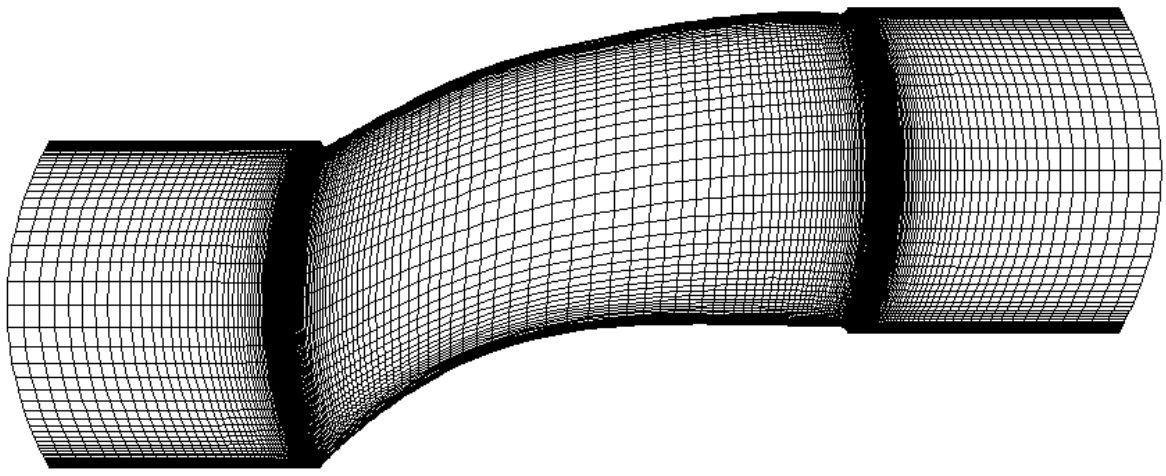

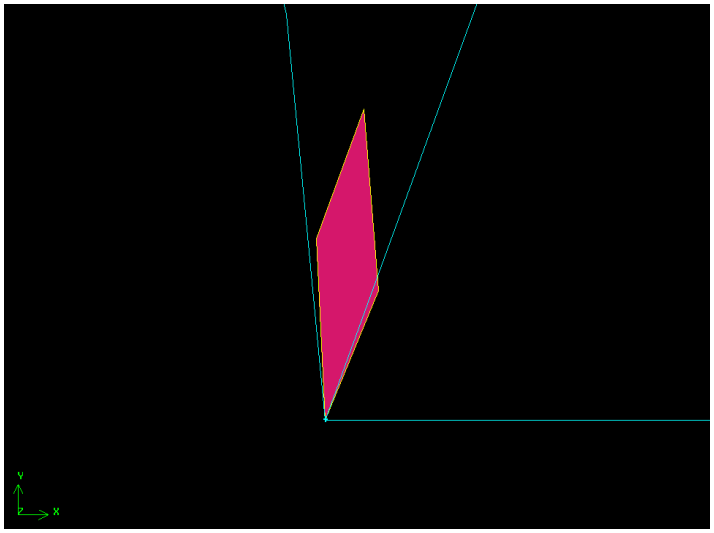

The worst element in the EquiSize and EquiAngle skew is the same one.

Worst element. EquiSize and EquiAngle Skew, structured

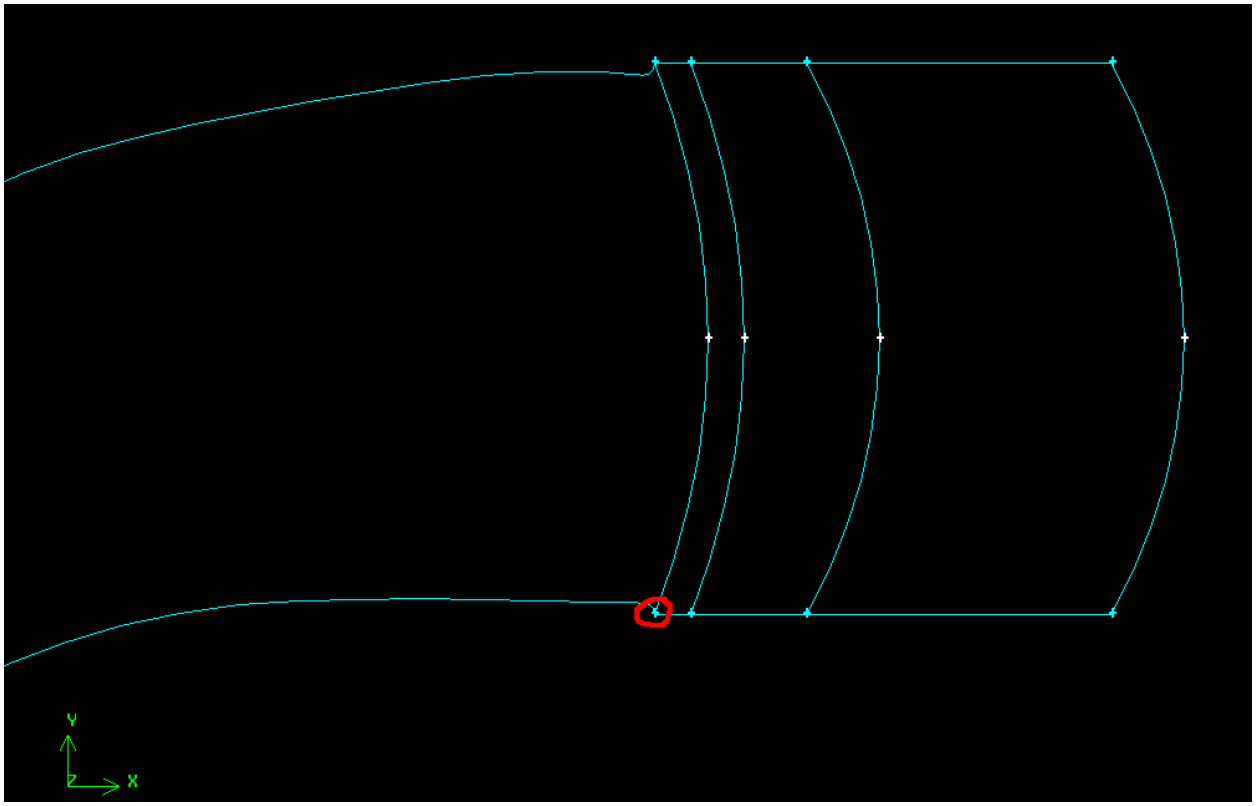

Worst element location. EquiSize and EquiAngle Skew in the structured mesh

4. IMPLEMENTATION OF CFD IN THE TWO-DIMENSIONAL LINEAR CASCADE.

4.1 Basics.

The solver selected to analyze and solve our problem is Fluent. Fluent is a computational fluid dynamics (CFD) software package to simulate fluid flow problems. It uses the finite-volume method to solve the governing equations for a fluid. It provides the capability to use different physical models such as incompressible or compressible, inviscid or viscous, laminar or turbulent, etc. Geometry and grid generation is done using Gambit which is the preprocessor bundled with Fluent

Some conditions are set before studying the two-dimensional linear cascade flow. We study only a steady state problem, a compressible flow, an ideal gas model (air), a viscous flow and as a test case, we also study an inviscid flow. As this project will show, the inviscid model for a compressible flow in this study, lacks completely of meaning.

Finding convergence for this problem was tricky and it got harder as the angle of attack increased from 0 to 46 and as the pressure ratio increased from 1.03 to 1.5.

4.2 Computational fluid dynamics theory.

To study the parameters/variables on the stator's blade of an axial compressor, where it's so difficult to arrive with a sensor and collect data, we used the numerical software that has been developed in the last two decades. The name of this tool is Computational Fluid Dynamics (CFD) and is used to predict the velocity, pressure, flow rate etc. in each point of the mesh. The $k-\epsilon\ model$ is the most used model in industries and it's enough strong and accurate for our calculations. This tool enable us to do several simulations rapidely.

4.2.1 Turbulence models.

It is important to distinguish if the flow is laminar or turbulent. The Reynolds number that compares the inertial forces with the viscous forces is used to predict it. When the Reynolds number increased, up to or approximately over 4000 the flow becomes turbulent. Depending on the values of the Reynolds number we can classify the flow as laminar, transient or turbulent.

Reynolds Number	Flow Regime
Re < 2300	Laminar
2300 < Re < 4000	Transient
4000 < Re	Turbulent

In a turbulent regime, the flow depends on four variables, (*x*, *y*, *z*, and *t*). The Navier-Stokes equations describes the conservation of momentum and mass.

$$\partial_i \widetilde{u_\iota} + \widetilde{u_j}\partial_j \widetilde{u_\iota} = -\frac{1}{\rho}\partial_i \tilde{p} + V\nabla^2 \widetilde{u_\iota}$$

$$\partial_i \widetilde{u_\iota} = 0$$

A direct numerical simulation (DNS) is a simulation in computational fluid dynamics in which the Navier-Stokes equations are numerically solved without any turbulence model. This means that the whole range of spatial and temporal scales of the turbulence must be resolved. All the spatial scales of the turbulence must be resolved in the computational mesh, from the smallest dissipative scales (Kolmogorov microscales), up to the integral scale L, associated with the motions containing most of the kinetic energy. However it is not possible actually because it requires a very thin mesh to take all the turbulent flow's variation. To solve later this mesh, we need a very strong computational power and nowadays, due to economical reasons this is not worthy.

Another way is to modify the Navier-Stokes equations to adapt to the turbulence problem. The change is to study the flow with a time scale larger than the turbulence ones and the velocities as a sum between the mean and a fluctuation. With this changes and applying another time the Navier-Stokes we arrive to the model called RANS (Reynolds Averaged Navier Stokes). This RANS model is similar to the Realizable k-Epsilon model with the exception of the dissipation term in the *K* equation.

$$\partial_i U_i + U_j \partial_j U_i = -\frac{1}{\rho}\partial_i P + V\nabla^2 U_i - \partial_j \overline{u_j u_\iota}$$

$$\partial_i U_i = 0$$

The term that appears is called the Reynolds stress tensor but is not a stress tensor, is an average effect of turbulent convection. This term is the key of this model. The mean flow equations are 4 but there are 10 unknowns so we have 6 that cannot be solved. To close the system we need more equations in order to solve the Reynolds stress tensor.

4.2.2 The *K-Epsilon* model.

The *K-Epsilon* model is the most used turbulence model. It is a two equation model, that means, it includes two extra transport equations to represent the turbulent properties of the flow. This allows a two equation model to account for history effects like convection and diffusion of turbulent energy.

The first transported variable is turbulent kinetic energy, k. The second transported variable in this case is the turbulent dissipation, ϵ. It is the variable that determines the scale of the turbulence, whereas the first variable, k, determines the energy in the turbulence.

There are two major formulations of K-epsilon models. That of Launder and Sharma is typically called the "Standard" K-epsilon Model. The original impetus for the K-epsilon model was to improve the mixing-length model, as well as to find an alternative to algebraically prescribing turbulent length scales in moderate to high complexity flows.

This method was developed in 1974 and was the first proposed two equation models to be used in Computational Fluid Dynamics. In the later 70s other models more accurate or more robust appear but nowadays they are less used due to this historical reason.

The model aims to know the eddy viscosity and relate it to the Reynolds stress and dissipation. If we know that the turbulence correlation time scale is about T~K/ε and k are the velocity squared, we can find the next formula:

$$\upsilon_T \sim u^2 T = C_\mu \frac{K^2}{\varepsilon}$$

The next step to evaluate the formulas to parameterize turbulent mixing with a model that predicts *k* and ε. From scalar eddy viscosity and the constitutive relation we calculate the mean flow formula.

$$-\overline{u_i u_j} = 2\upsilon_T S_{ij} - \frac{2}{3} k \delta_{ij}$$

Where S_{ij} is the mean rate of strain tensor.

The equation called the constitutive assumes that there's a balance between the Reynolds Stress and the mean rate of strain in most of Newton's fluid flows as in our case (water). The formula help us with cutting the vt predict to the values in the spatial and temporal distribution of k and epsilon.

$$\upsilon_T = C_\mu \frac{k^2}{\varepsilon}$$

Finally we have the two equations that close the system knowing that we added an empirical constant to get the ε-equation final form.

$$\frac{\partial \varepsilon}{\partial t} + U_j \frac{\partial \varepsilon}{\partial x_j} = -C_{\varepsilon 1} \frac{\varepsilon}{k} \overline{u_i u_j} \frac{\partial U_i}{\partial x_j} - C_{\varepsilon 2} \frac{\varepsilon^2}{k} + \frac{\partial}{\partial x_j} \left(\left(\upsilon + \frac{\upsilon_T}{\sigma_\varepsilon} \right) \frac{\partial \varepsilon}{\partial x_j} \right)$$

$$\frac{\partial k}{\partial t} + U_j \frac{\partial k}{\partial x_j} = -\overline{u_i u_j} \frac{\partial U_i}{\partial x_j} - \varepsilon + \frac{\partial}{\partial x_j}\left((\upsilon + \upsilon_T)\frac{\partial k}{\partial x_j}\right)$$

The standard value for the constant are:

$$C_\mu = 0.09 \qquad C_{\varepsilon 1} = 1.44 \qquad C_{\varepsilon 2} = 1.92 \qquad \sigma_\varepsilon = 1.3$$

4.2.3 Near wall modeling.

Near the walls the viscosity effect becomes very important and there is a strong velocity gradient. That made the Reynolds stress vary and finally disappear close to the wall.

Some expressions are important to know in the boundary layer.

$\frac{U}{u*} = f\left(y\frac{u*}{v}\right)$	*Law of the wall*
$y_+ = y\frac{u*}{v}$	$Y^+ definition$
$u_* = sqrt\left(\frac{\tau_0}{\rho}\right)$	Friction velocity or velocity scale
$\frac{v}{u*}$	Length scale

We can distinguish three zones near the wall. From the wall to the outside:

- The first is the viscous sub-layer where the viscous effect dominates the flows and the Reynolds stress is still small.
- In the sub-layer, it can be assume that the stress is constant and is equal to the wall shear stress.
- In the outer region, there is the logarithmic sub-layer. The velocity and other variables do not depend on viscosity because this layer is far enough from the wall.

Between the two sub-layers explained before, there is another one where the effects are mixed. This layer is very important dynamically since there is a maximum of the turbulence production.

The next pictures shows the typical velocities and shear distribution in turbulent flow near the wall.

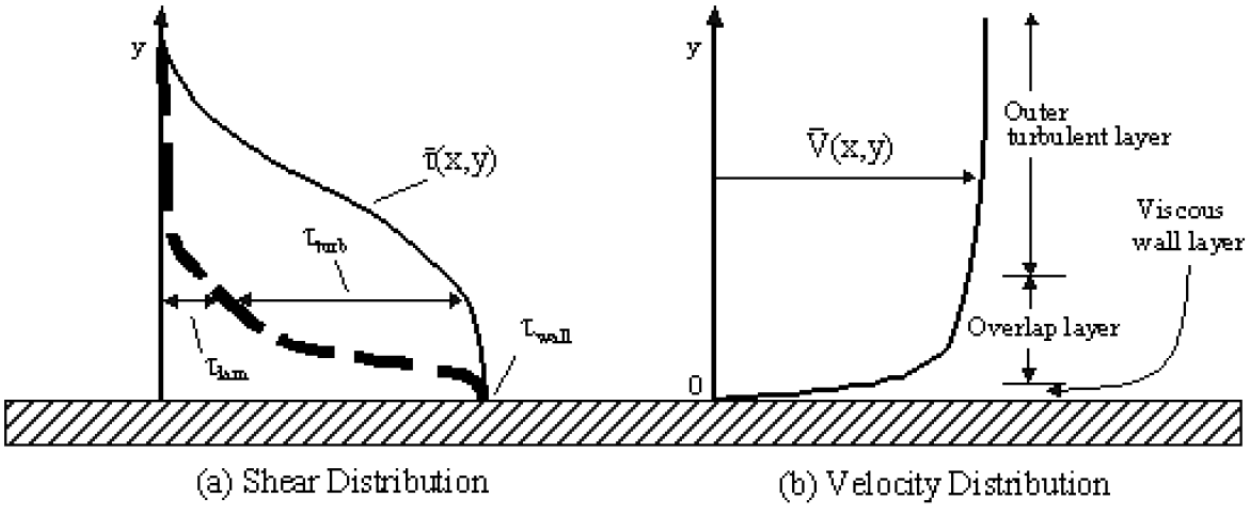

When the K-Epsilon tries to solve the flow near the wall it fails drastically near the logarithmic layer. There are two different ways of solving it.

The first one consist to solve the boundary layer formed near the wall and change and change it for suitable conditions which are based on empirical formulas. It allows to work with less dens mesh near the wall and save computer storage because we don't need to solve difficult equations. To obtain good results with this model the y_+ must be between 30 and 100 where the boundary is.

The second one consists in using a very thin grid near the wall to solve the boundary layer. This method is called low-Re method, because the Reynolds number decreases in the viscous layer where the flow becomes laminar. It is easy to understand that this method is going to need an important computer requirement and time because the grid must be very thin and the software will have to solve a lot of points near the wall. This is the method used in this project.

4.2.4 Scheme order and influence.

The finite difference method is an old method to obtain numerical solutions of a differential equation. The finite difference model needs a mesh where each element is similar to the others that are around it. This way is based on the Taylor's developments and on the derivative definition. The method used the derivation's definition with the values of the points near the studied point, to find the derivate in this point.

The derivation definition is:

$$u_x = \frac{\partial u}{\partial x} = \lim_{\Delta x \to 0} \frac{u(x + \Delta x) - u(x)}{\Delta x}$$

An approximation of this value can be obtained by using the Taylor's development of $u(x+\Delta x)$ around the x point.

If we develop this expression we found the next polynomial:

$$u(x+\Delta x) = u(x) + \Delta x * u_x(x) + \frac{\Delta x}{2} * u_{xx}(x) + \cdots$$

We write it like in the derivation definition and we group the Taylor's development in an expression such as

$$\frac{u(x+\Delta x) - u(x)}{\Delta x} = u_x(x) + 0(\Delta x)$$

We consider a one dimension analysis (in the *x* axis) where we know the function value, u_i, in the point x_i, with *i=1,……,N* and $x_{i+1} - x_i = \Delta x$, where Δx is the constant value for any *i*. We can define the finite difference approximation for the first derivative:

$$(u_x)_i = \left(\frac{\partial u}{\partial x}\right)_{x=x_i} = \frac{u_{i+1} - u_i}{\Delta x} + 0(\Delta x)$$

$$(u_x)_i = \left(\frac{\partial u}{\partial x}\right)_{x=x_i} = \frac{u_i - u_{i-1}}{\Delta x} + 0(\Delta x)$$

These first order approximations are called forward difference and backward difference and are consider as one sided difference formulas.

If we calculate the approximation between the points *i-1* and *i+1* we obtain a second order approximation called the central difference.

$$(u_x)_i = \left(\frac{\partial u}{\partial x}\right)_{x=x_i} = \frac{u_{i+1} - u_{i-1}}{2\Delta x} + 0(\Delta x^2)$$

We can also think in forward differences as the central difference respect to the point $x_{i+\frac{1}{2}}$

$$(u_x)_{i+\frac{1}{2}} = \left(\frac{\partial u}{\partial x}\right)_{x=x_i+\frac{1}{2}} = \frac{u_{i+1} - u_i}{\Delta x} + 0(\Delta x^2)$$

So, the same formula can be used with the same mesh points (*I and i+1*) being a first order forward difference if we study the point $(u_x)_i$ or a second order central approximation if we study the point $(u_x)_{i+\frac{1}{2}}$. We obtain the same for the backward difference

$$(u_x)_{i+\frac{1}{2}} = \left(\frac{\partial u}{\partial x}\right)_{x=x_i+\frac{1}{2}} = \frac{u_i - u_{i-1}}{\Delta x} + 0(\Delta x^2)$$

An order of accuracy is gained by using the same expressions as an approximation to the middle points (*i+1/2 or i-1/2*).

4.3 Case set up.

To begin a case in FLUENT, the program is initiated and the user is asked to choose a

solver type. The options are 2D single-precision, 2D double-precision, 3D singleprecision, and 3D double-precision. The FLUENT Users Guide states that "For most cases, the single precision solver will be sufficiently accurate." A list of possible applications that would benefit from a double-precision solver does not include anything that resembles the type of case for the two-dimensional linear cascade and therefore, a 2D single-precision solver is used for all the studies done in this project.

Once the solver is chosen, the program loads and is ready to read in a mesh file. Under "File-Read-Case", the user can find the appropriate .msh file created by the preprocessor and FLUENT imports the created mesh (grid). Once the grid is read into Fluent, a grid check should be ran to ensure that there are no negative volumes contained within the grid as Fluent is unable to provide a solution to a grid with negative volumes. Because the grid was created in centimeters and the default grid setting in Fluent is in meters, the grid must be scaled to centimeters using the "Grid-Scale" command. It is possible to display the grid to assure that everything looks good.

4.4 Defining the model, materials and solver.

The next step in setting up a case to run in Fluent is to choose the appropriate models Fluent will run from the "Define-Models" menu. We select the pressure-based solver type, the steady option under the time menu, and absolute velocity formulation and the planar option under the 2d space menu. We use the pressure-based solver instead of the density-based solver because we are doing a steady state calculation and therefore, the pressure-based solver does not contain time-dependent terms. Modeling the flows as steady-state allows pertinent flow features to be captured while not placing an excessive computational load on the computer.

We allow the energy equation as we set our material as a compressible ideal gas. Fluent automatically enables the solution of the energy equation when the ideal gas law is used, in case we did not already enable it manually in the energy panel. In order to activate the turbulence

model a viscous model is needed to be selected. The viscous model used in this project is the *k-epsilon*, as is the most commonly used and our problem does not include any special phenomenon such as combustion or supersonic flow etc.

Once all the appropriate models are specified, the user must ensure that the fluid material used by Fluent is air. This is found under the "Define-Materials" menu. The appropriate values for density and viscosity should be entered under the "Material Properties" section of the menu. Unless otherwise stated, these values corresponded to standard atmosphere sea level conditions for the CFD runs presented in this project.

The desired pressure ratio and angle of attack for a given case are specified under the "Define-Boundary Conditions" menu. For the pressure inlet boundary condition specified in Gambit, the pressure magnitude and direction is specified in Fluent. For example, to run a Fluent case of 1 atmosphere as the static pressure in the outlet, the magnitude is specified in the boundary condition menu and we need to be careful as the pressure inputted here is relative to the operating pressure defined in the operating conditions panel. As for the angle of attack, this is specified in the inlet boundary condition menu with the *x*- component and *y*-component flow direction options. Refer to the next section (4.5) for more information.

4.5 Boundary conditions.

In differential equations, a boundary value problem is a differential equation together with a set of additional restraints, called the boundary conditions. A solution to a boundary value problem is a solution to the differential equation which also satisfied the boundary conditions.

All CFD problems are defined in terms of initial and boundary conditions. Boundary conditions specify the flow and thermal variables on the boundaries of our physical model. They are, therefore, a critical component of our CFD simulation and it is important that the user specifies these appropriately and understands their role in the numerical algorithm.

In FLUENT we have several boundary types available:

- Flow inlet and exit boundary:
    1. *Pressure inlet*
    2. *Velocity inlet*
    3. *Mass flow inlet*
    4. *Inlet*
    5. *Vent*
    6. *Intake fan*
    7. *Pressure outlet*

8. *Pressure far-field*
9. *Outflow*
10. *Outlet vent*
11. *Exhaust fan*

- Wall, repeating and pole boundaries:
  1. *Wall*
  2. *Symmetry*
  3. *Periodic*
  4. *Axis*
- Internal cell zones:
  1. *Fluid*
  2. *Solid (porous is a type of fluid zone)*
- Internal face boundaries:
  1. *Fan*
  2. *Radiator*
  3. *Porous jump*
  4. *Interior*

In FLUENT, boundary conditions are associated with zones and not with individual cells or faces.

Generally, a pressure condition cannot be used at a boundary where velocities are also specified, due to the fact that velocities are influenced by pressure gradients.

In our problem, the boundary conditions given to our two dimensional linear compressor cascade flow are shown as follow:

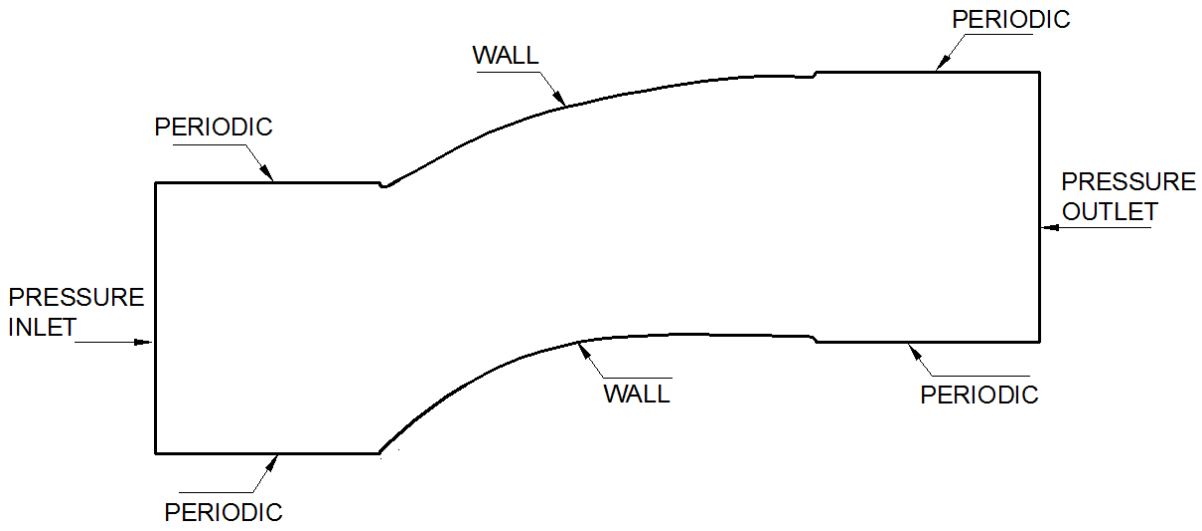

Periodic boundary type cannot be set up through GAMBIT and it has to be specified first as a wall boundary condition and then create it in FLUENT.

PRESSURE INLET:

This boundary condition is used to define the fluid pressure at flow inlets, along with all other scalar properties of the flow. We use this boundary conditions in this problem because we know the inlet pressure and we don't know the velocity or the flow rate.

We study different pressure ratios in this problem:

$$\frac{P^0}{P_e} = 1.03 \qquad \frac{P^0}{P_e} = 1.2 \qquad \frac{P^0}{P_e} = 1.5$$

Where P^0 is the stagnation pressure at the inlet, and P_e is the static pressure at the outlet.

The stagnation pressure is the static pressure at a stagnation point in a fluid flow. At a stagnation point, the fluid velocity is zero and all kinetic energy has been converted into pressure energy.

In FLUENT, stagnation pressure at the inlet equals total pressure, hence for uncomprensible flows:

$$Total\ Pressure = P^0 = P_e + \frac{1}{2}\rho V^2$$

And for compressible flows:

$$\frac{P^0}{P_e} = \left(1 + \frac{\gamma - 1}{2} M^2\right)^{\frac{\gamma}{\gamma - 1}}$$

Where:

$\rho = density$
M = mach number
V = velocity
$\gamma = ratio\ of\ specific\ heats\ \left(\frac{C_p}{C_v}\right)$

The operating pressure is set as the atmospheric pressure, 101325 Pascals. We must be careful as the pressures are defined with respect to the operating pressure.

If we set the static pressure at the outlet as the atmospheric pressure, we can simply calculate the stagnation pressure at the inlet.

$$P_e = 101325\ Pascals$$

$\frac{P^0}{101325} = 1.03 \longrightarrow P^0 = 104364.75\ Pascals \longrightarrow$ P inputted 3039.75

$\frac{P^0}{101325} = 1.2 \longrightarrow P^0 = 121590\ Pascals \longrightarrow$ P inputted 20265

$\frac{P^0}{101325} = 1.5 \longrightarrow P^0 = 151987.5\ Pascals \longrightarrow$ P inputted 50662.5

Regarding the direction of the flow at the inlet:

Angle of attack	**0**	**28**	**39**	**46**
X-Component of flow direction	1	0.882947592	0.777145961	0.694658637
Y-Component of flow direction	0	0.469471562	0.629320391	0.7193398

Same thing could have been done setting up the operating pressure to 0 as the only thing that matters is the pressure gradient.

PRESSURE OUTLET:

This boundary condition requires to specify a static (gauge) pressure at the outlet. This value is only used while the flow is subsonic.

We set the operating pressure to the atmospheric pressure (101325 Pa). We also set the static pressure at the outlet as the atmospheric pressure, and therefore the pressure inputted is 0 as this value is relative to the operating pressure. In CFD, the absolute pressure is defined as follows

$$Absolut\ pressure = Operating\ pressure + Static\ pressure$$

PERIODIC:

As said before, we cannot set the periodic condition through GAMBIT, so we first need to set the boundary condition as a wall and then create the periodic zones in FLUENT.

To do so, we need to attach a periodic zone with a shadow zone, it means, the initial and end zones of the periodic conditions. The next figure explains these zones in our problem:

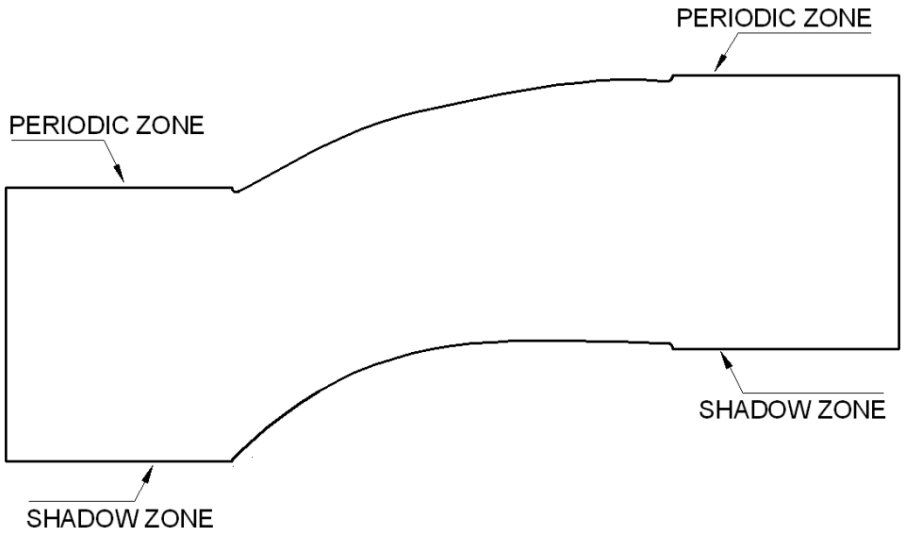

To create periodic zones in FLUENT we need to write some commands on the console:

1. Press enter to get the command prompt (>)
2. Write and press enter ⟶ Grid ⟶ modify-zones ⟶ make-periodic
3. Write the periodic zone ID
4. Write the shadow zone ID
5. Select translational as this is a two dimensional linear cascade flow
6. Create periodic zones ⟶ Yes
7. Auto detect translation vector ⟶ Yes

The flow is allowed to escape through this boundary type.

WALL:

This boundary condition is used to bound fluid and solid regions. If we set a viscous model, the no-slip condition would be enforced on the wall by default. It is possible to model a slip wall in a viscous model by using the symmetry boundary type, or specifying a tangencial velocity component of the wall boundary or just by specifying shear.

The shear stress and heat transfer between the fluid and wall are computed based on the flow details in the local flow field.

This study does not include the effect of heat transfer, and therefore, we only focus on the flow motion.

4.6 Solution initialization and Setup.

Before a case can run in Fluent, the solution must be initialized to provide an initial guess for the solution flow field. To begin the initialization process, the governing equations must first be converted to algebraic equations that can be solved numerically. This is accomplished through a control volume technique that involves integrating the governing equations about each control volume to yield discrete equations from which each quantity is conserved on a control volume basis. A mathematical example of this can be found in section 26.2 of the FLUENT Users Guide.

For our project, in the solution method, the Simplec scheme is used because of our steady state problem, and we can benefit with it against the Simple scheme because of the increased under-relaxation factors that can be applied and therefore, we can obtain a more quickly converged solution.

For the spatial discretization, we use the standard option for the pressure equation, and we set other equations as a second order upwind in order to obtain a more accurate solution. However, sometimes due to convergence problems, a first order upwind and a PRESTO option for the pressure equation was selected. The first order upwind can sometimes lead to wiggly shapes on the contours due to the first order of the equations used.

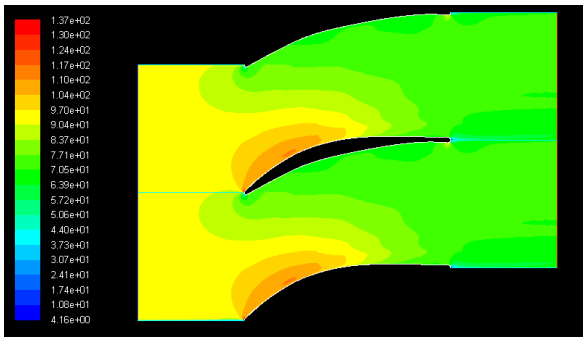

1st order discretization (wiggly shapes)

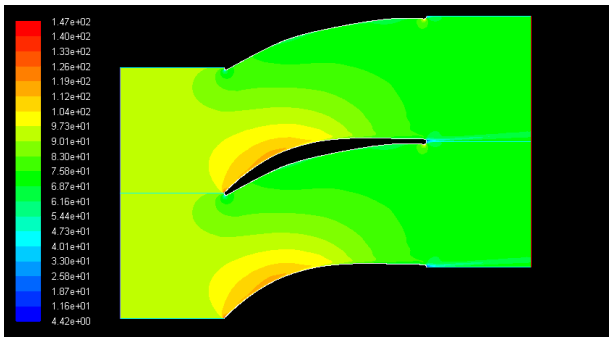

2nd order discretization (smooth shapes)

Once the solution controls have been specified, the solution is ready to be initialized. Under the "Solution initialization" menu in Fluent, the user specifies where the solution is to be initialized from. For the cases of this project, the solution is computed from the inlet face. Once this is specified, the "Initial Values" field automatically updates to include all previously specified values for Gauge Pressure, Velocity Components, and Modified Turbulent Viscosity. Clicking the "Init" button initializes the solution.

Several steps remain before the case is ready to be run. Under the "Solve-Monitors-

Residual" menu, the convergence criteria for continuity and x, y, and z velocity are specified as 0.0001. We uncheck this criteria as we want to judge the convergence for this project ourselves. The lower the residuals are, the better and therefore we do not want to stop the iterations at

0.0001 or at a lower value. The plotting of the residuals is allowed in this same menu and we can see when the convergence is reached.

To begin iterations of the cases, the "Run Calculation" menu is opened and the user specifies the number of iterations to be run. A high number, such as 2,000 iterations, should be specified at first to ensure enough iterations for solution convergence. Clicking on the "Iterate" button begins the iterative process. Fluent will automatically stop iterating when the maximum number of specified iterations occur. By monitoring the residuals values during the iterative process, the user can determine if it is feasible to continue iterations prior to Fluent automatically stopping the process. For example, if none of the equations are converging or they are converging really slow, the user can stop the iterations and make some changes in order to find a better convergence.

A summary of the actions taken to setup a case in FLUENT is shown in Table 4.1. Note that once a case has been setup in FLUENT, the case may be saved so that only the steps 5 to 12 need to be addressed for each new case to be ran. In addition, after each case is run, the case and data files should be written in order to save all the information pertaining to the case.

Step	Action	Result
1	Chose solver type	2D
2	Import mesh file (.msh)	N/A
3	Grid Check	Not negative volumes
4	Grid Scale	Centimeters
5	Define Models	Pressure-Based, Steady, k-Epsilon,
6	Define Material	Air. Enable ideal gas law
7	Define Boundary Conditions	Set pressure ratios and flow direction
8	Solution Method	Set Simplec scheme, and 2nd order discretization
9	Initialize Solution	From the inlet
10	Enable the ploting of residuals	Check convergence
11	Specify Reference Values	Average from the inlet
12	Iterate	Number of Iterations

5. RESULTS

5.1 Organization of the results.

There are many results in this project as we ran several cases through Fluent. For both, the structured and unstructured meshes, we ran the cases 12 times so overall, we ran 24 cases. For each pressure ratio (1.03, 1.2, and 1.5) we ran four different cases, one for each angle of attack (0, 28, 39, and 46) and we did it twice as we are studying two different types of grid.

In this chapter, we distribute the results by showing for each different contour plot or vector plot the results according to the different pressure ratios. For each pressure ratio, the four results from the four different angles of attack and the two results from the two different types of grid are shown. For example,

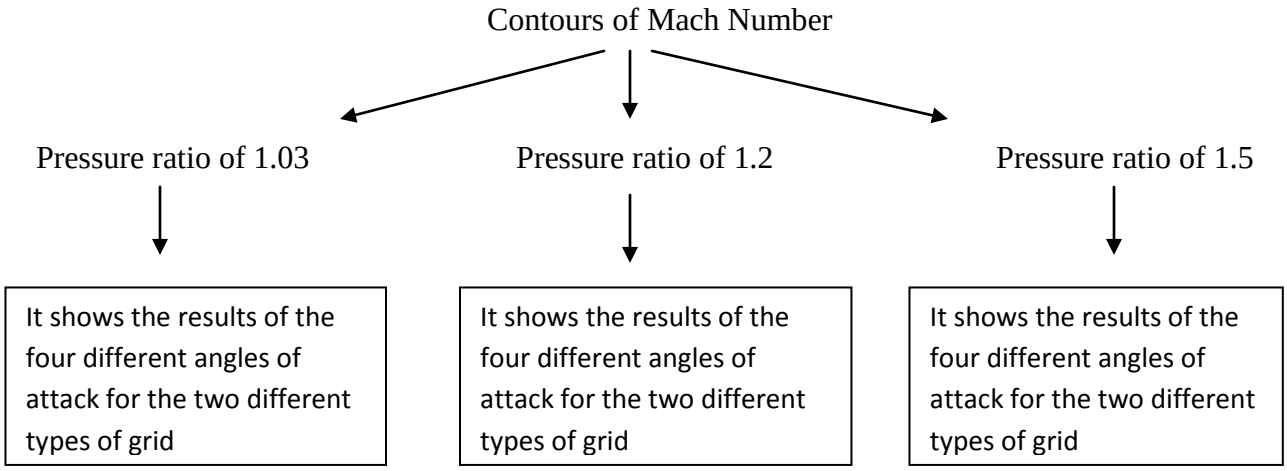

This project is always going to show the results of the structured mesh first, as this type of mesh is more appropriate for this study, and then it shows the results of the unstructured mesh.

The case run for the pressure ratio of 1.5 at the angle of attack of 46 degrees turned out to be a transient problem, so for this pressure ratio and angle of attack, we don't show any results.

The units are Pascal for the pressure, and m/s for the velocity magnitude.

5.2 Contours of velocity magnitude.

5.2.1 Pressure ratio of 1.03.

Structured mesh

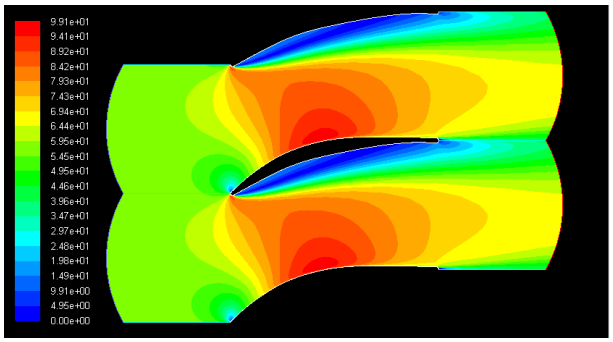

Angle of attack = 0

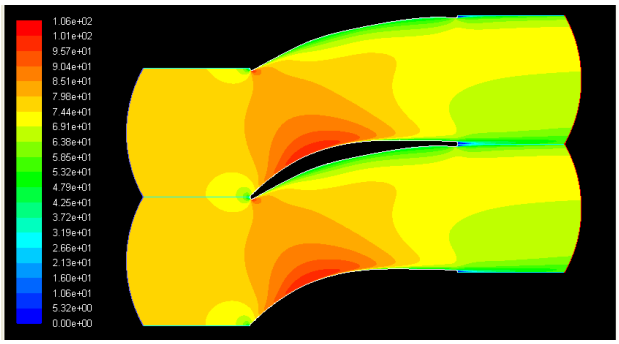

Angle of attack = 28

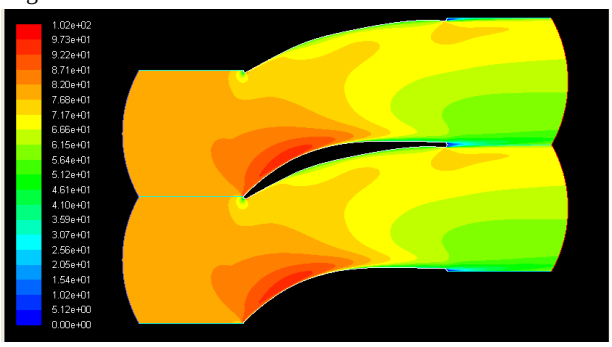

Angle of attack = 39

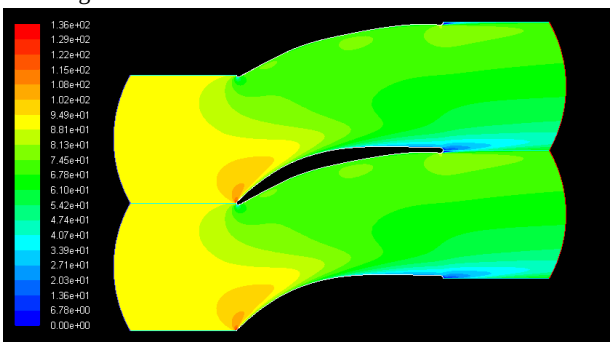

Angle of attack = 46

Unstructured mesh

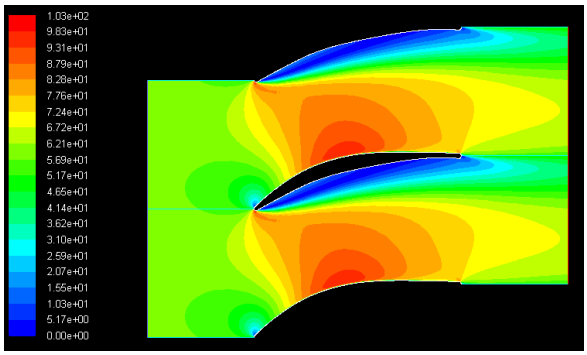

Angle of attack = 0

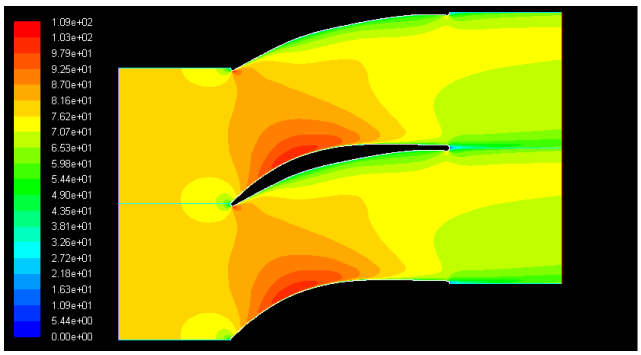

Angle of attack = 28

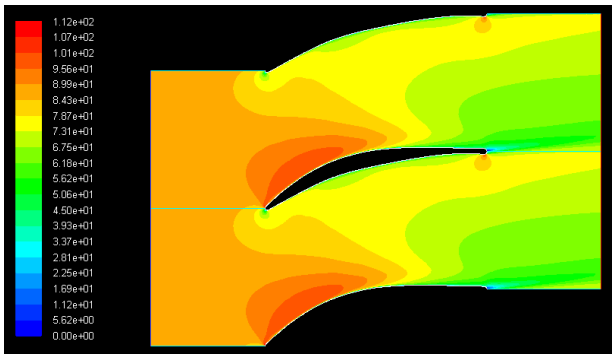

Angle of attack = 39

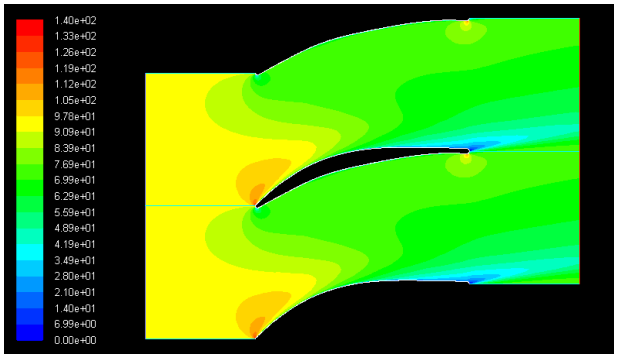

Angle of attack = 46

5.2.2 Pressure ratio of 1.2

Structured mesh

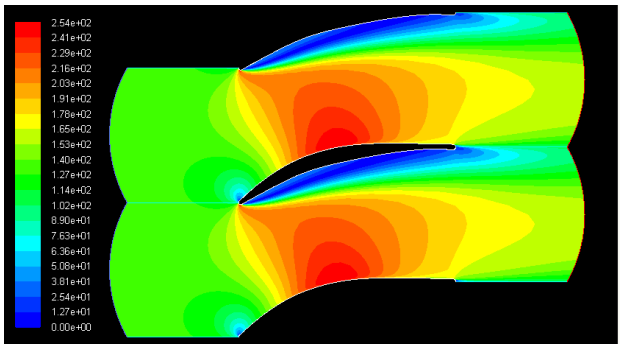

Angle of attack = 0

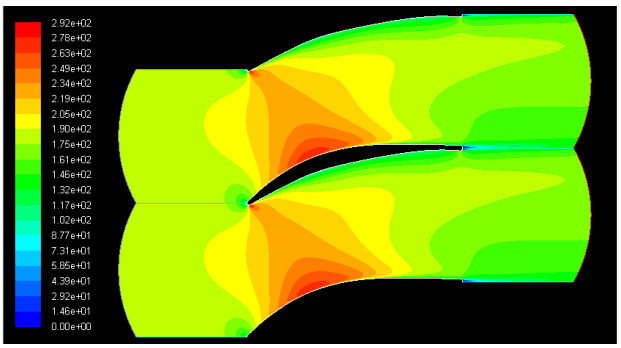

Angle of attack = 28

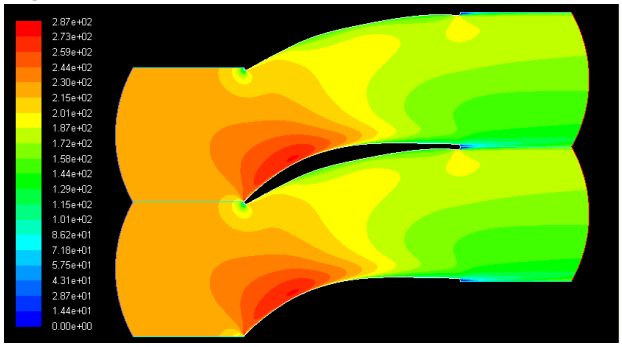

Angle of attack = 39

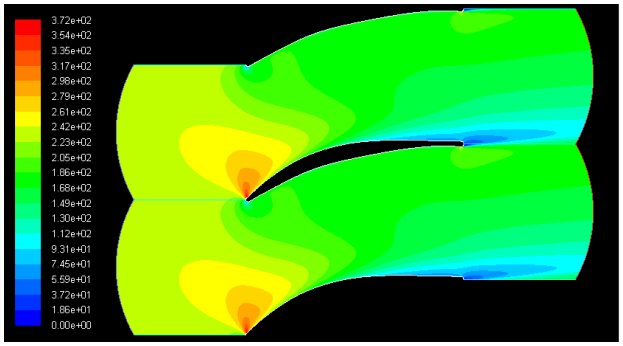

Angle of attack = 46

Unstructured mesh

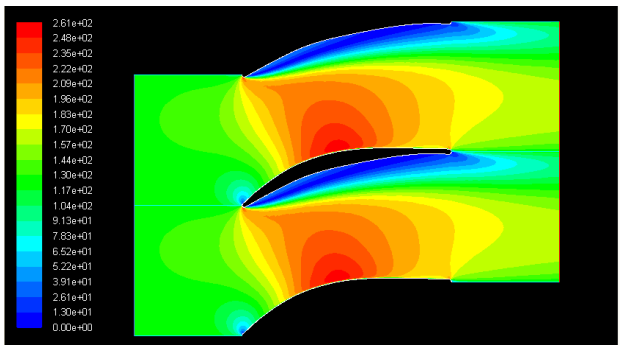

Angle of attack = 0

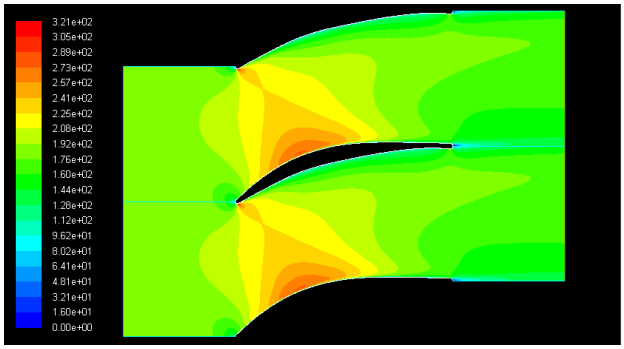

Angle of attack = 28

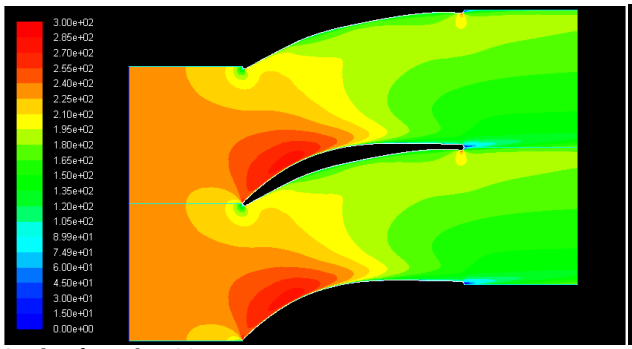

Angle of attack = 39

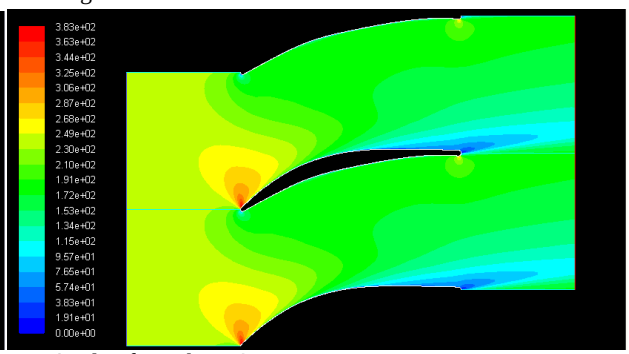

Angle of attack = 46

5.2.3 Pressure ratio of 1.5

Structured mesh

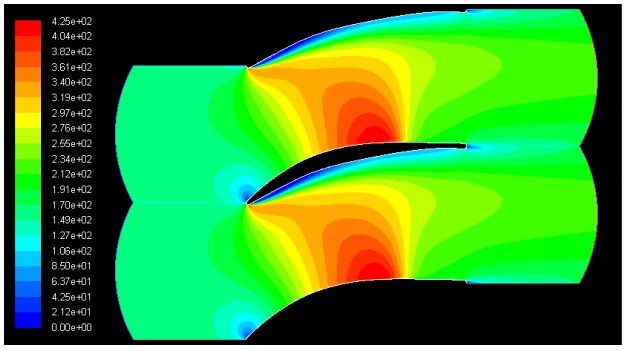

Angle of attack = 0

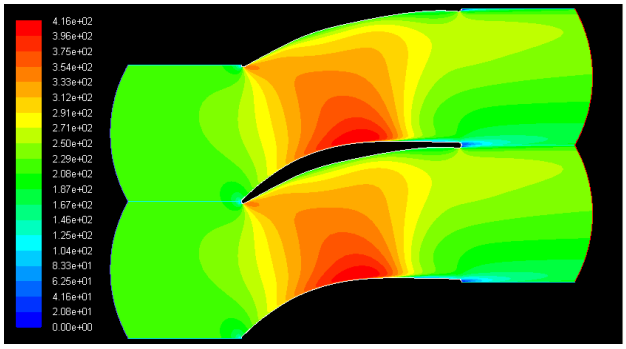

Angle of attack = 28

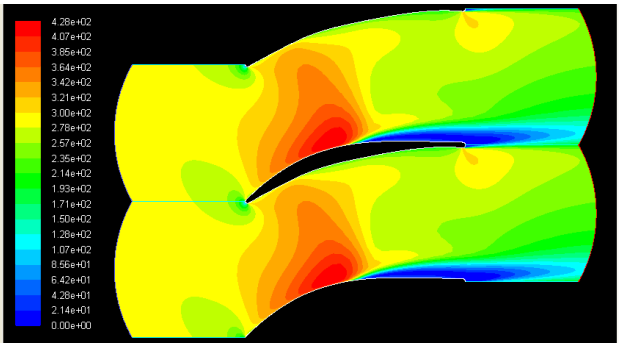

Angle of attack = 39

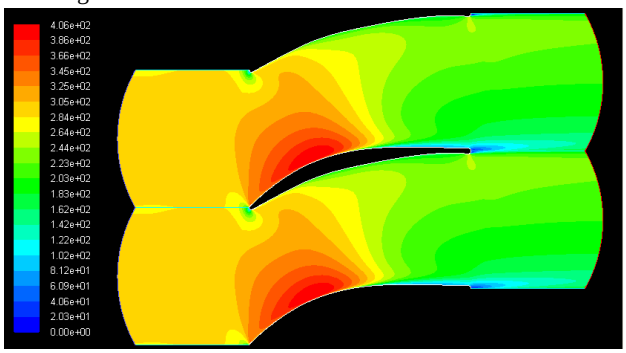

Angle of attack = 46

Unstructured mesh

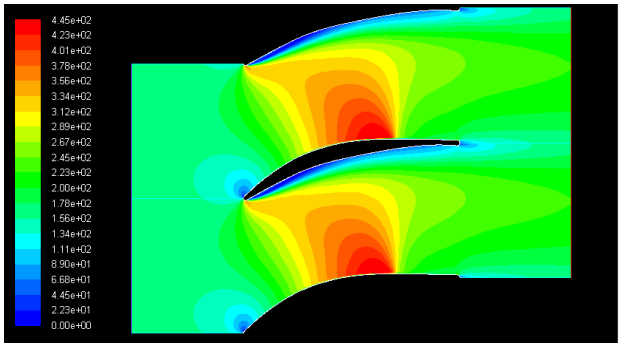

Angle of attack = 0

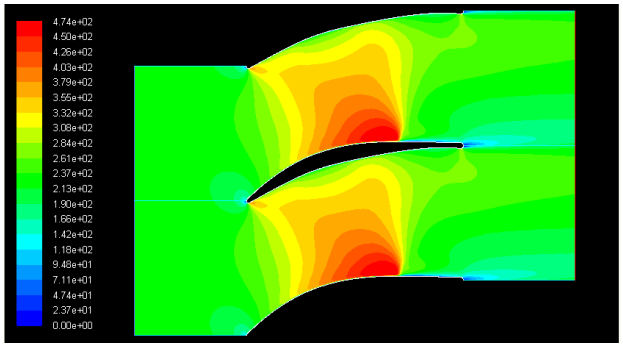

Angle of attack = 28

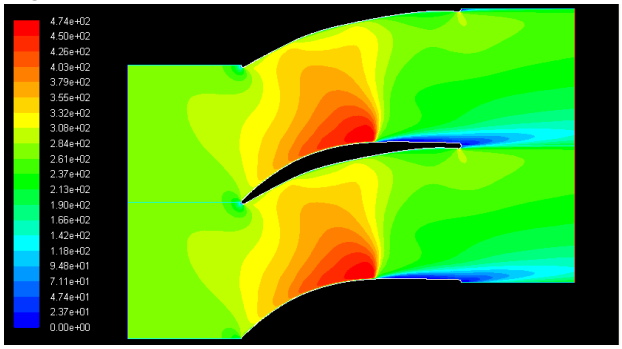

Angle of attack = 39

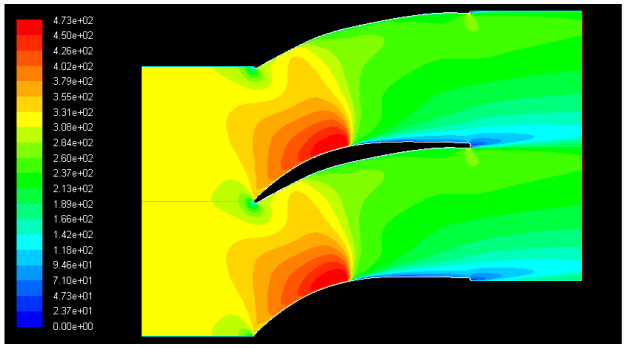

Angle of attack = 46

5.3 Contours of Mach number.

5.3.1 Pressure ratio of 1.03

Structured mesh

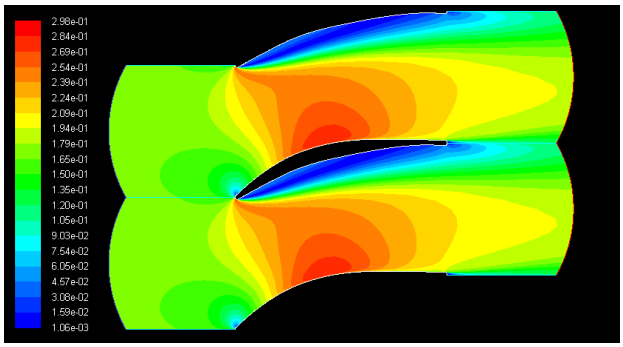

Angle of attack = 0

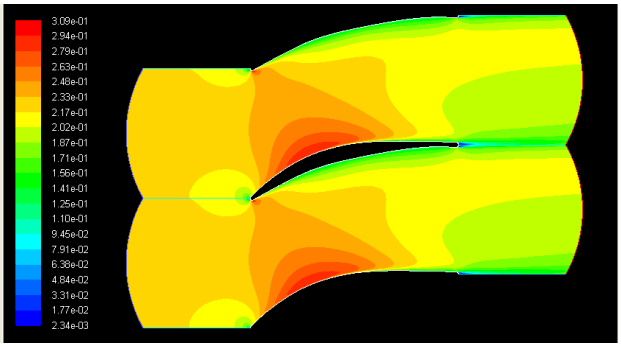

Angle of attack = 28

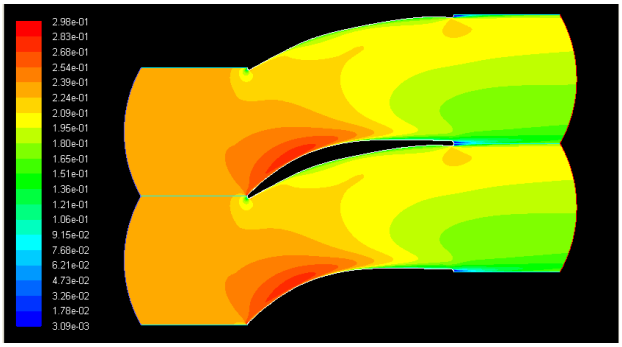

Angle of attack = 39

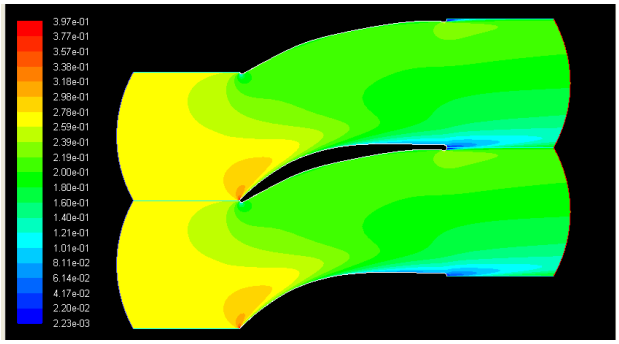

Angle of attack = 46

Unstructured mesh

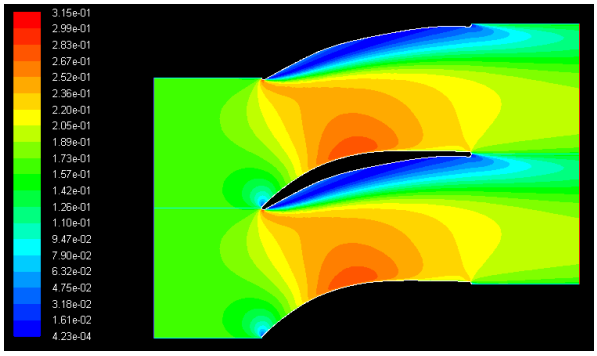

Angle of attack = 0

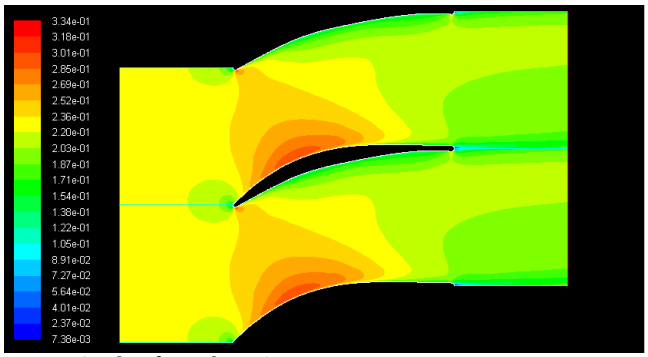

Angle of attack = 29

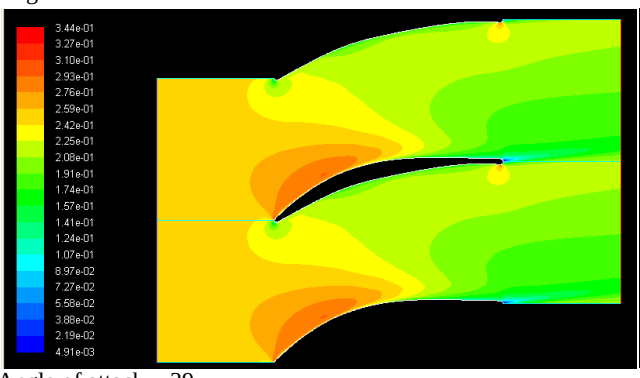

Angle of attack = 39

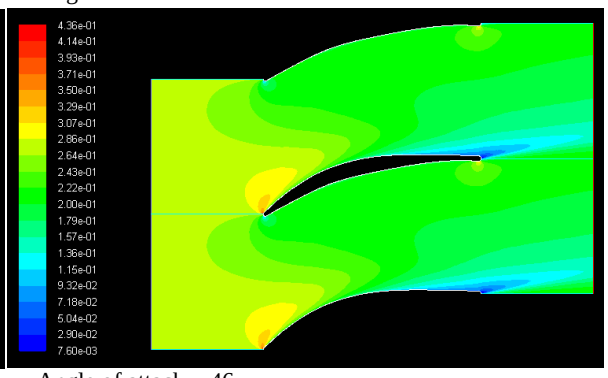

Angle of attack = 46

5.3.2 Pressure ratio of 1.2.

Structured mesh

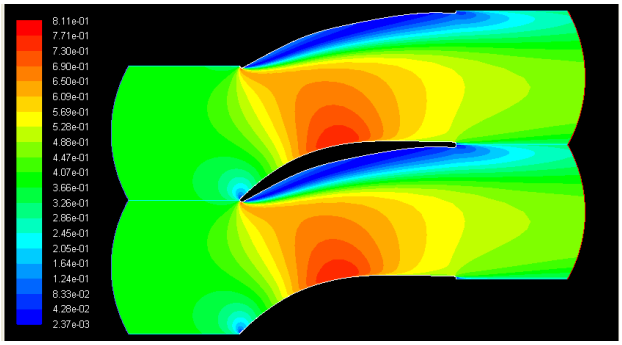

Angle of attack = 0

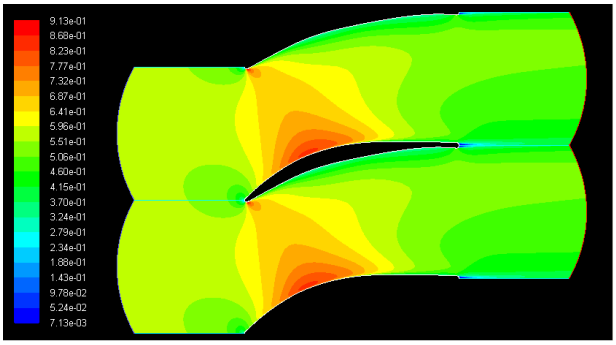

Angle of attack = 28

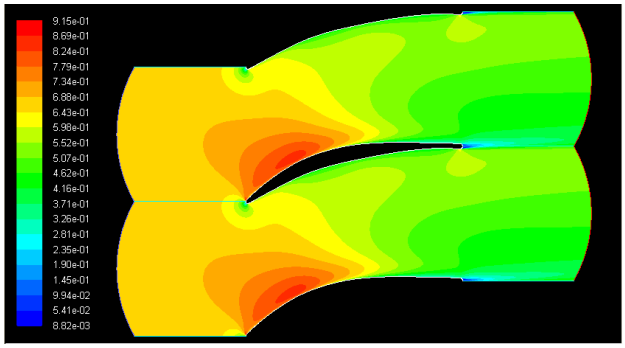

Angle of attack = 39

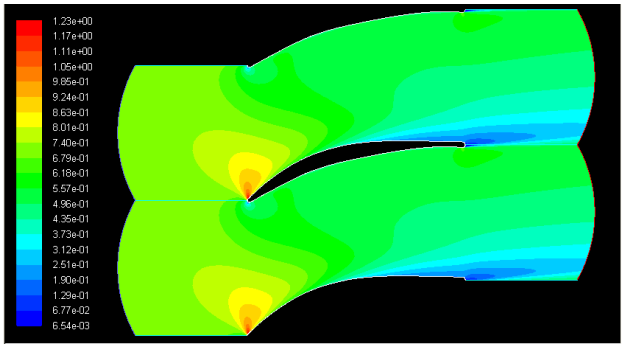

Angle of attack = 46

Unstructured mesh

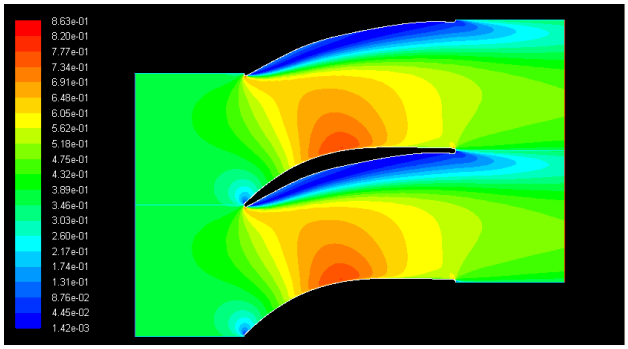

Angle of attack = 0

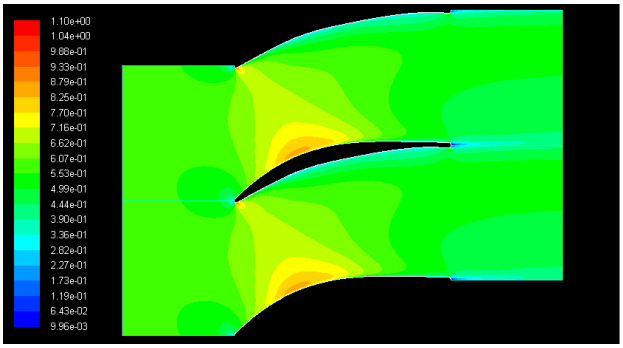

Angle of attack = 28

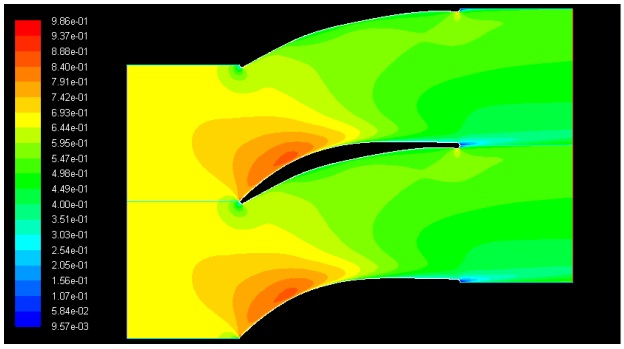

Angle of attack = 39

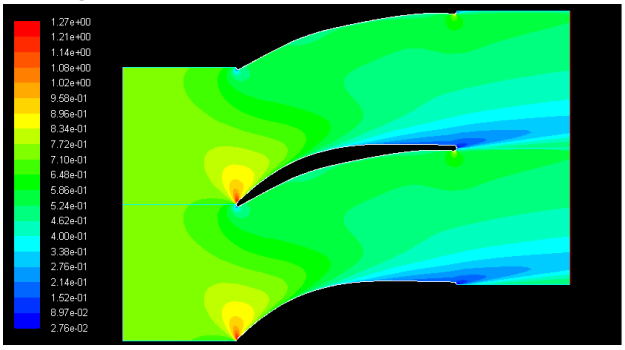

Angle of attack = 46

5.3.3 Pressure ratio of 1.5

Structured mesh

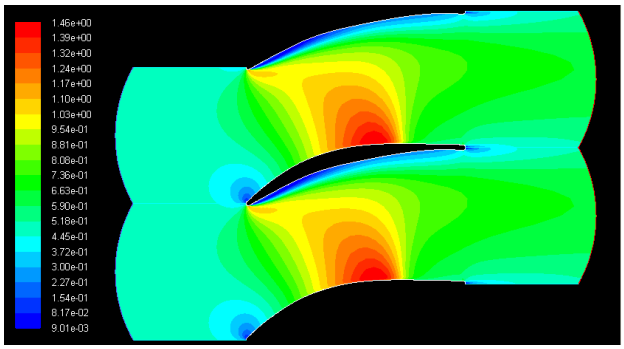

Angle of attack = 0

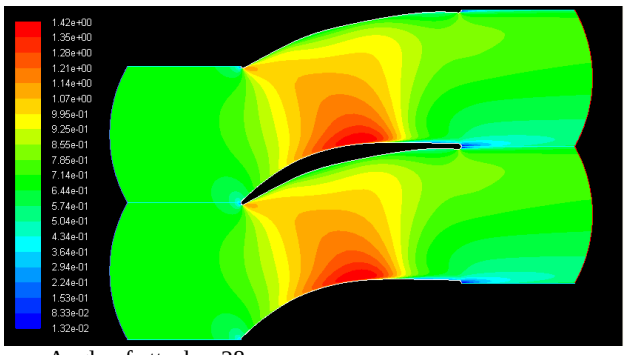

Angle of attack = 28

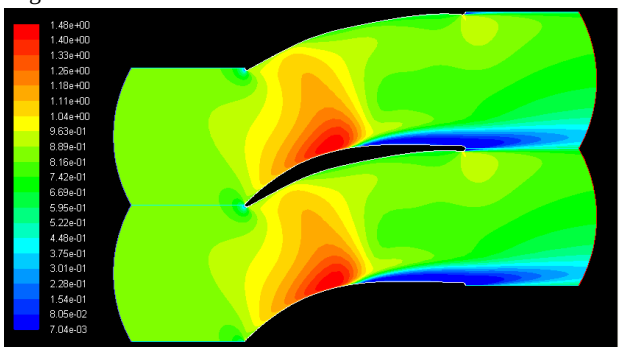

Angle of attack = 39

Unstructured mesh

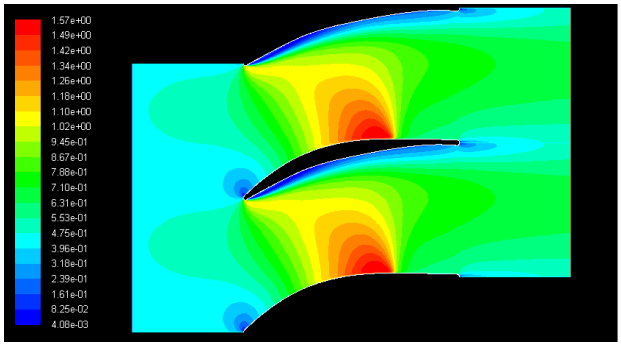

Angle of attack = 0

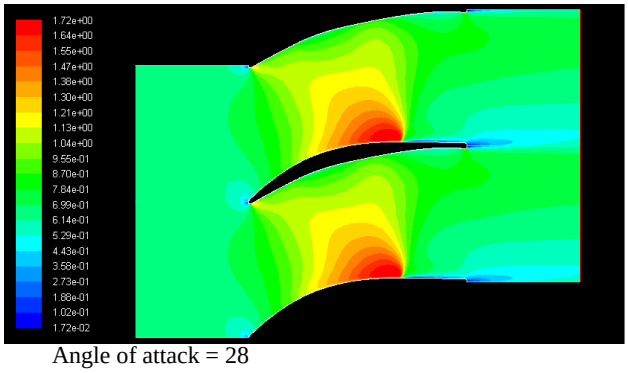

Angle of attack = 28

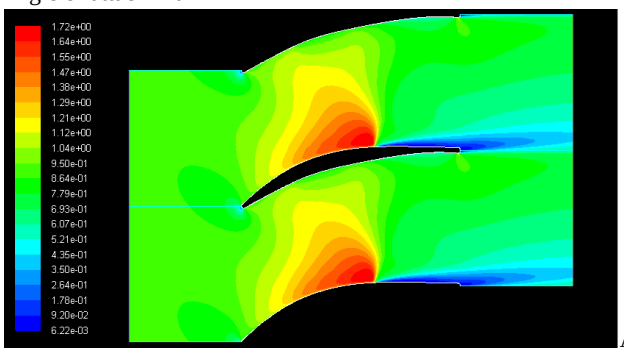

Angle of attack = 39

5.4 Vectors of velocity magnitude.

5.4.1 Pressure ratio of 1.03

Structured mesh

- Leading edge

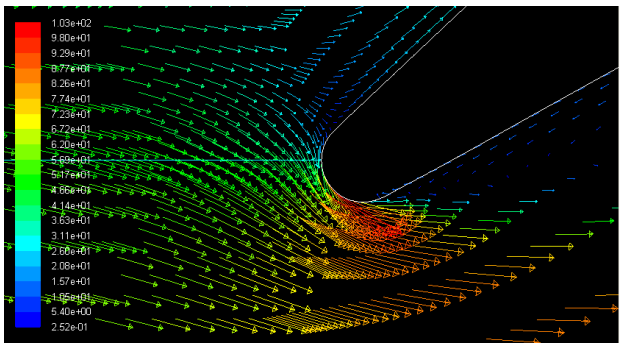

Angle of attack = 0

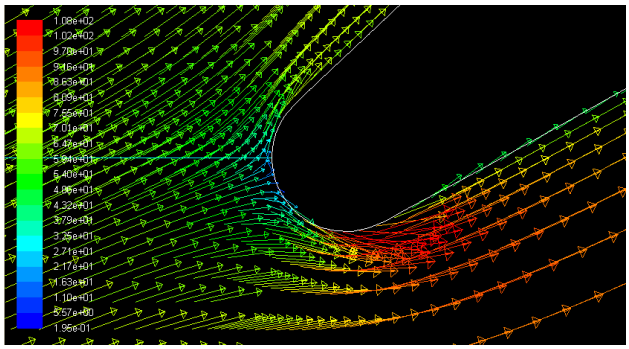

Angle of attack = 28

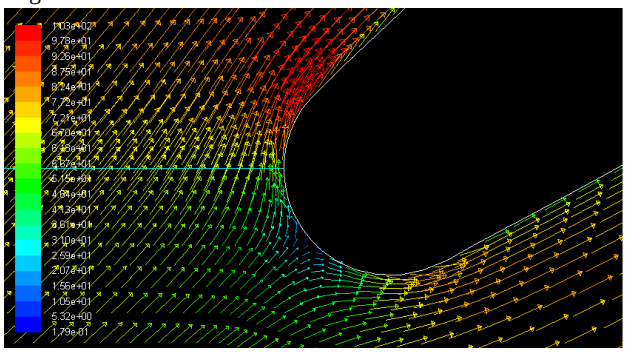

Angle of attack = 39

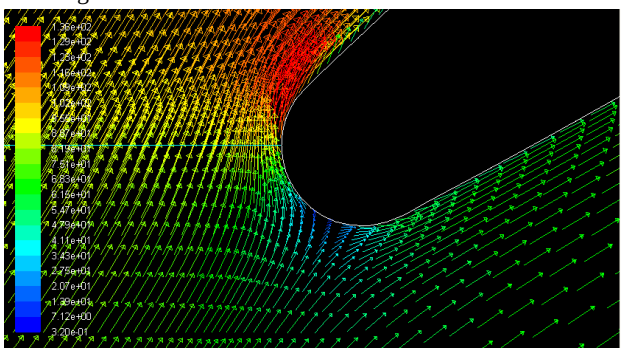

Angle of attack = 46

- Trailing edge

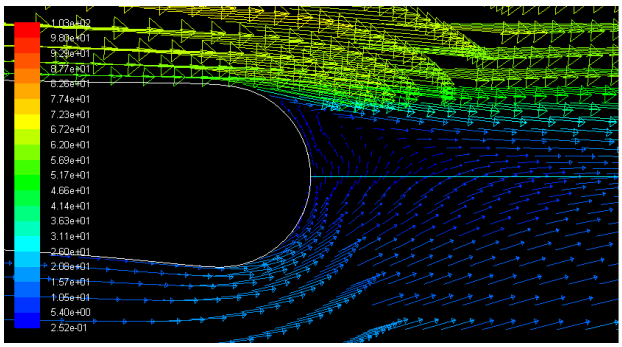

Angle of attack = 0

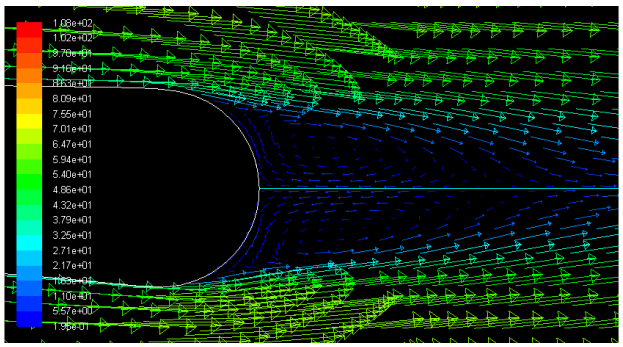

Angle of attack = 28

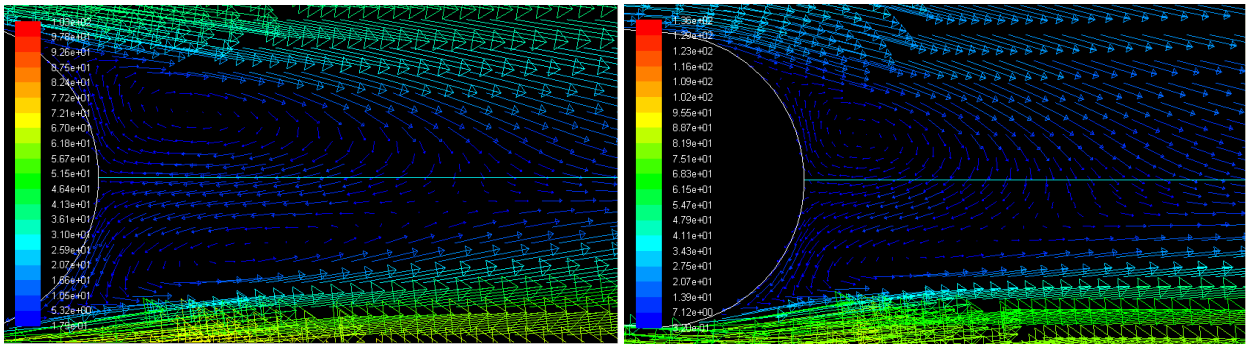

Angle of attack = 39 Angle of attack = 46

Unstructured mesh

- Leading edge

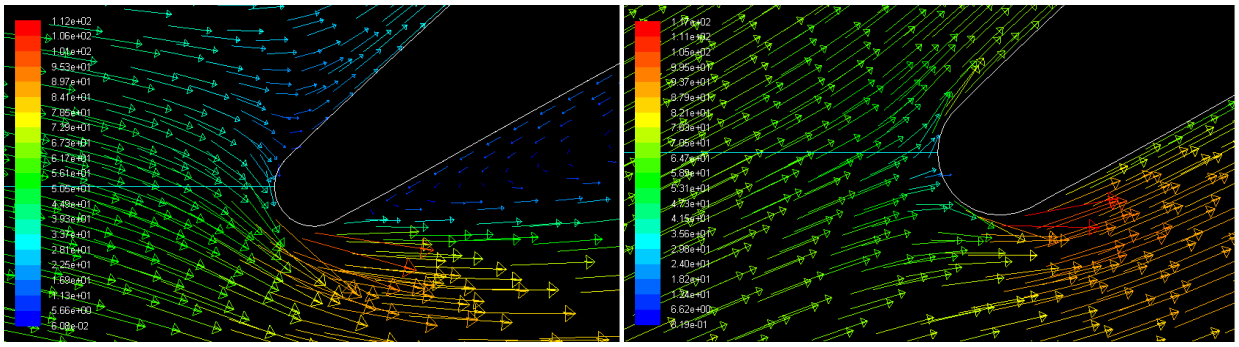

Angle of attack = 0 Angle of attack = 28

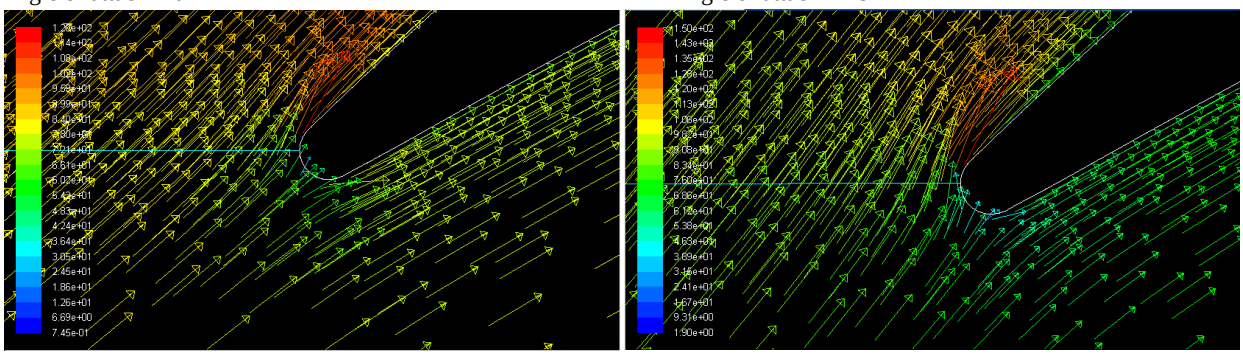

Angle of attack = 39 Angle of attack = 46

- Trailing edge

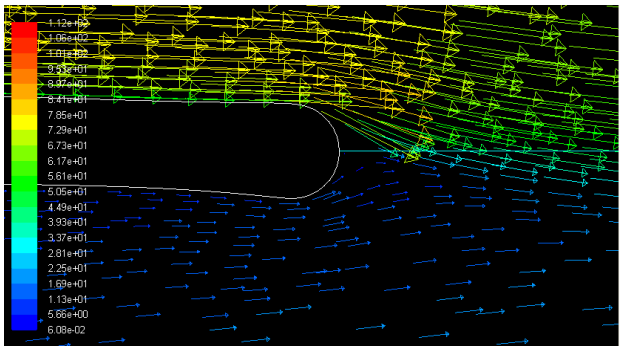

Angle of attack = 0

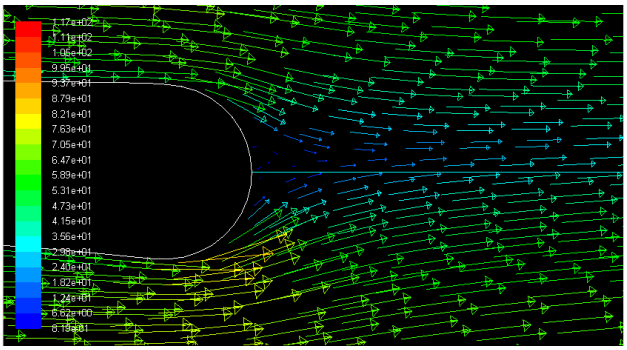

Angle of attack = 28

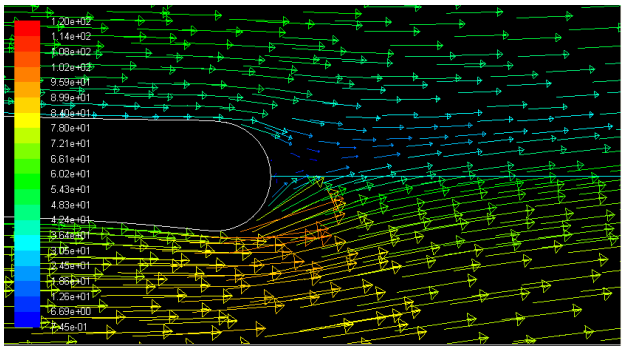

Angle of attack = 39

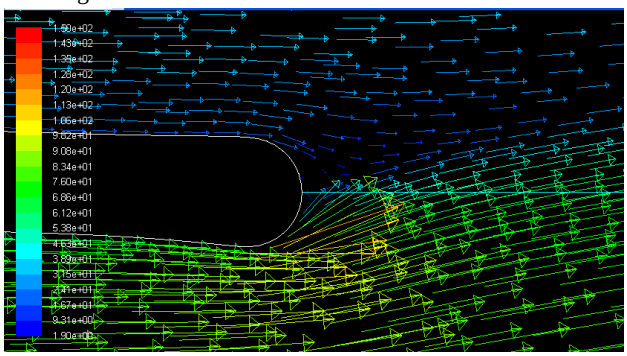

Angle of attack = 46

5.4.2 Pressure ratio of 1.2.

<u>Structured mesh</u>

- Leading edge

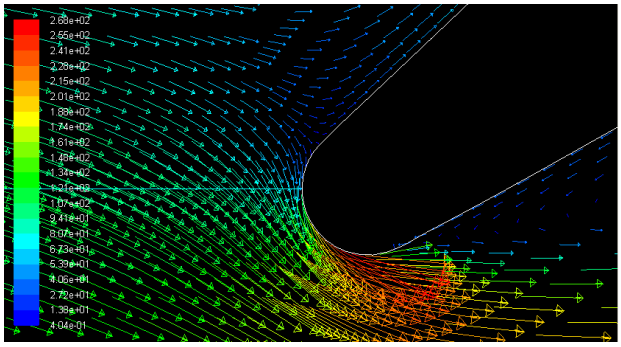

Angle of attack = 0

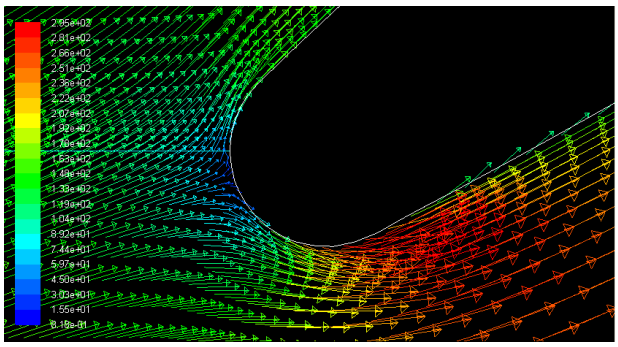

Angle of attack = 28

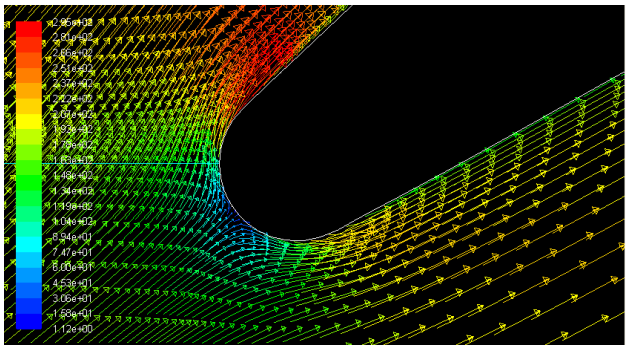
Angle of attack = 39

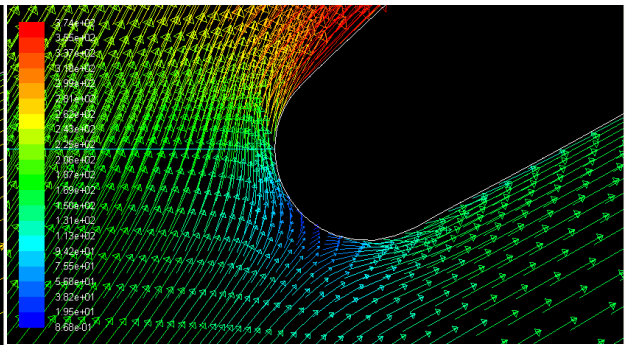
Angle of attack = 46

- Trailing edge

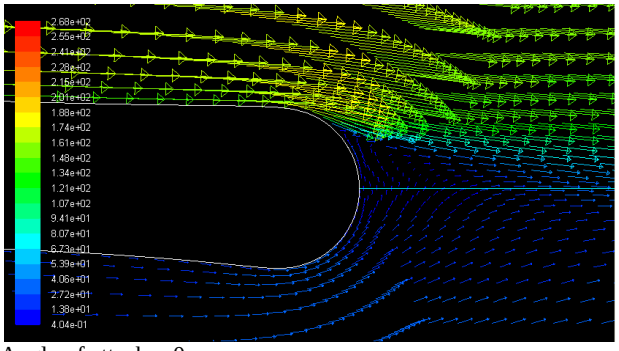
Angle of attack = 0

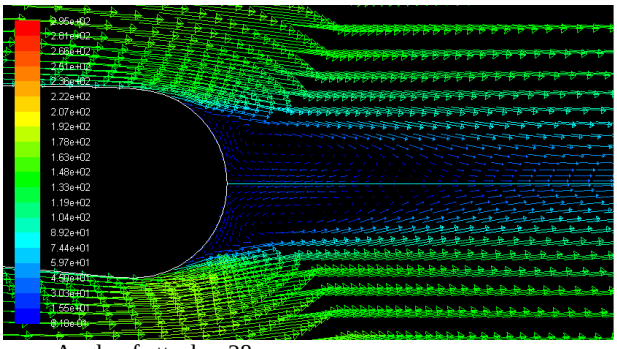
Angle of attack = 28

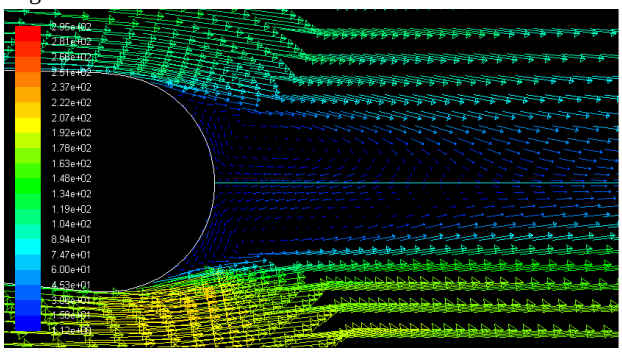
Angle of attack = 39

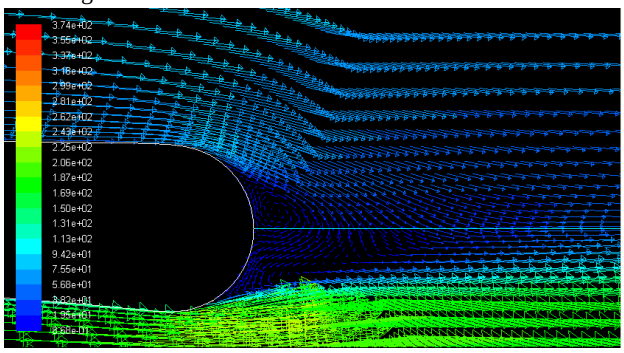
Angle of attack = 46

Unstructured mesh

- Leading edge

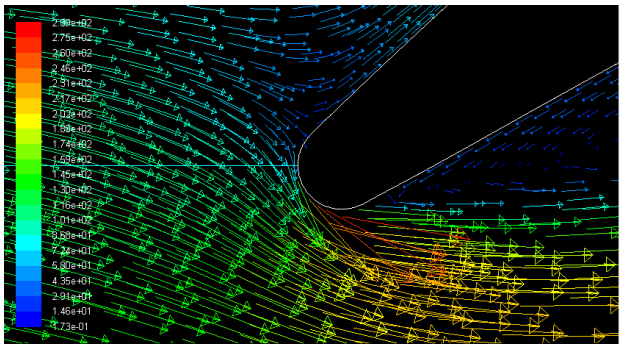

Angle of attack = 0

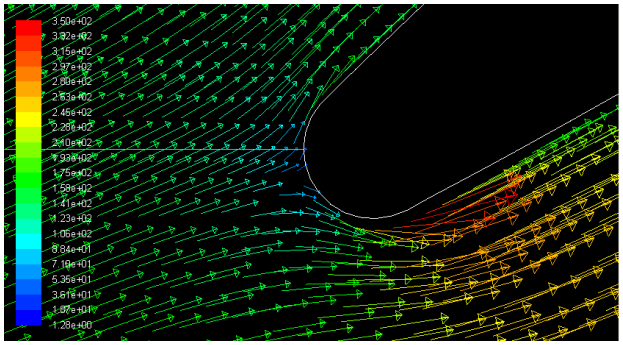

Angle of attack = 28

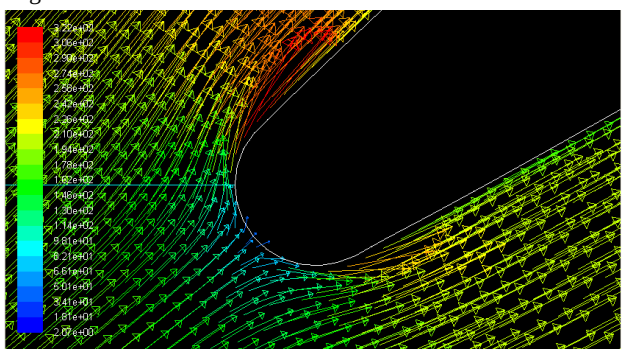

Angle of attack = 39

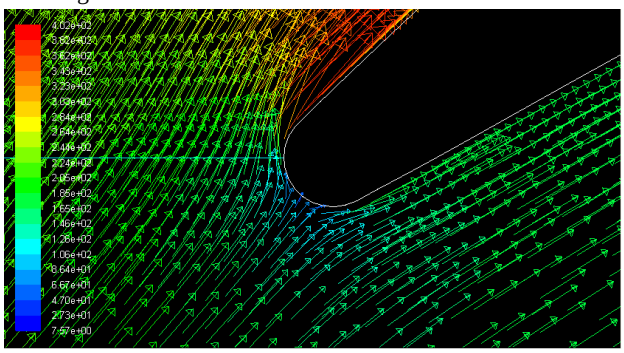

Angle of attack = 46

- Trailing edge

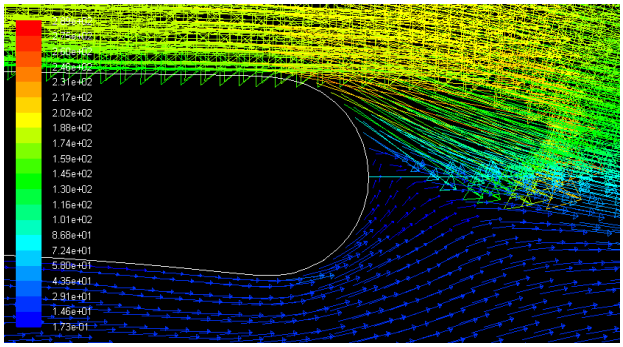

Angle of attack = 0

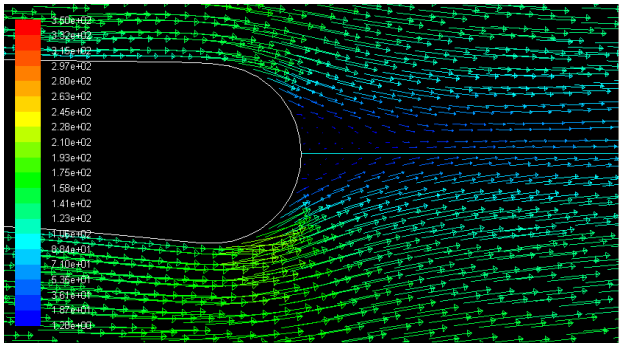

Angle of attack = 28

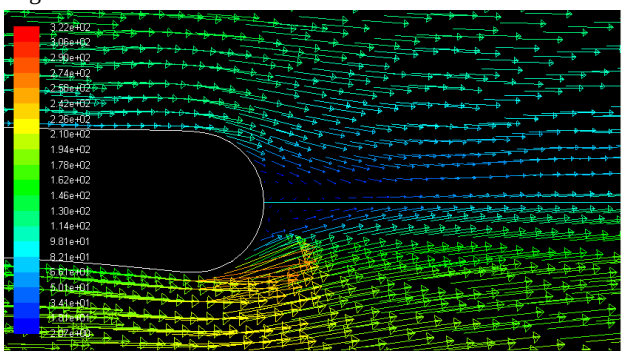

Angle of attack = 39

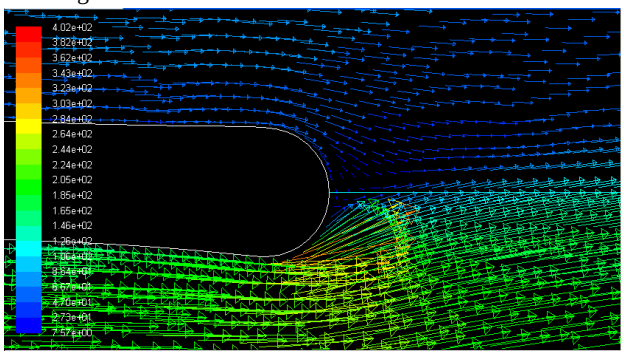

Angle of attack = 46

5.4.3 Pressure ratio of 1.5.

Structured mesh

- Leading edge

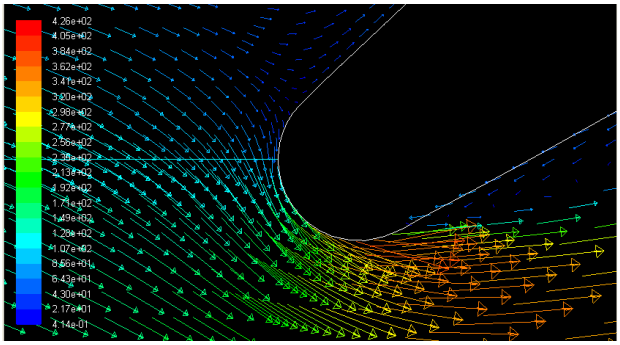

Angle of attack = 0

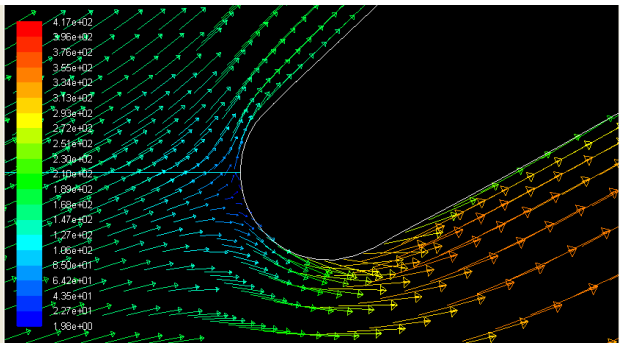

Angle of attack = 28

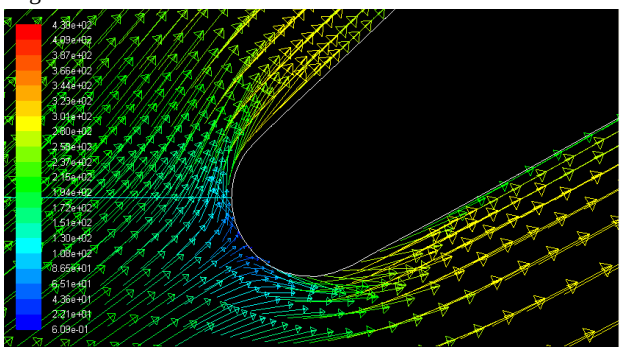

Angle of attack = 39

- Trailing edge

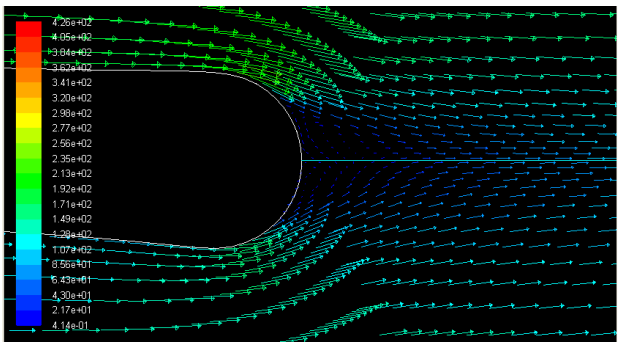

Angle of attack = 0

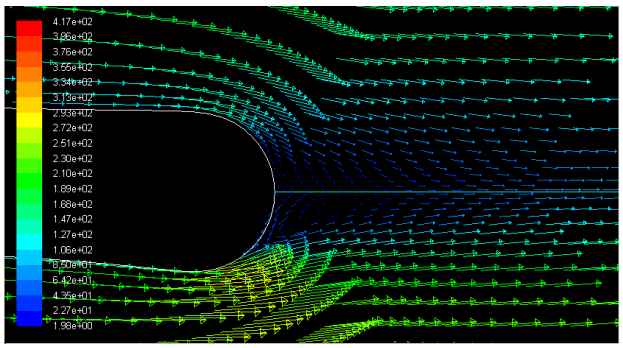

Angle of attack = 28

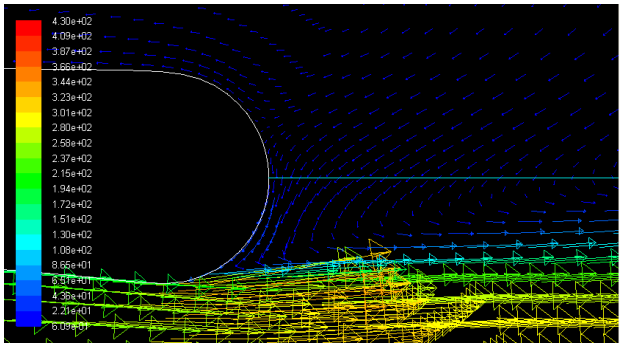

Angle of attack = 39

Unstructured mesh

- Leading edge

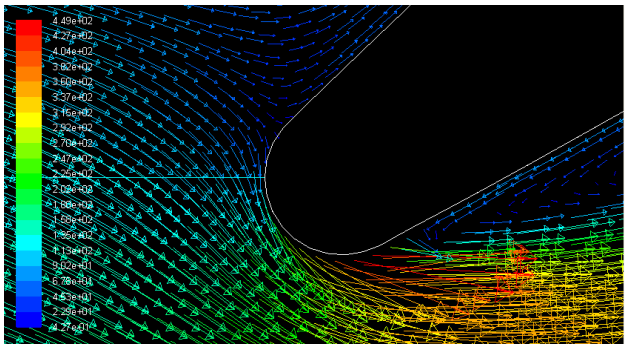

Angle of attack = 0

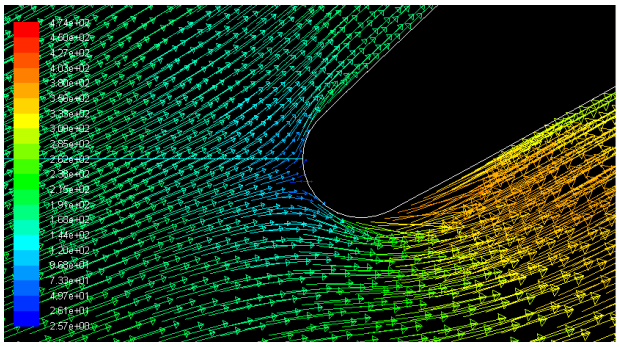

Angle of attack = 28

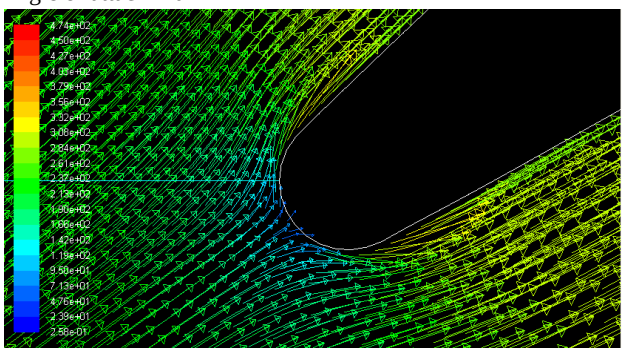

Angle of attack = 39

- Trailing edge

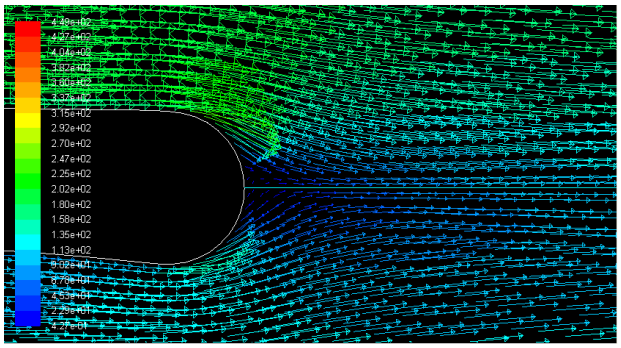

Angle of attack = 0

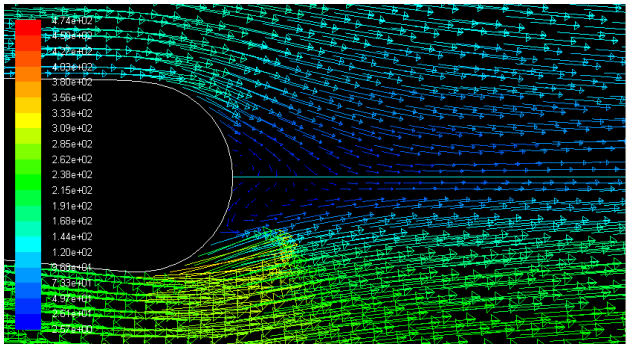

Angle of attack = 28

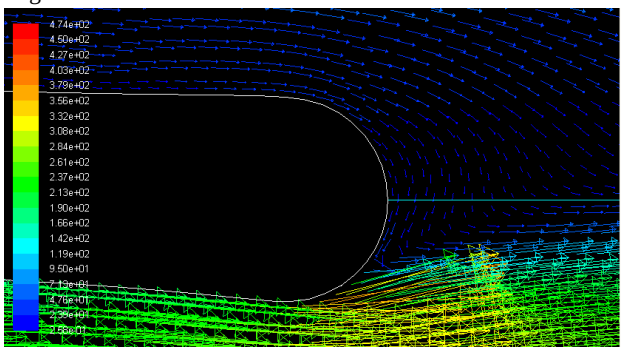

Angle of attack = 39

5.5 Contours of static pressure

5.5.1 Pressure ratio of 1.03

Structured mesh

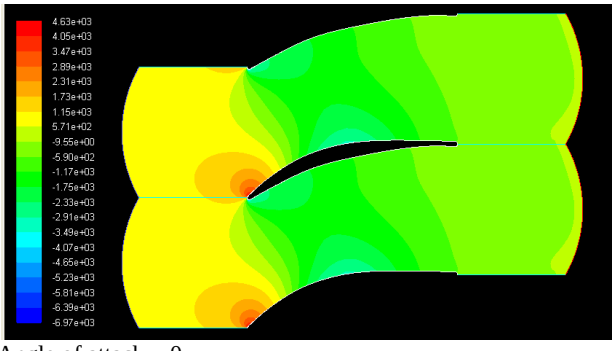

Angle of attack = 0

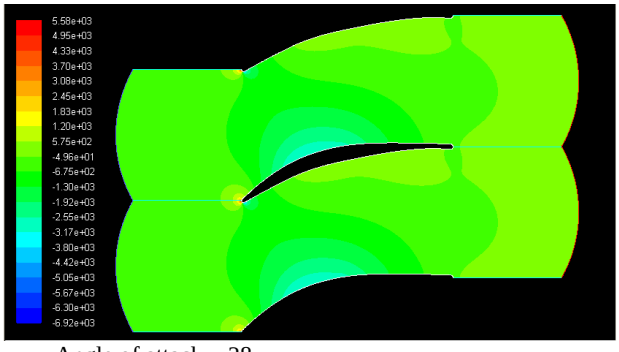

Angle of attack = 28

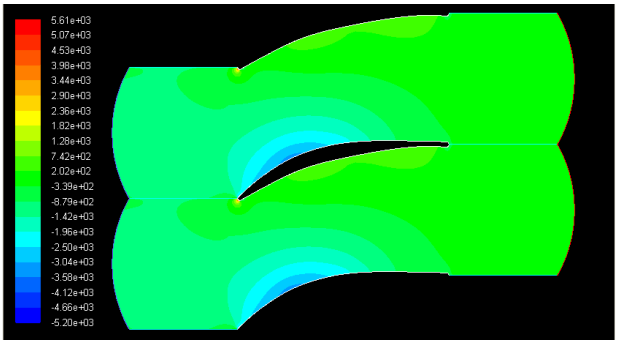

Angle of attack = 39

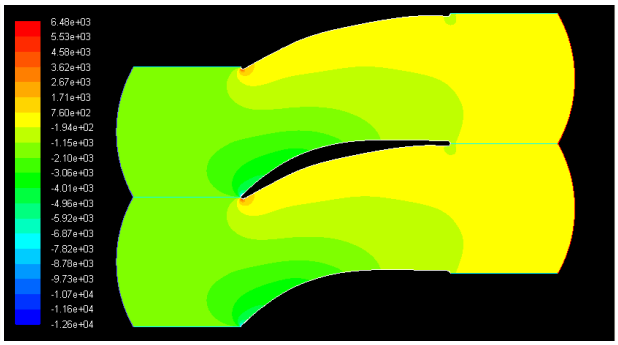

Angle of attack = 46

Unstructured mesh

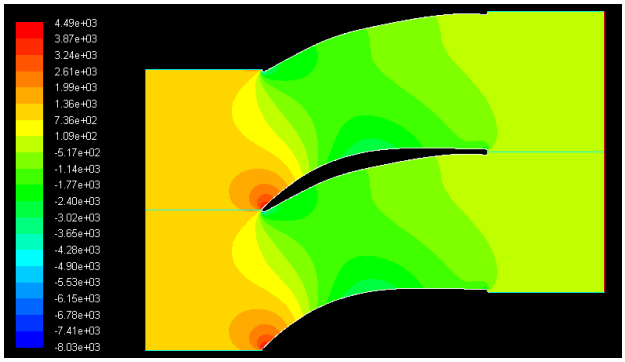

Angle of attack = 0

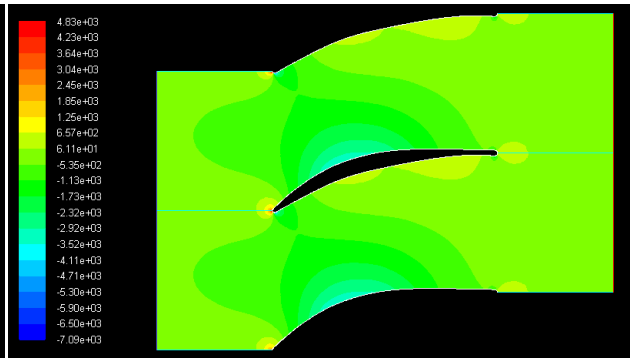

Angle of attack = 28

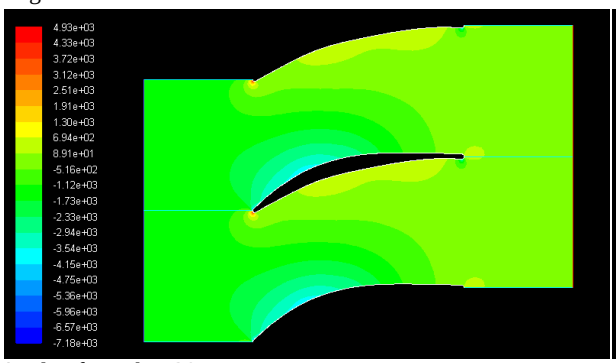

Angle of attack = 39

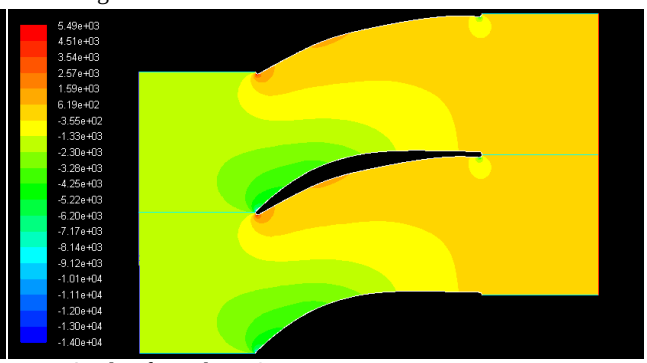

Angle of attack = 46

5.5.2 Pressure ratio of 1.2.

Structured mesh

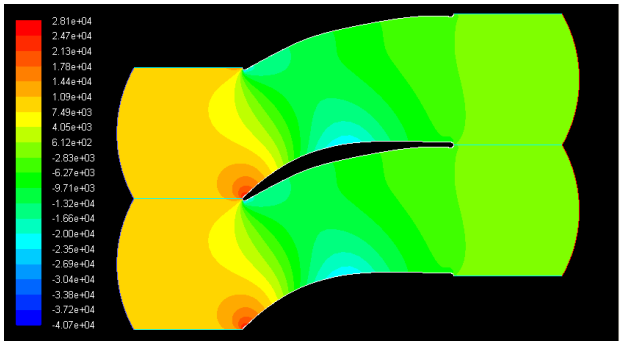

Angle of attack = 0

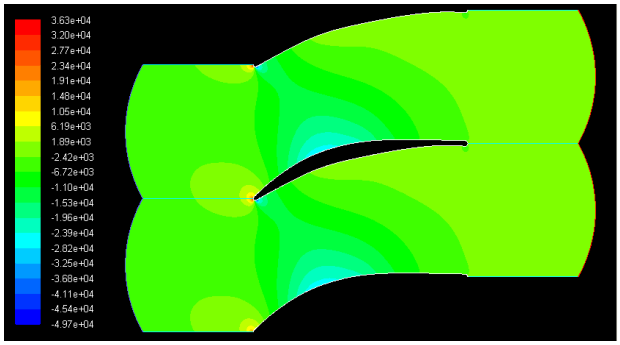

Angle of attack = 28

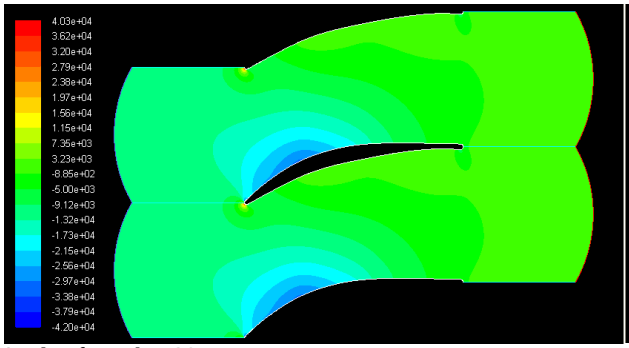

Angle of attack = 39

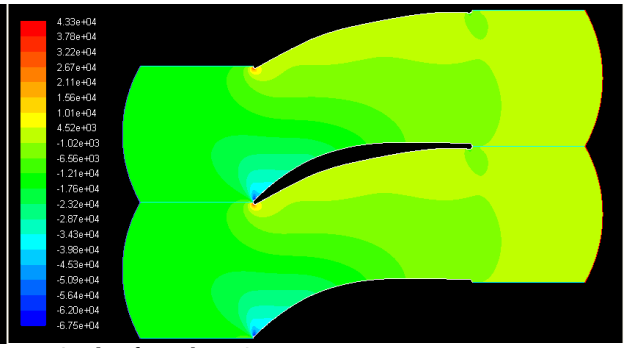

Angle of attack = 46

Unstructured mesh

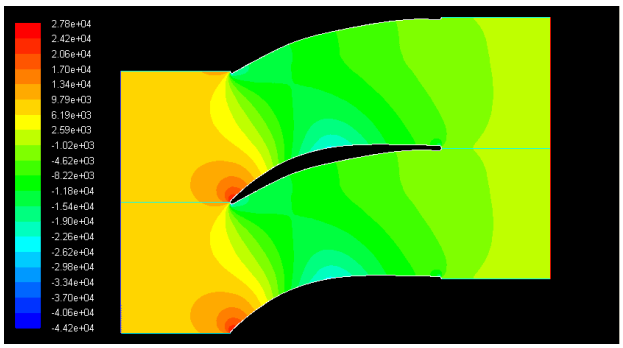

Angle of attack = 0

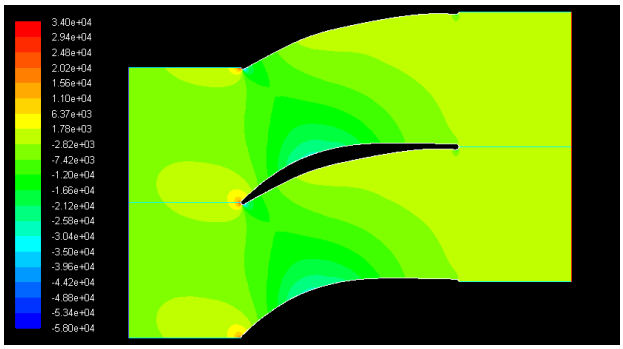

Angle of attack 0 28

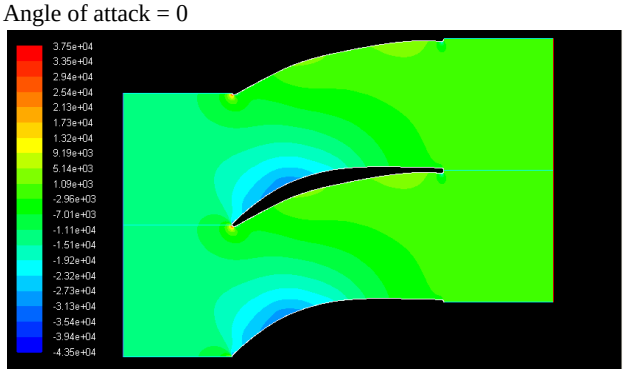

Angle of attack = 39

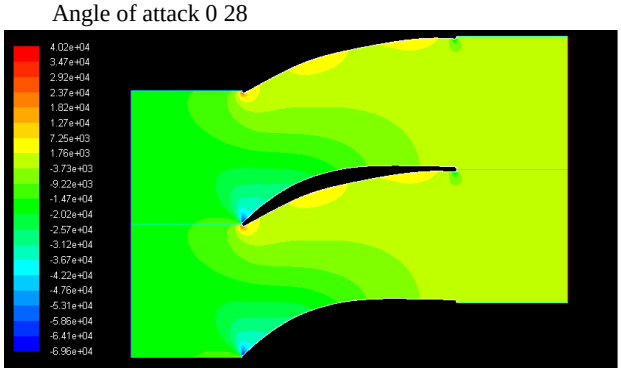

Angle of attack = 46

5.5.3 Pressure ratio of 1.5

Structured mesh

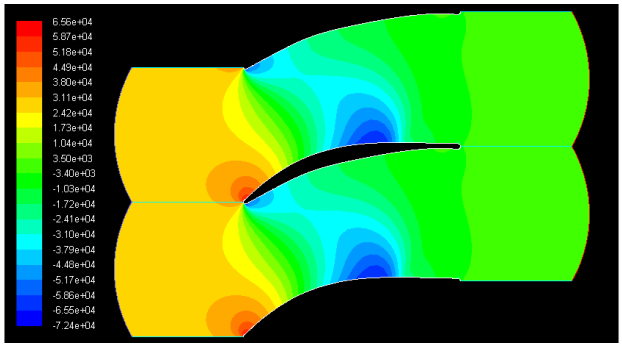

Angle of attack = 0

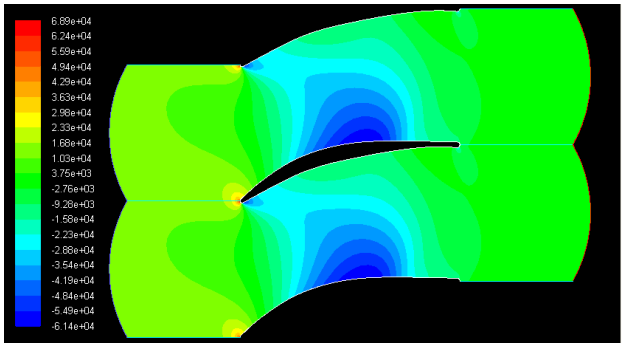

Angle of attack = 28

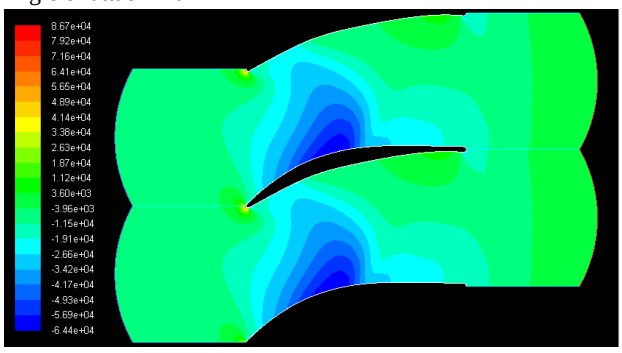

Angle of attack = 39

Unstructured mesh

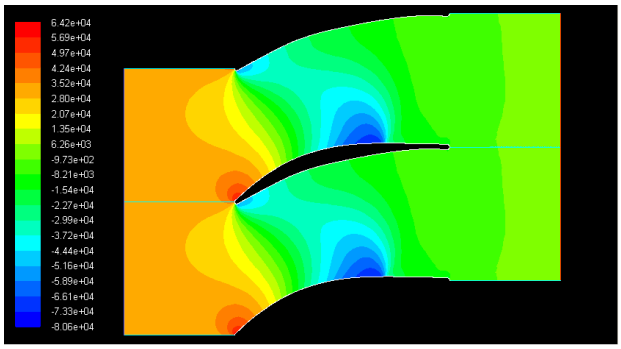

Angle of attack = 0

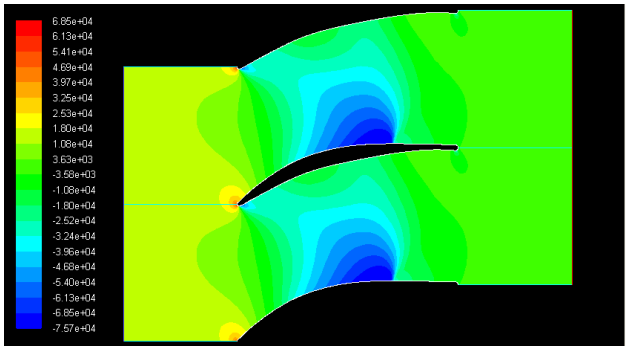

Angle of attack = 28

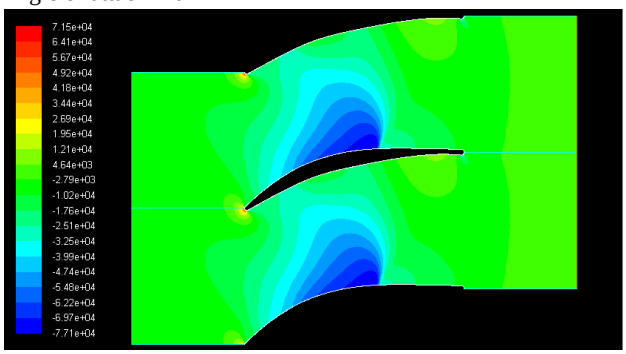

Angle of attack = 39

5.6 Contours of dynamic pressure.

5.6.1 Pressure ratio of 1.03

Structured mesh

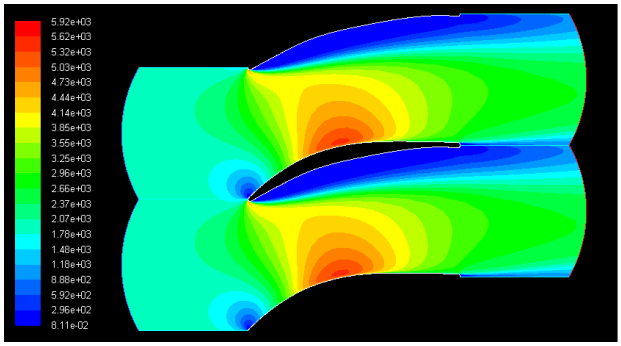

Angle of attack = 0

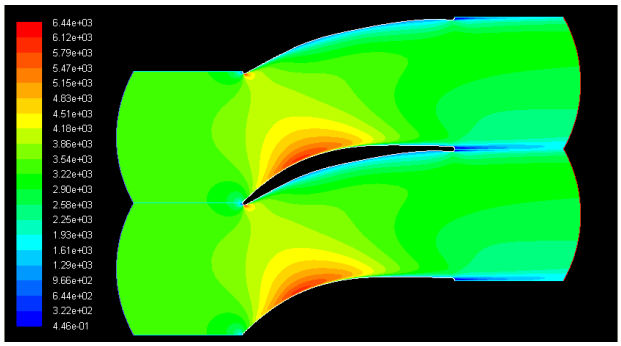

Angle of attack = 28

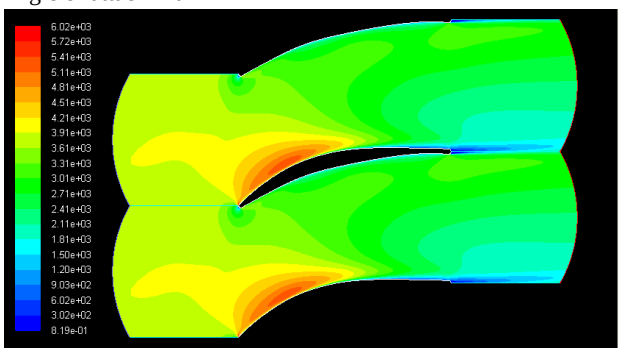

Angle of attack = 39

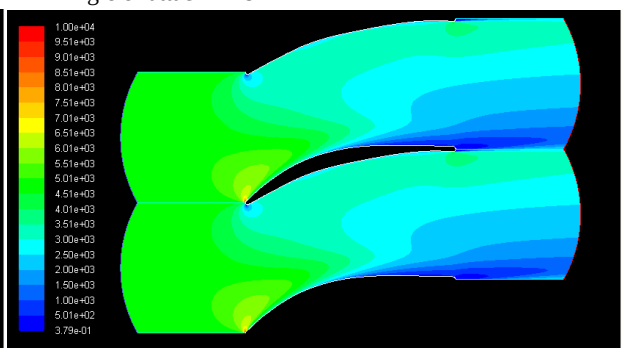

Angle of attack = 46

Unstructured mesh

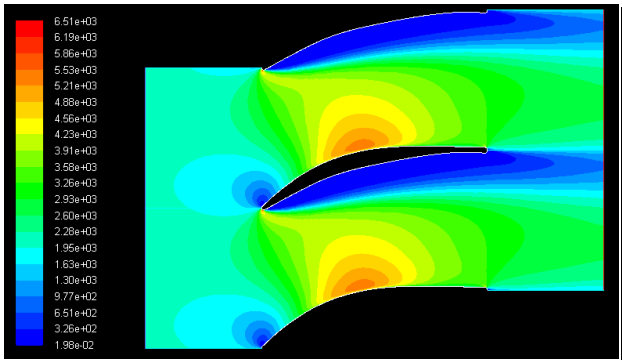

Angle of attack = 0

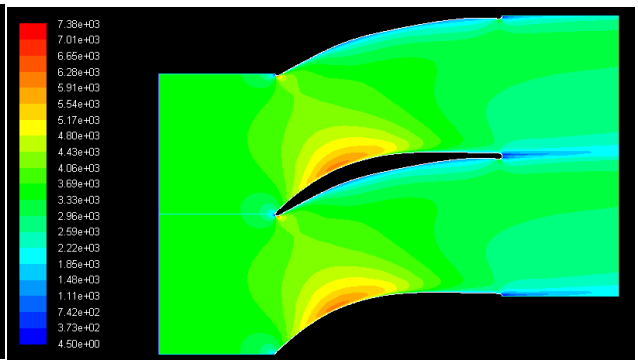

Angle of attack = 28

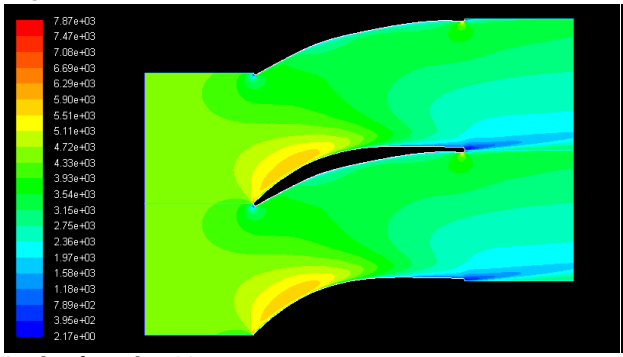

Angle of attack = 39

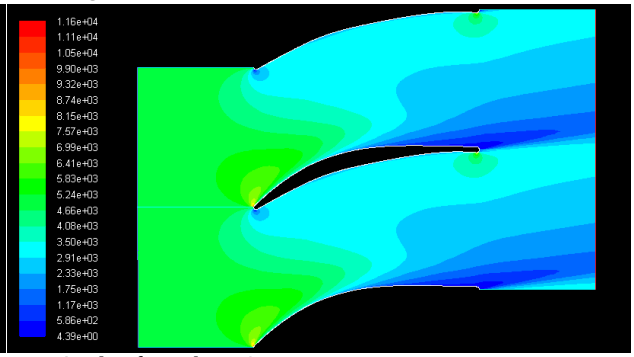

Angle of attack = 46

5.6.2 Pressure ratio of 1.2

Structured mesh

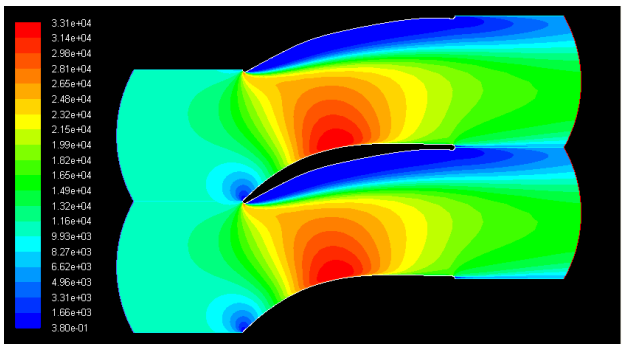

Angle of attack = 0

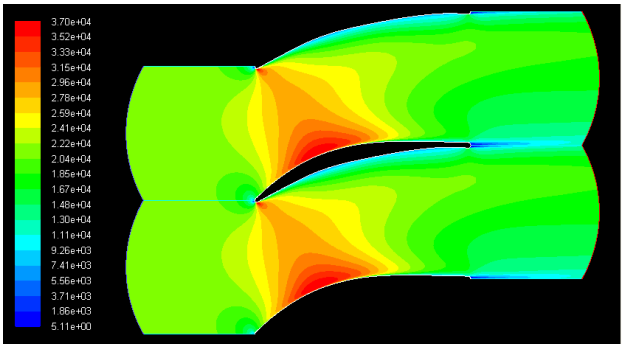

Angle of attack = 28

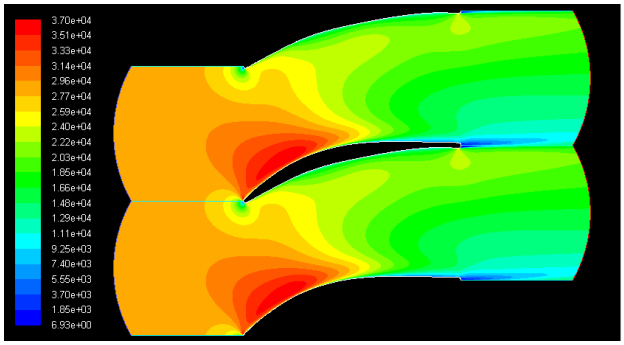

Angle of attack = 39

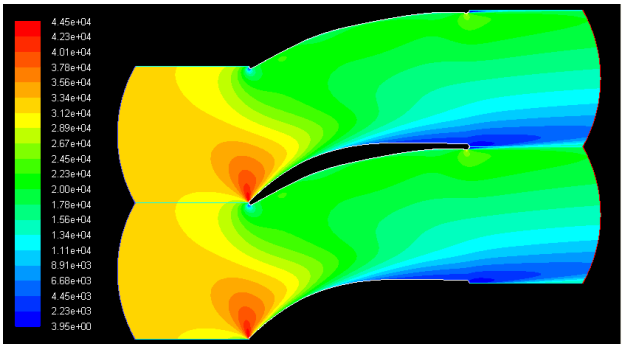

Angle of attack = 46

Unstructured mesh

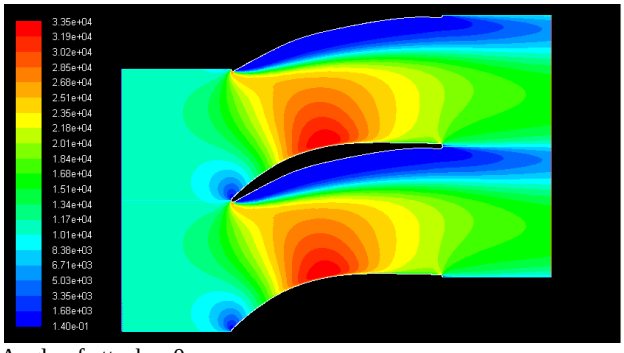

Angle of attack = 0

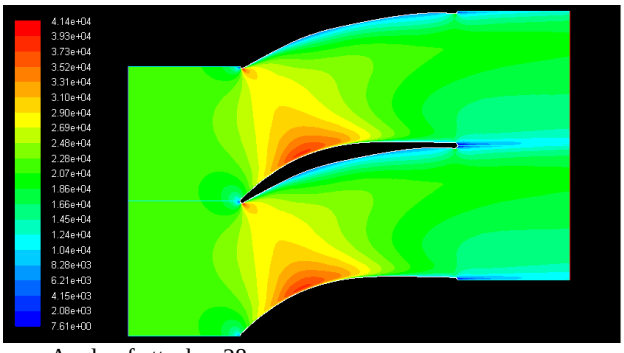

Angle of attack = 28

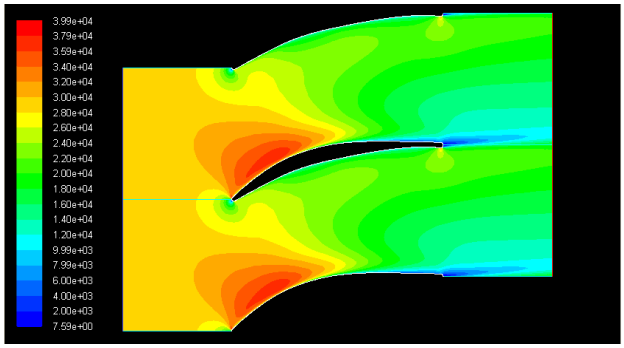

Angle of attack = 39

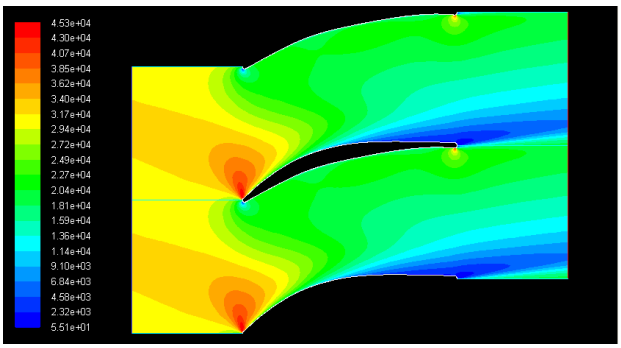

Angle of attack = 46

5.6.3 Pressure ratio of 1.5.

Structured mesh

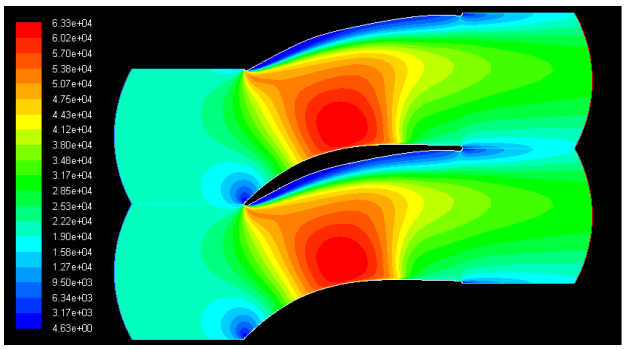

Angle of attack = 0

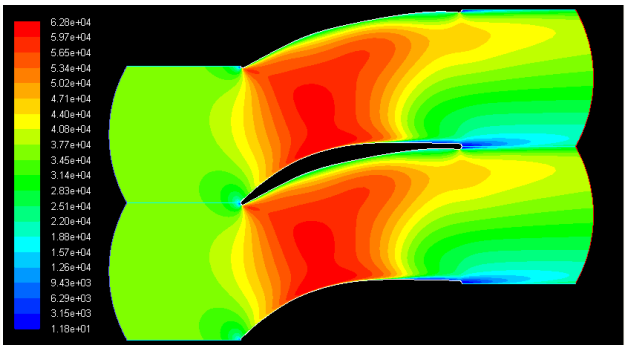

Angle of attack = 28

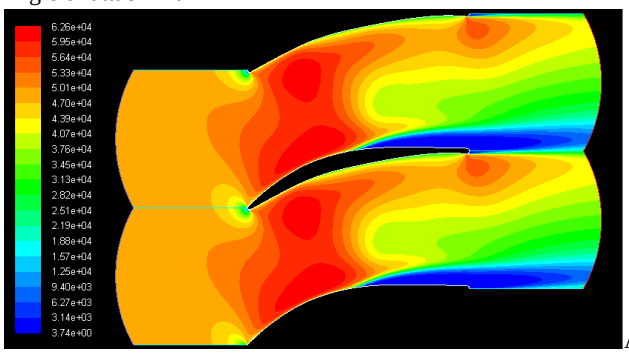

Angle of attack = 39

Unstructured mesh

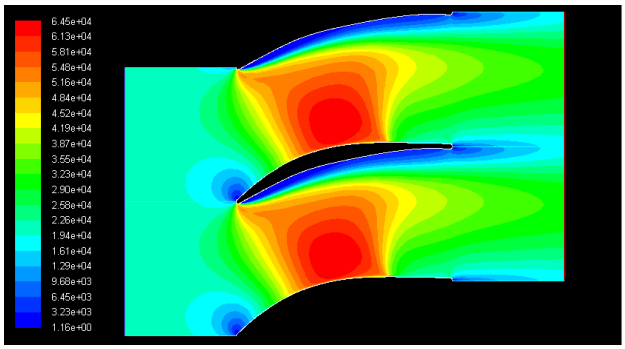

Angle of attack = 0

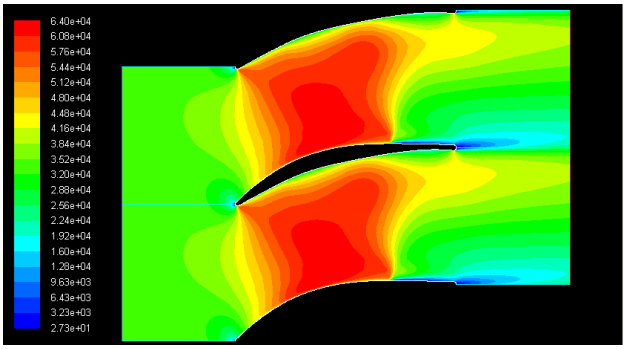

Angle of attack = 28

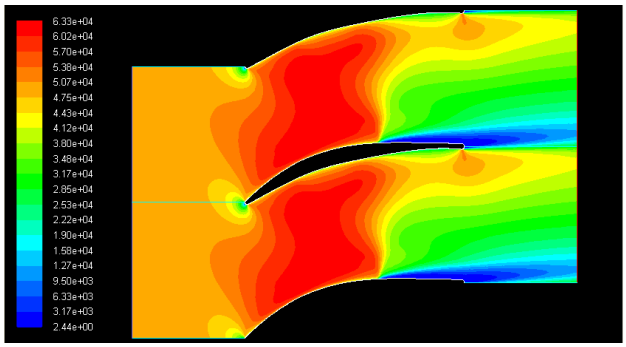

Angle of attack = 39

5.7 Contours of total pressure.

5.7.1 Pressure ratio of 1.03

Structured mesh

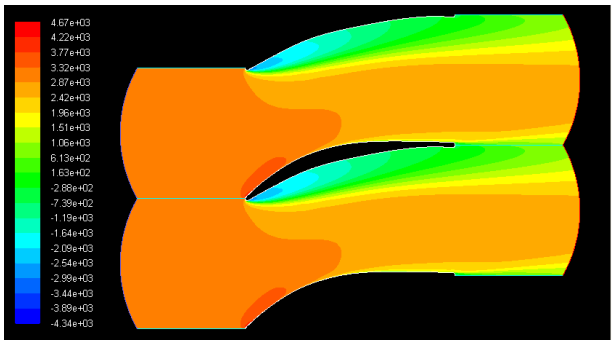

Angle of attack = 0

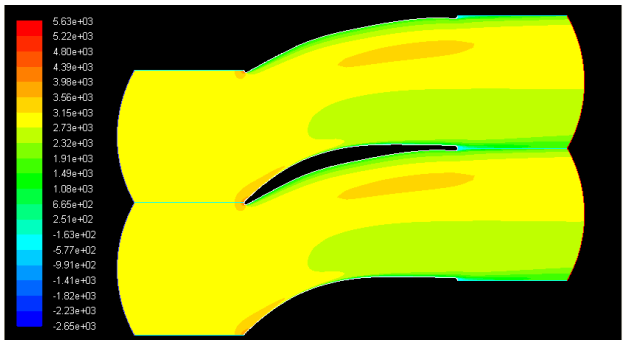

Angle of attack = 28

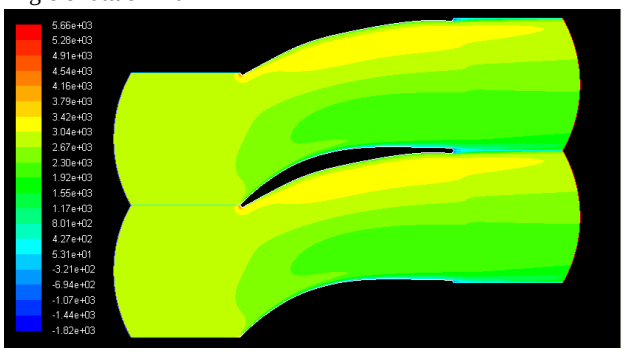

Angle of attack = 39

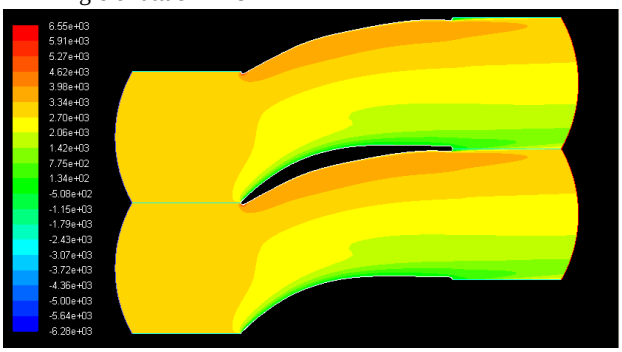

Angle of attack = 46

Unstructured mesh

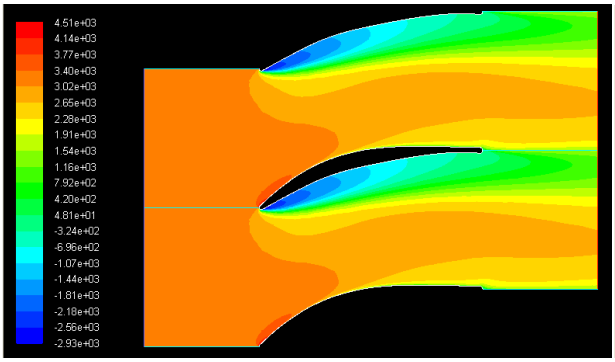

Angle of attack = 0

Angle of attack = 28

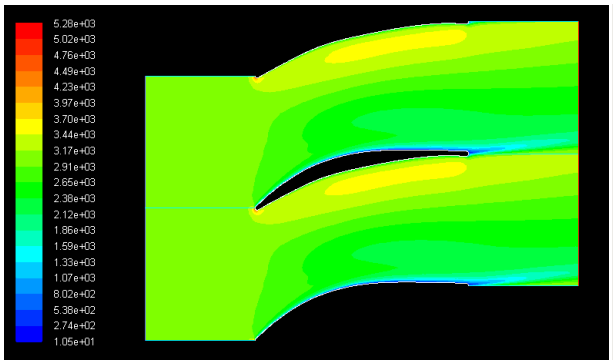

Angle of attack = 39

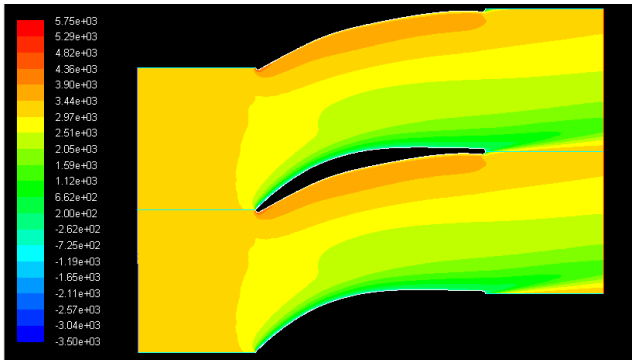

Angle of attack = 46

5.7.2 Pressure ratio of 1.2

Structured mesh

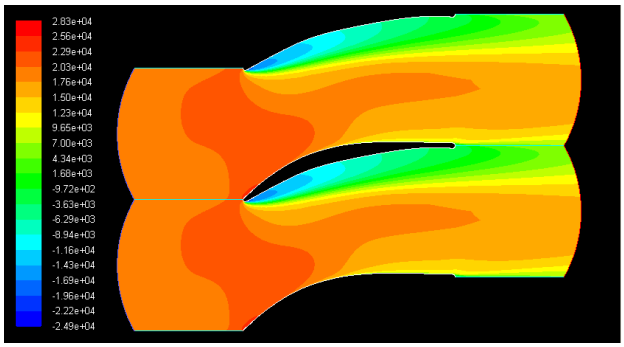

Angle of attack = 0

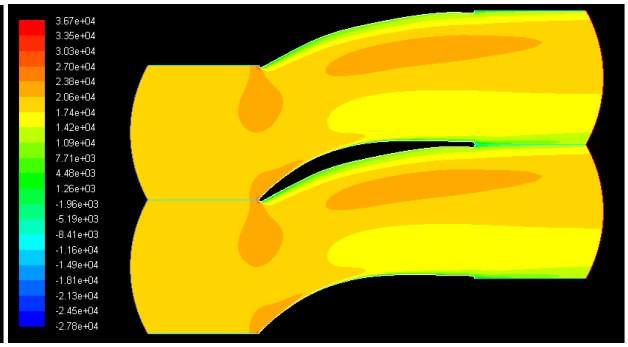

Angle of attack = 28

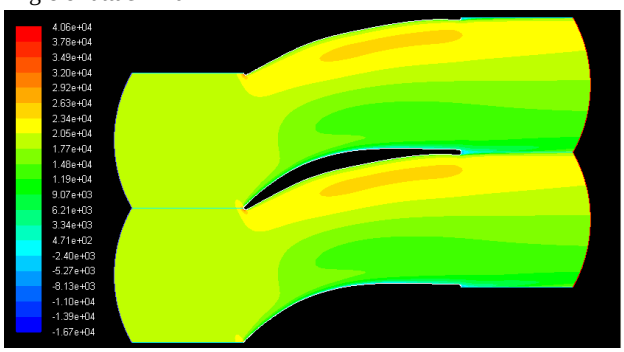

Angle of attack = 39

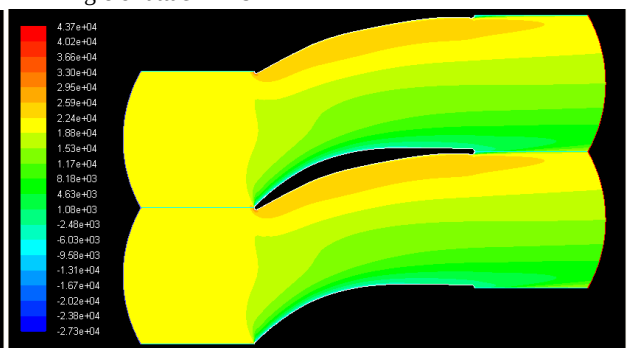

Angle of attack = 46

Unstructured mesh

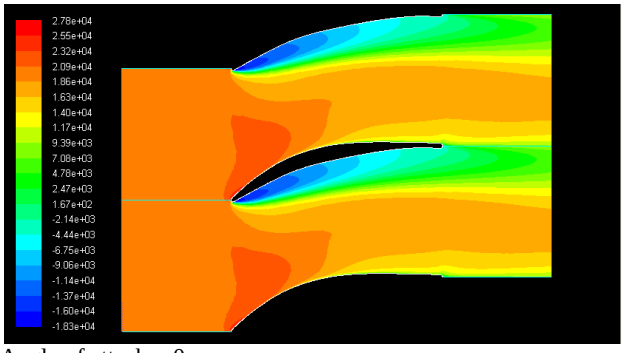

Angle of attack = 0

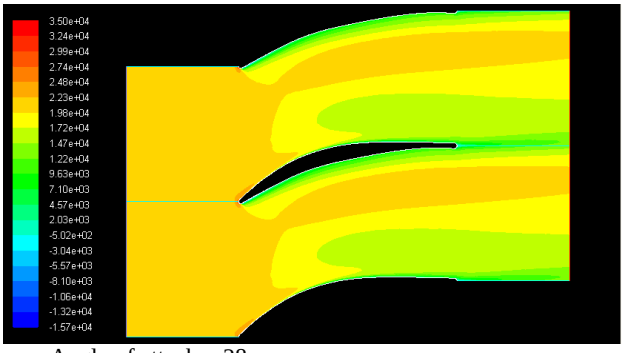

Angle of attack = 28

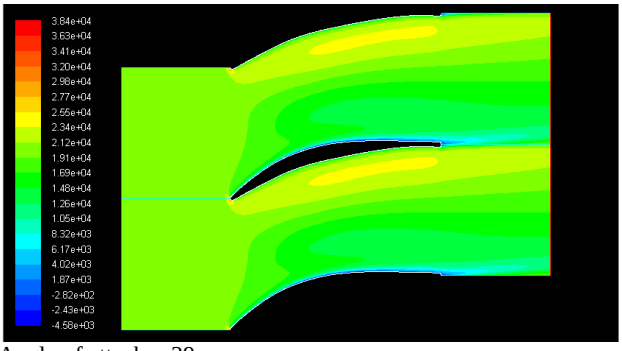

Angle of attack = 39

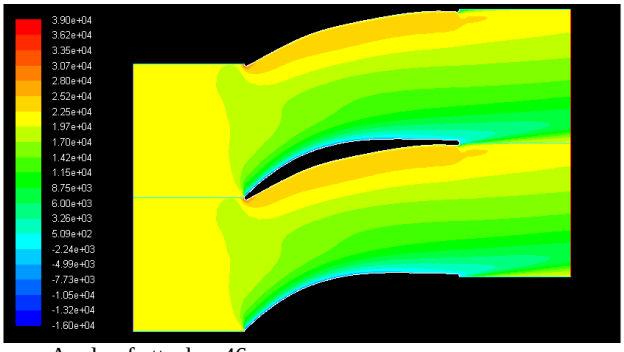

Angle of attack = 46

5.7.3 Pressure ratio of 1.5

Structured mesh

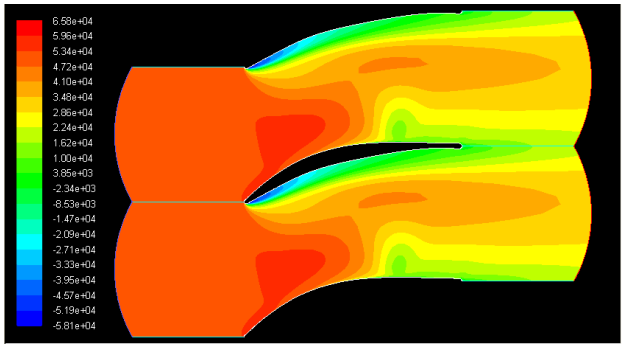

Angle of attack = 0

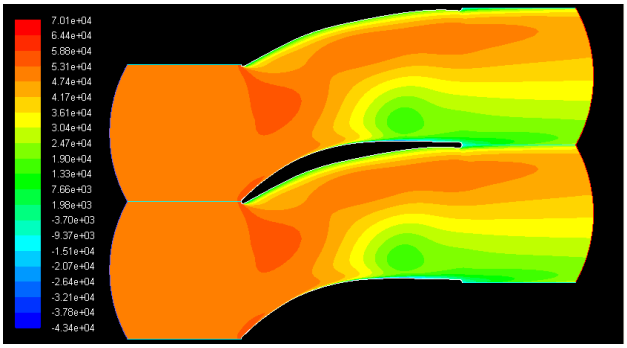

Angle of attack = 28

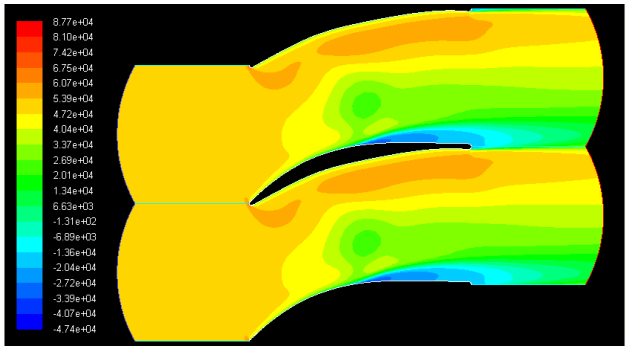

Angle of attack = 39

Unstructured mesh

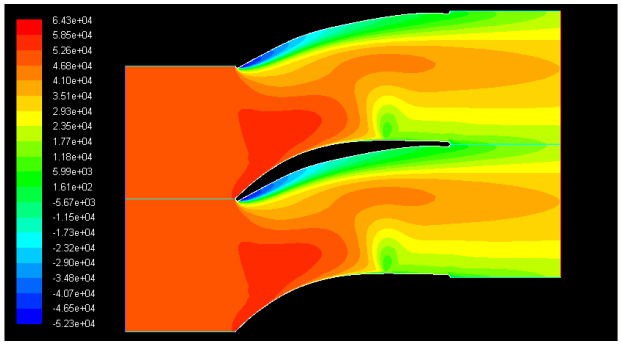

Angle of attack = 0

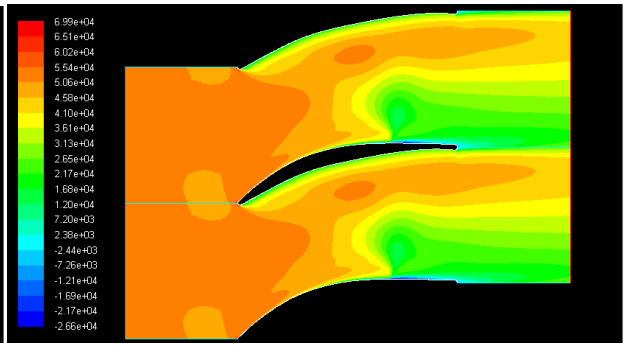

Angle of attack = 28

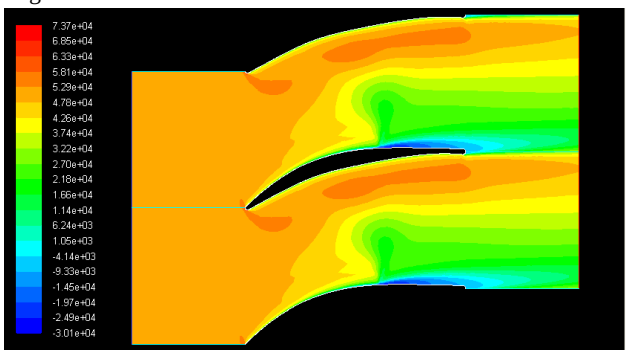

Angle of attack = 39

5.8 Inviscid flow. Test case (Pressure ratio 1.03).

Structured mesh & unstructured mesh

- Angle of attack = 0

For the angle of attack of zero degrees, there is a separation of the flow from the wall. We could not find a good convergence for this case file. This indicates that the problem may be transient. By studying the problem for different number of iterations we could see an eddy moving down the stream.

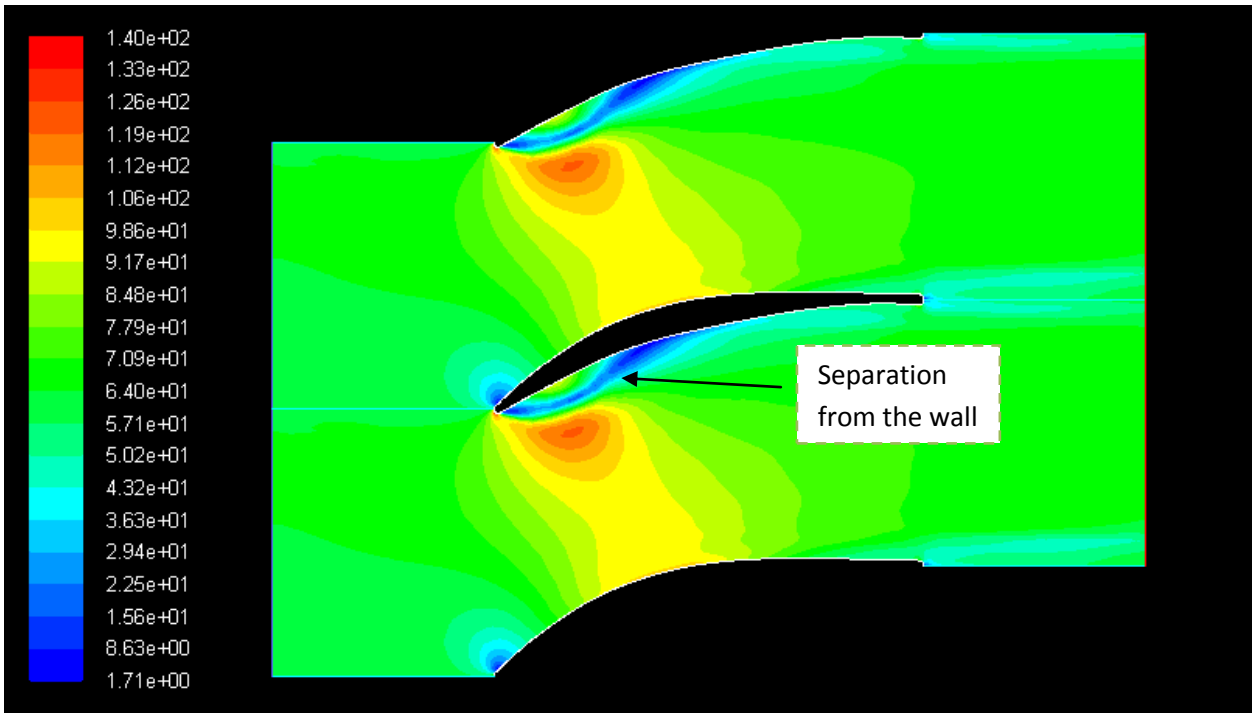

In the next images it is possible to see the eddy moving towards the cascade,

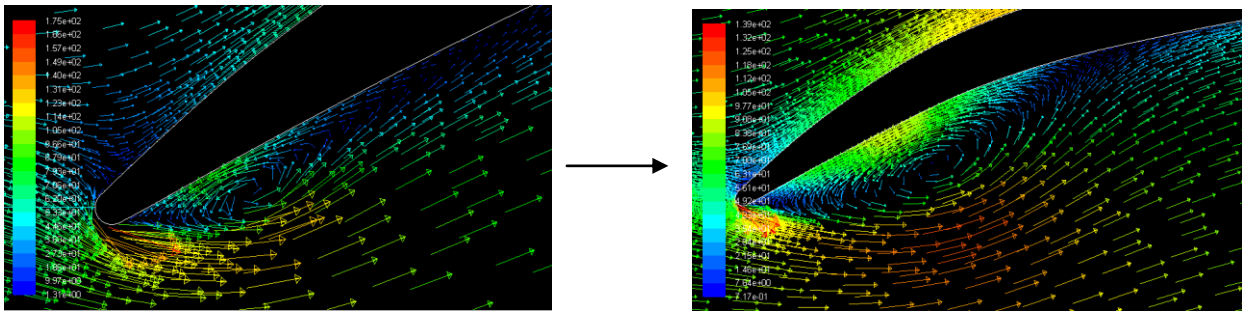

2500 iterations 5500 iterations

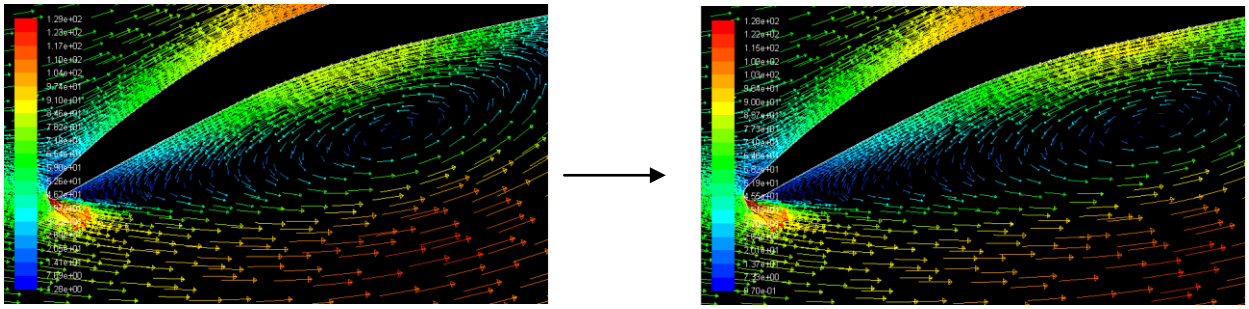

15000 iterations 20000 iterations

This project does not show the rest of the results as we do not study transient problems.

- Angle of attack = 28

For this case it was easier to find convergence. The unstructured mesh shows a better convergence

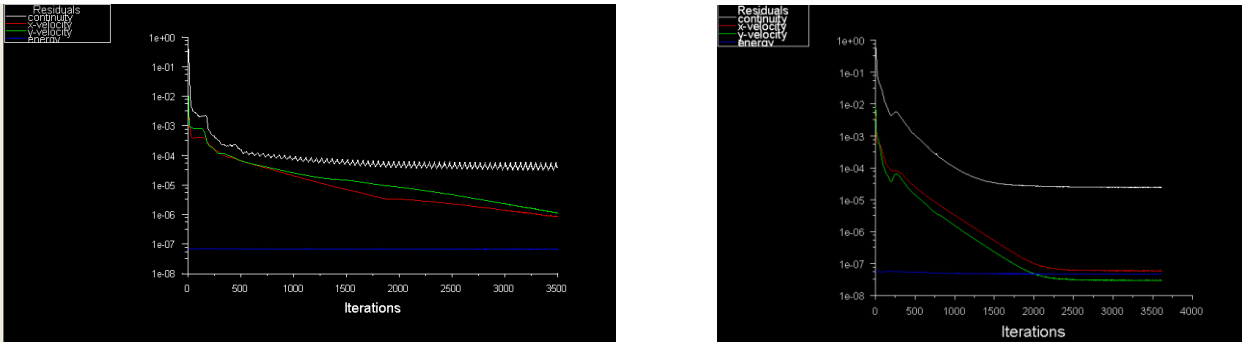

Residuals of the structured grid Residuals of the unstructured grid

For the contours of velocity magnitude and Mach number, we can see that the flow velocity does not decrease near the wall because there is not viscosity

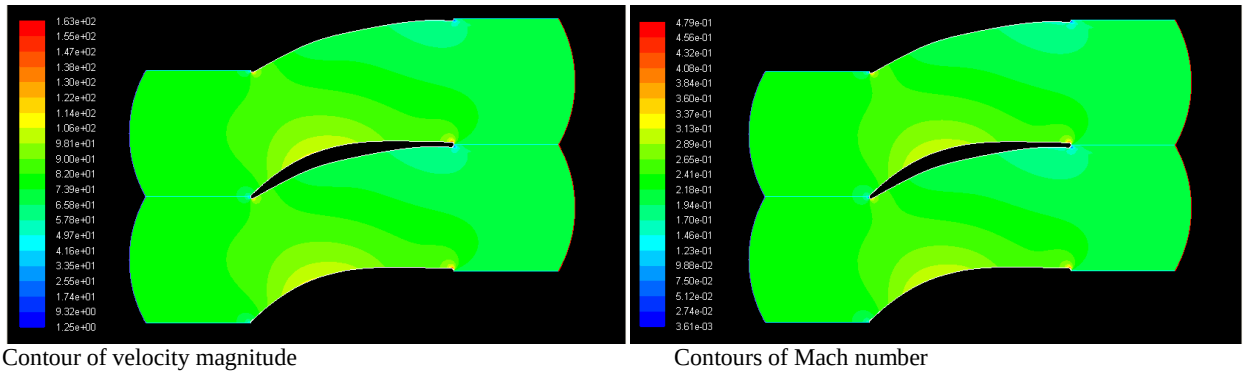

Contour of velocity magnitude Contours of Mach number

The vectors may show this better. We can see that the velocity profile near the wall. The no-slip condition does not apply for an inviscid problem.

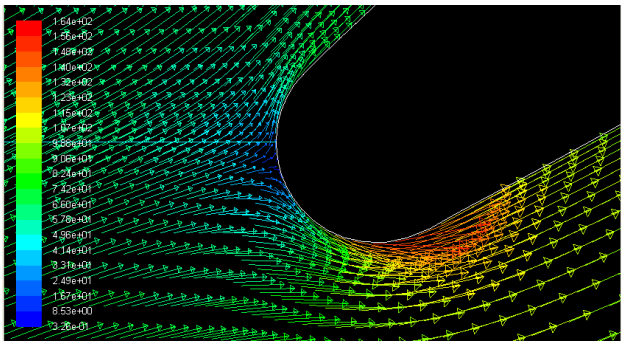
Leading edge

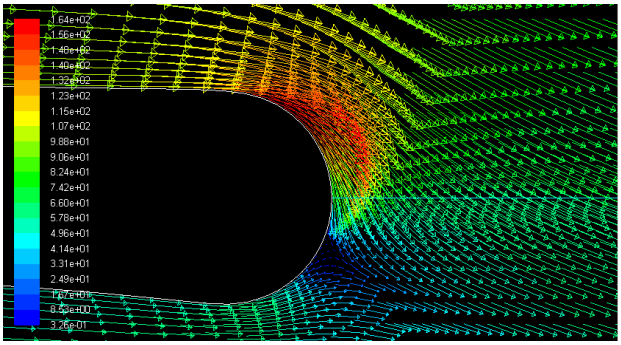
Trailing edge

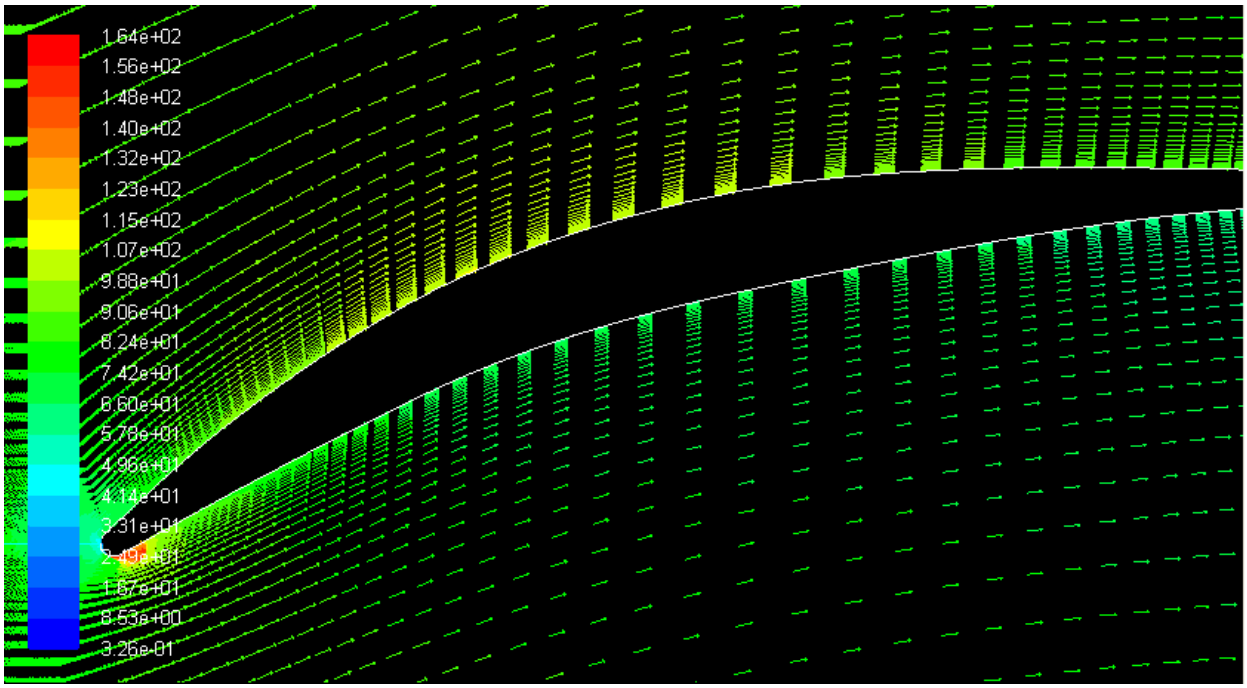

Vectors distribution along the blade. The no-slip condition does not apply for this case.

For this inviscid problem, we can see an increase of the static pressure at the outlet. For the dynamic pressure we cannot see almost any change due to the fact that the motion of the flow does not decrease on the wall


Contour static pressure

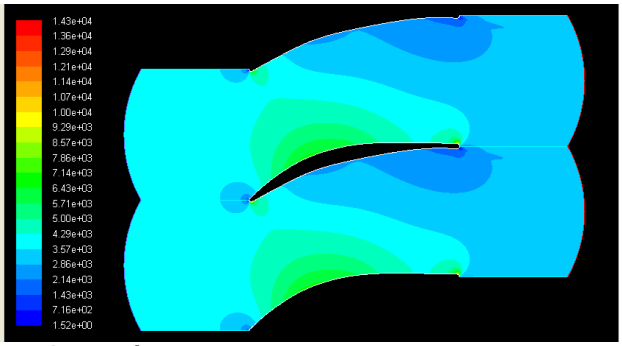
Contour dynamic pressure

The total pressure barely changes because there is no viscosity on the wall.

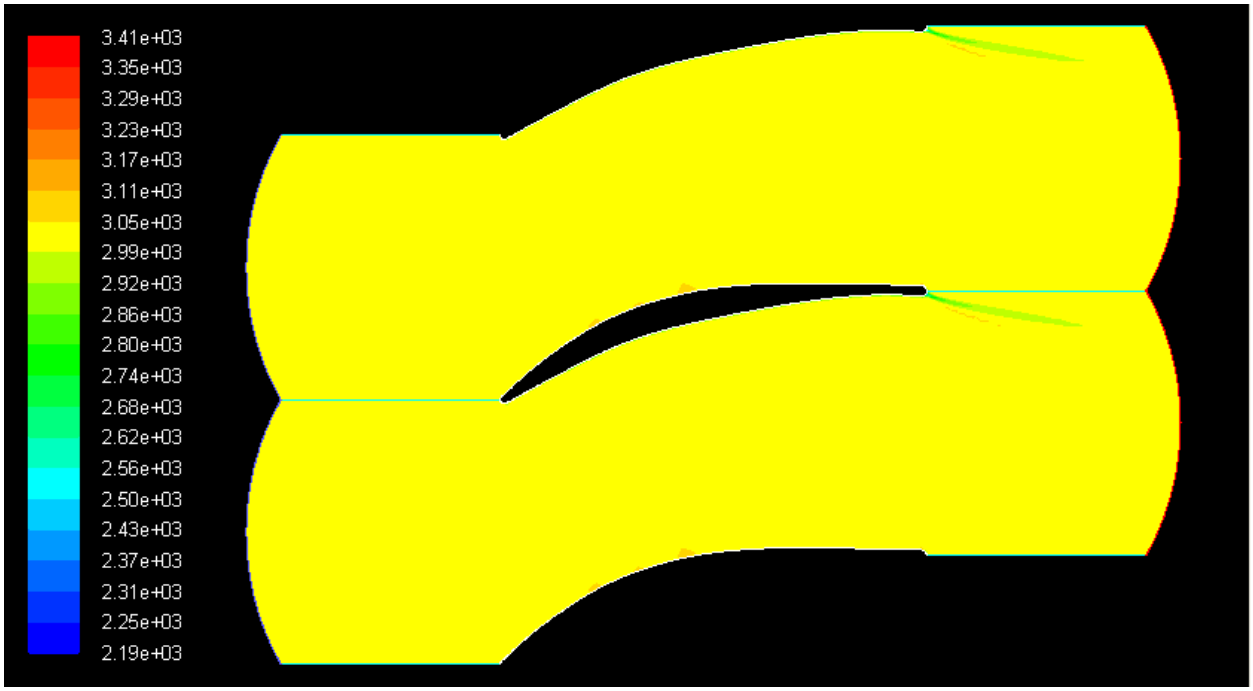

Contours of total pressure

- Angle of attack = 39

The convergence obtained for the structured grid is commonly seen in the transient problems, however, the small value of the residuals allow us to study the problem as a steady one. Once again, the residuals seems better for the unstructured grid. What we commented for the angle of attack of 28 degrees is totally valid for this contours and it is not mentioned again.

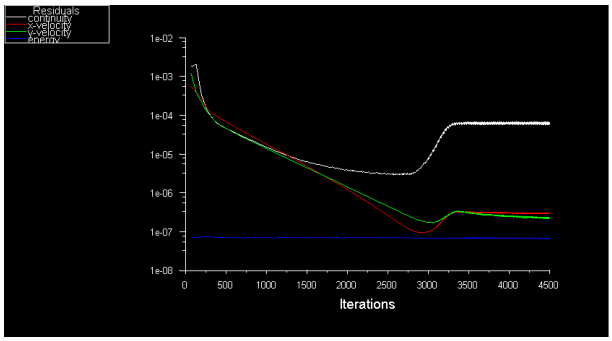

Residuals of the structured grid

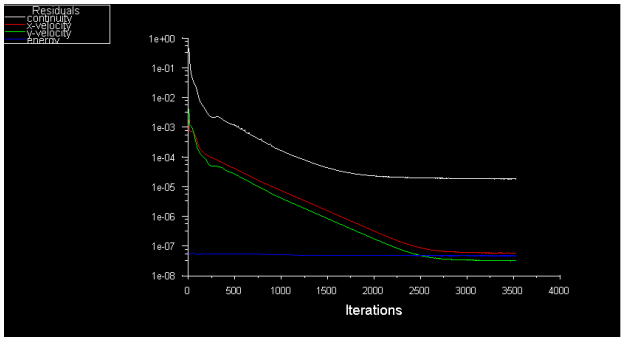

Residuals of the unstructured grid

Contours of velocity magnitude.

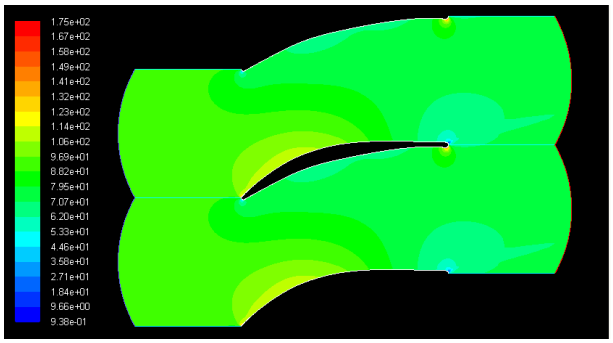

Contours of velocity magnitude. Structured grid

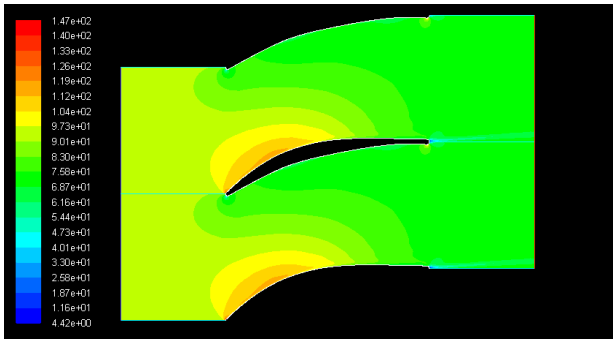

Contours of velocity magnitude. Unstructured grid

Contours of Mach Number.

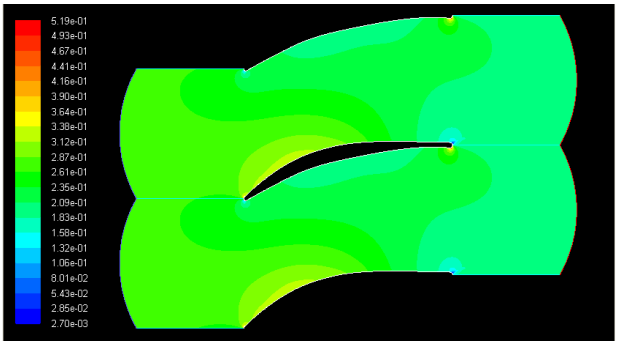

Contours of Mach Number. Structured mesh

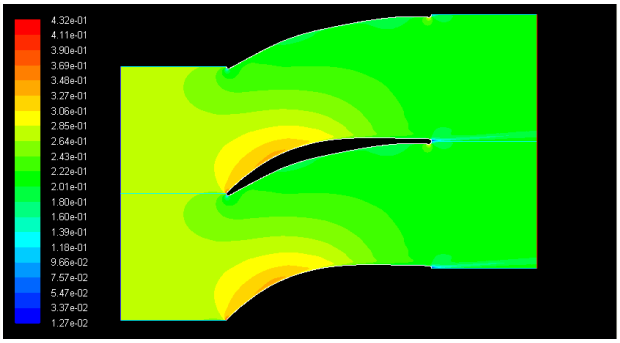

Contours of Mach Number. Unstructured mesh

Vectors of velocity magnitude.

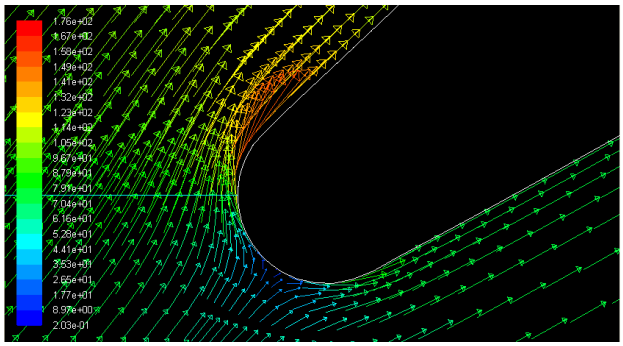

Vectors at the leading edge

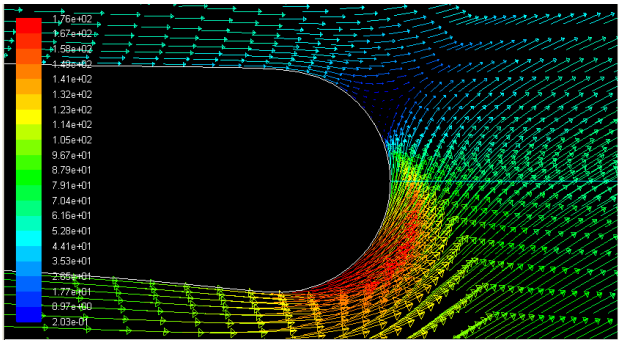

Vectors at the trailing edge

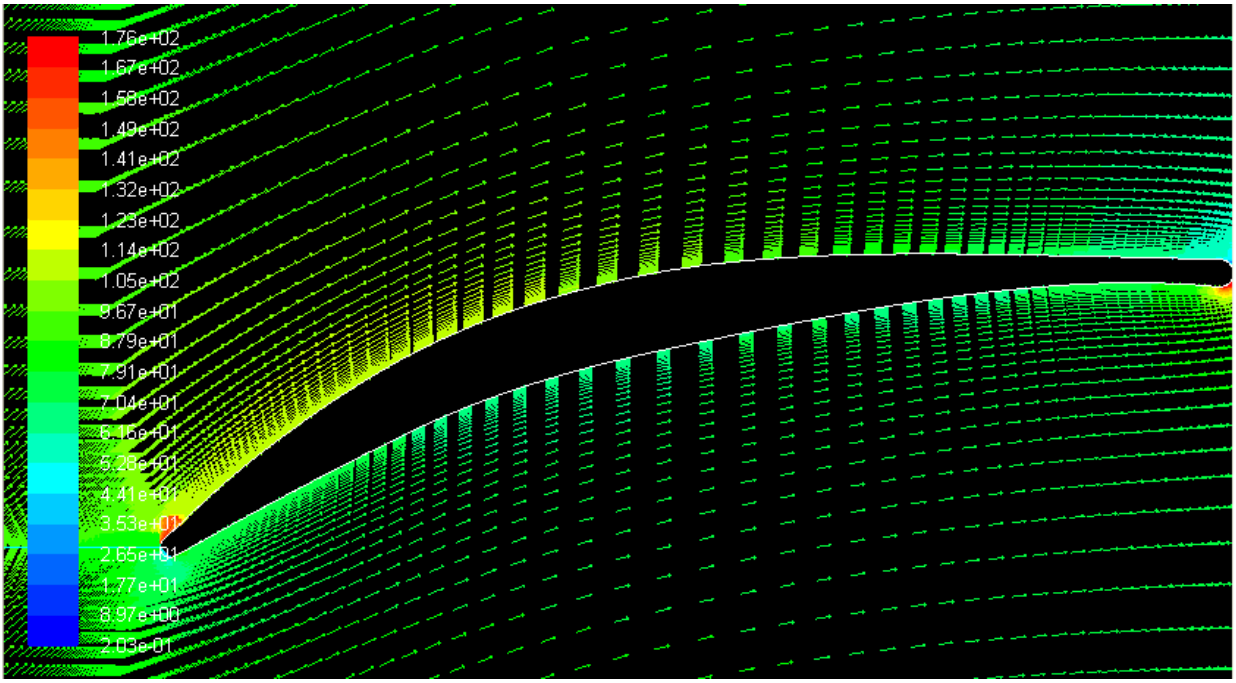

Vectors along the blade. The no-slip condition does not apply here.

Contours of static pressure.

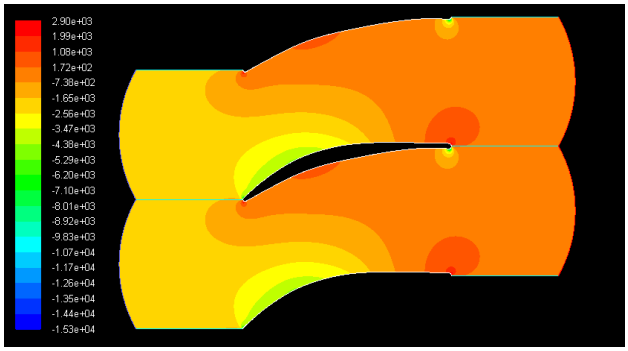

Contours of static pressure. Structured grid

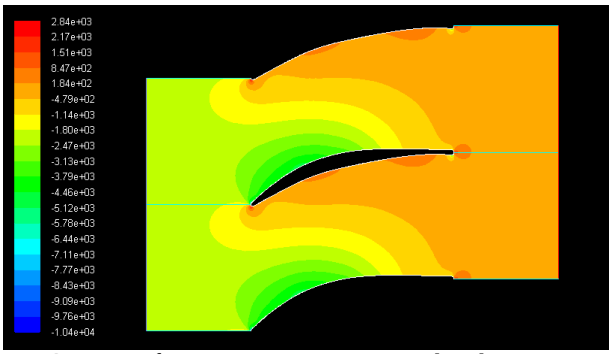

Contours of static pressure. Unstructured grid

Dynamic pressure.

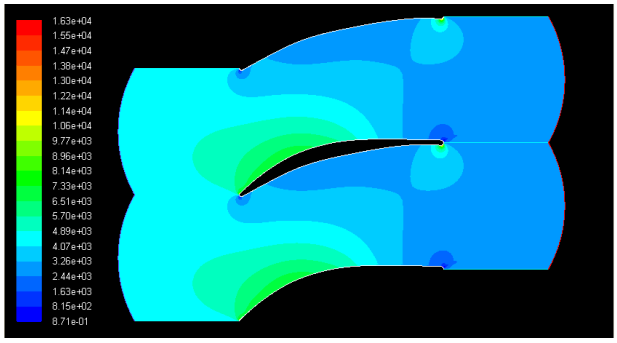

Contours of dynamic pressure. Structured grid

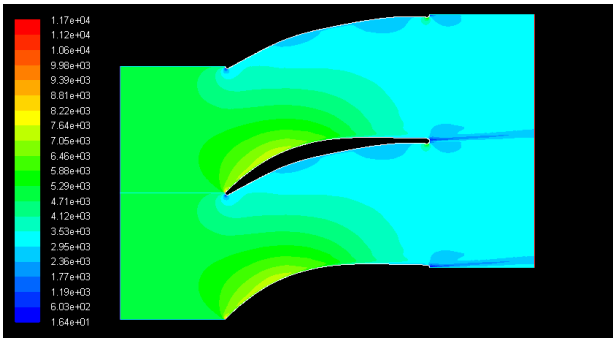

Contours of dynamic pressure. Unstructured grid

Contour of total pressure.

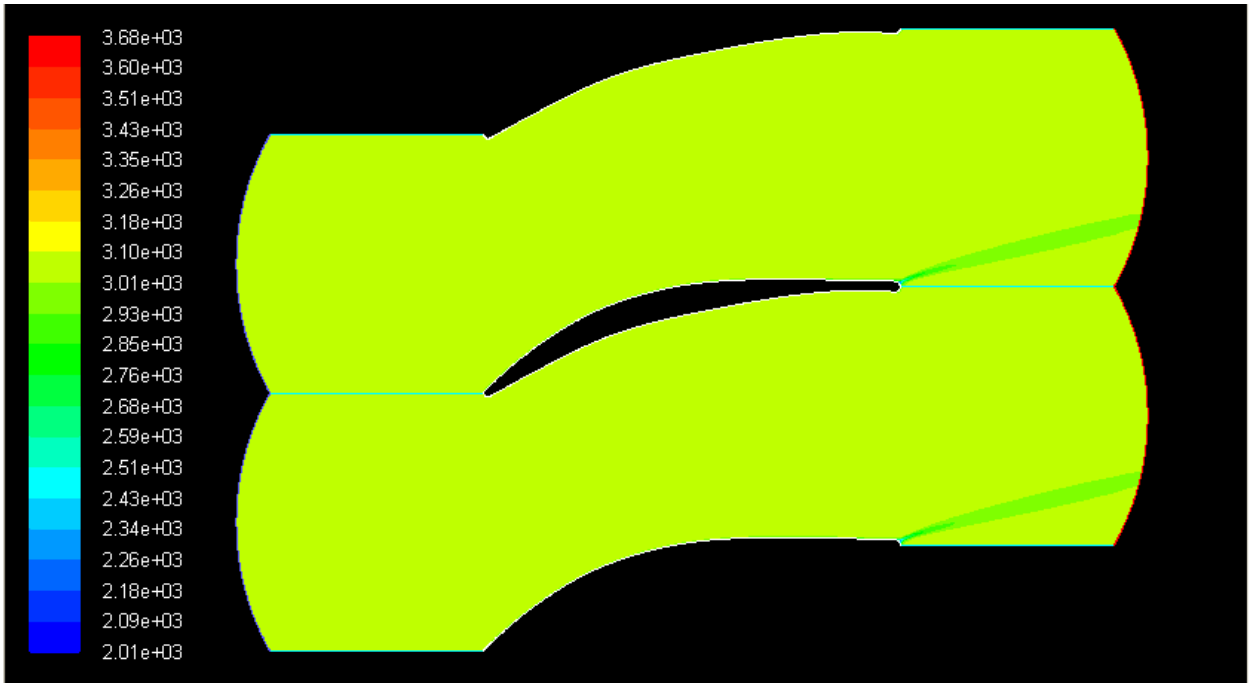

Contour of total pressure

- Angle of attack = 46

For this angle of attack, it was not possible to find convergence. It seems like is a transient problem and it should be study as one. Therefore, this case has not been studied.

5.9 Residuals.

All the residuals of all the cases are shown in this chapter. Is it possible to see that as we keep increasing the angle of attack, the convergence keeps getting worst. This has been discussed in the chapter three.

- Pressure ratio of 1.03

Structured mesh

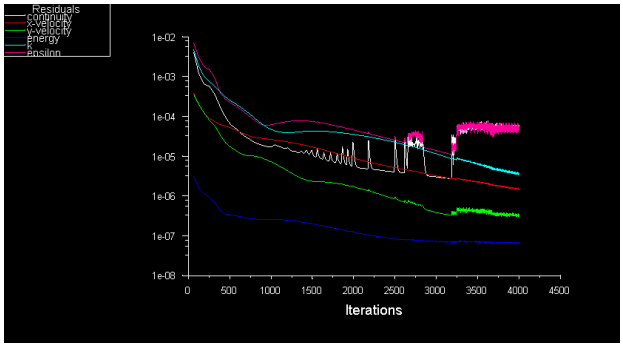

Angle of attack = 0

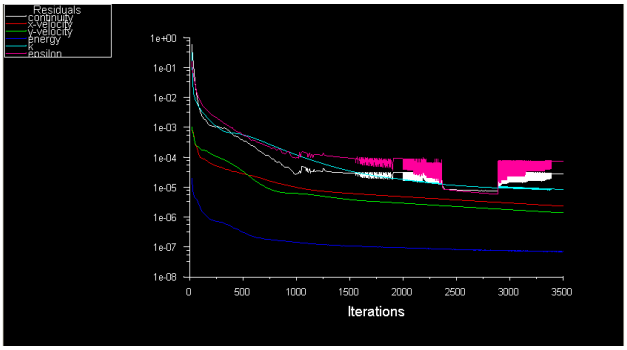

Angle of attack = 28

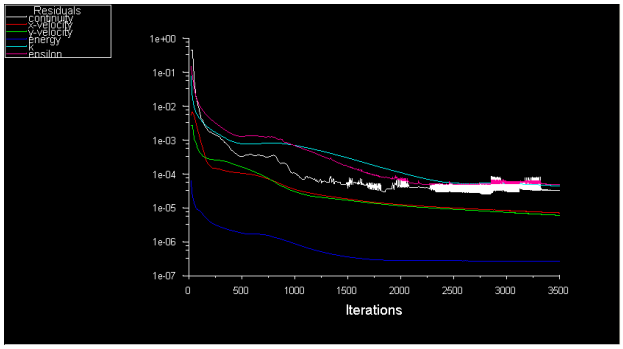

Angle of attack = 39

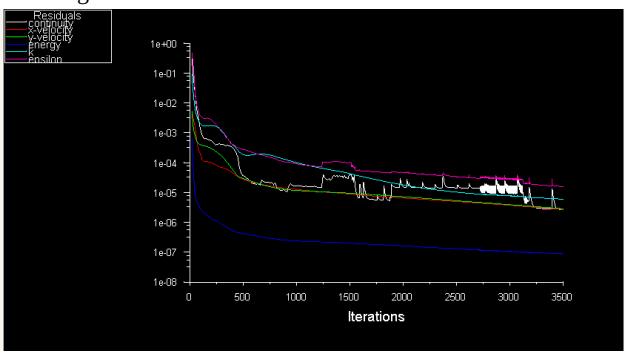

Angle of attack = 46

Unstructured mesh

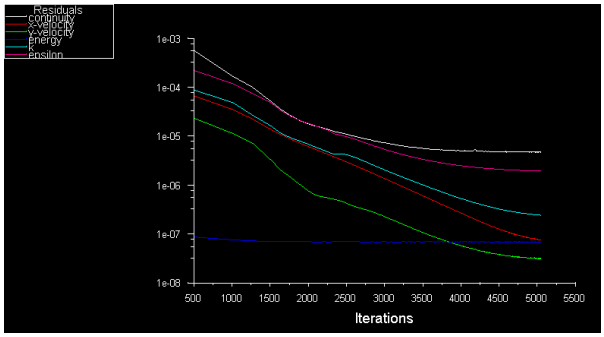

Angle of attack = 0

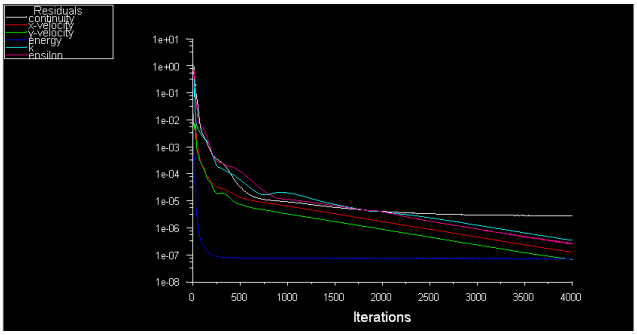

Angle of attack = 28

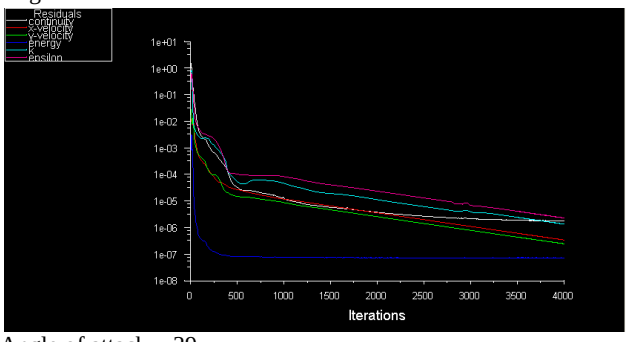

Angle of attack = 39

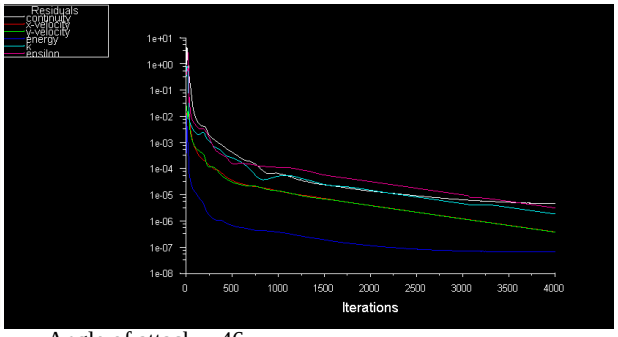

Angle of attack = 46

- Pressure ratio of 1.2

Structured mesh

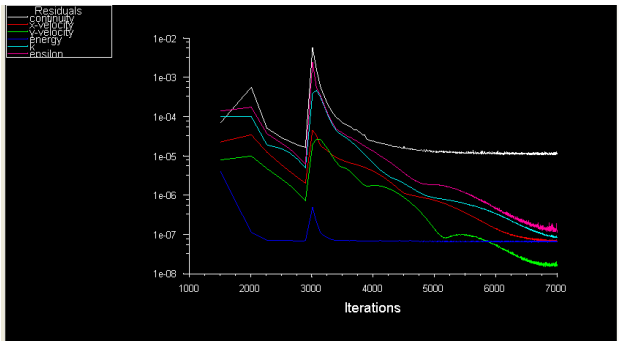

Angle of attack = 0

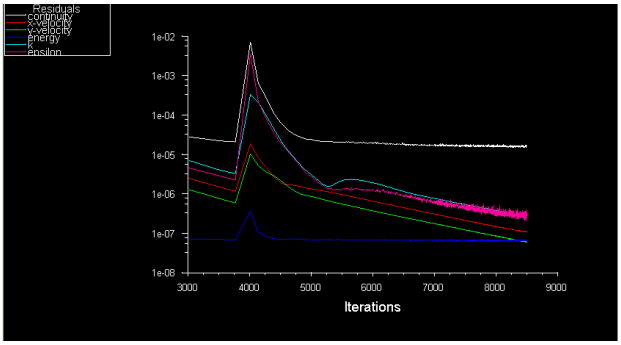

Angle of attack = 28

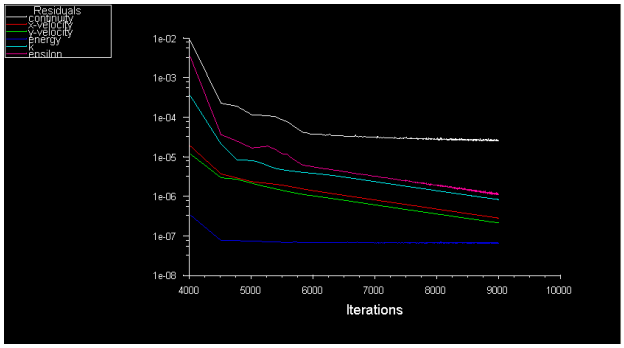

Angle of attack = 39

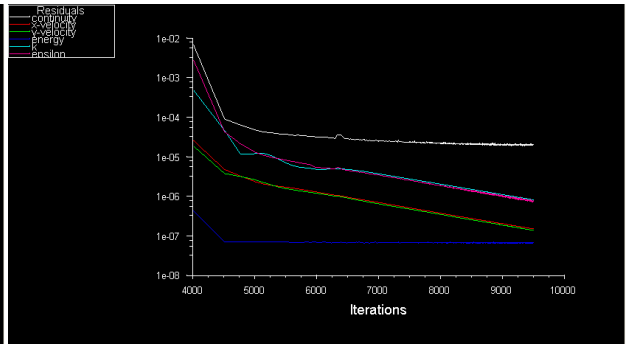

Angle of attack = 46

Unstructured mesh

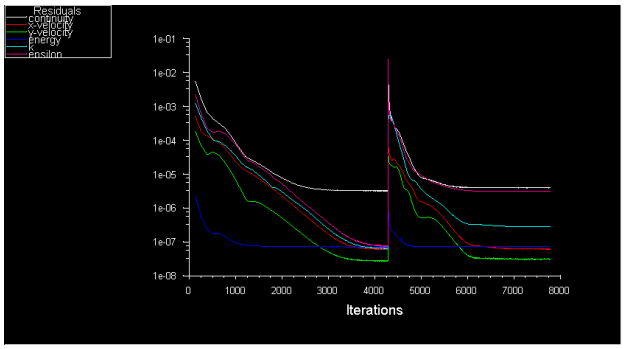

Angle of attack = 0

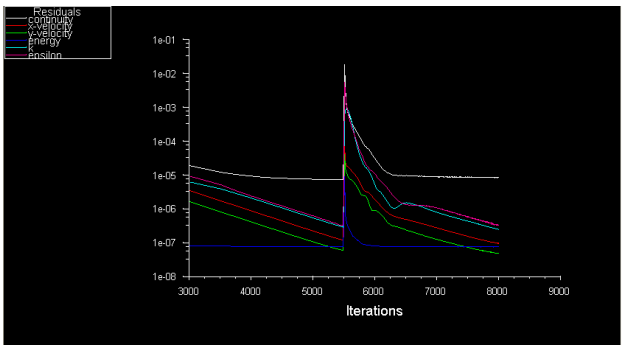

Angle of attack = 28

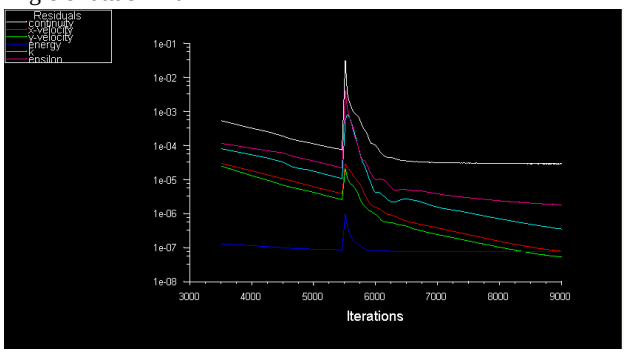

Angle of attack = 39

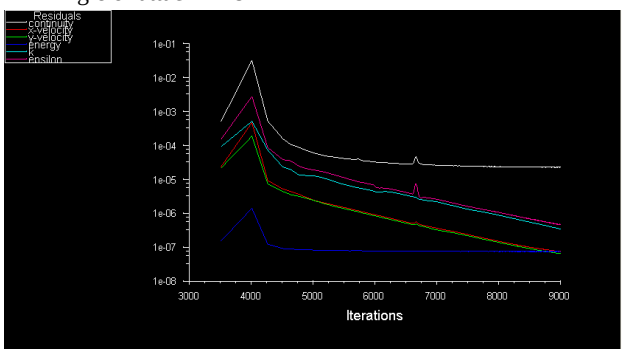

Angle of attack = 46

- Pressure ratio of 1.5

Structured mesh

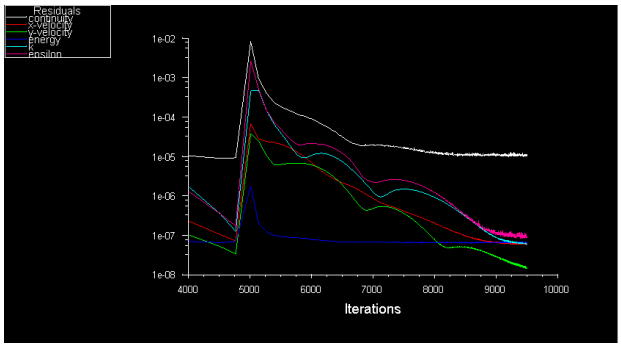

Angle of attack = 0

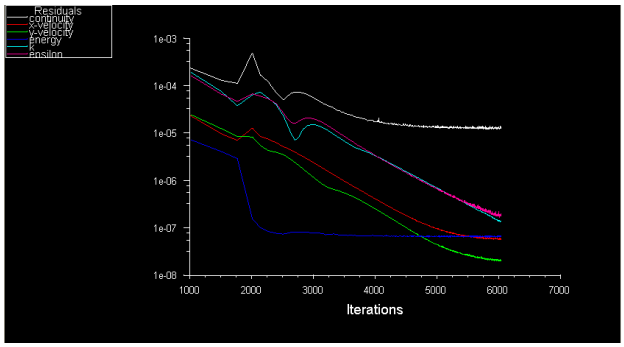

Angle of attack = 28

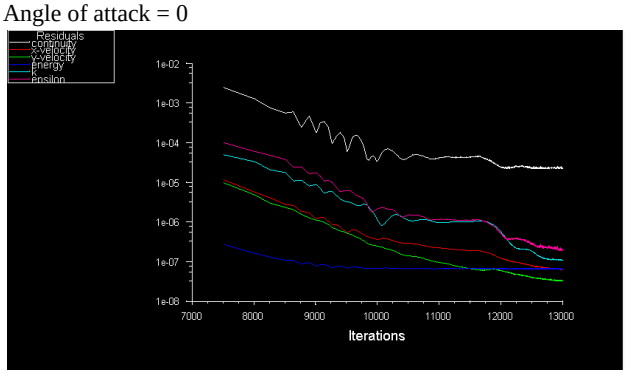

Angle of attack = 39

Unstructured mesh

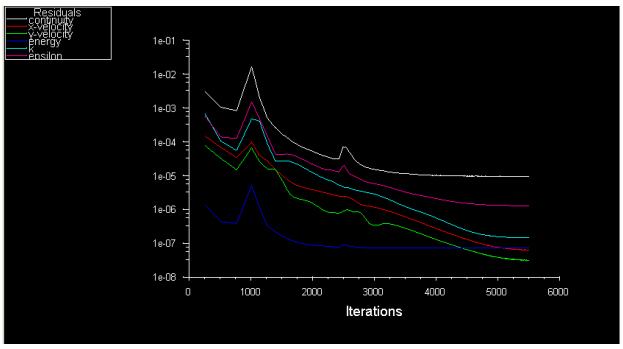

Angle of attack = 0

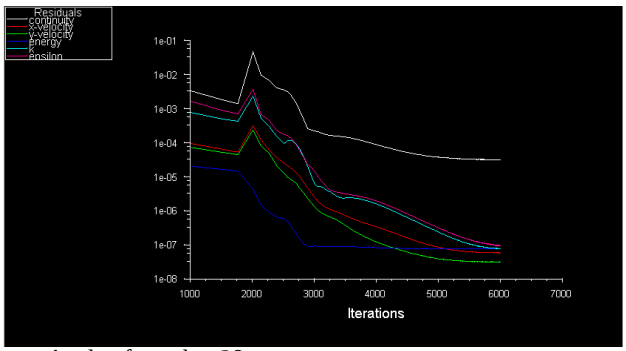

Angle of attack = 28

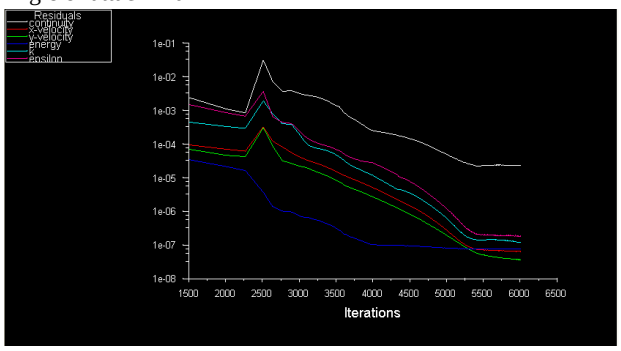

Angle of attack = 39

5.10 Tables

This section shows the values of the significant variables of our problem.

With the attack angle of zero degrees, the compressor blade cannot increase the pressure of the flow. As we go increasing the angle, the pressure goes up more and more. We can also see that the maximum pressure correspond with the maximum decrease of the velocity. This is due to the Navier-Stokes equations for a compressible flow moving at low Mach numbers. It is obvious that the maximum increase of pressure belongs to the higher pressure ratio 1.5.

$\frac{p^0}{p_e}$ = 1.03

ANGLE OF ATTACK	0		28		39		46	
Type of grid	U	S	U	S	U	S	U	S
Mass flow rate (Kg/s)	5.241072	5.236536	6.12946	6.029363	6.024508	5.675168	5.70937	5.596841
Inlet Pressure (Pa)	102372.3	102375.9	100810.9	100931.1	99889.37	100418.1	99302.3	99511.38
Outlet Pressure (Pa)	101325	101325	101325	101325	101325	101325	101325	101325
$P_{exit} - P_{inlet}$	-1047.3	-1050.9	514.1	393.9	1435.63	906.9	**2022.7**	1813.62
Inlet velocity(m/s)	57.53847	57.4857	77.05402	75.72557	86.61037	81.26069	92.21217	90.25629
Outlet velocity(m/s)	59.66077	59.53088	68.07597	67.01739	67.2514	63.42702	64.50999	63.22742
$\lvert\Delta V\rvert$	2.1223	2.04518	8.97805	8.70818	19.35897	17.83367	27.70218	27.02887
Outlet average density (Kg/m^3)	1.183753	1.183831	1.185759	1.185354	1.185583	1.182834	1.184886	1.184367
Inlet average density (Kg/m^3)			1.182329	1.183324	1.174593	1.178961	1.169653	1.171389

Table 1 Pressure Ratio 1.03

$\frac{p^0}{p_e}$ = 1.2

ANGLE OF ATTACK	0		28		39		46	
Type of grid	U	S	U	S	U	S	U	S
Mass flow rate (Kg/s)	13.01091	13.03944	15.35701	15.29616	15.1744	15.10407	13.95772	13.94247
Inlet Pressure (Pa)	110102.7	110046.7	98403.31	98650.9	88966.1	89471.28	85505.45	85670.13
Outlet Pressure (Pa)	101325	101325	101325	101325	101325	101325	101325	101325
$P_{exit} - P_{inlet}$	-8777.7	-8721.7	2921.69	2674.1	12358.9	11853.72	**15819.55**	15654.87
Inlet velocity(m/s)	129.8149	130.143	188.0458	186.9593	226.8813	224.9057	240.1881	239.5636
Outlet velocity(m/s)	144.3179	143.6483	164.3234	163.6289	163.2609	162.5773	153.7538	153.6422
$\lvert\Delta V\rvert$	14.503	13.5053	23.7224	23.3304	63.6204	62.3284	86.4343	85.9214
Outlet average density (Kg/m^3)	1.2194	1.218981	1.231869	1.231477	1.231347	1.230994	1.22537	1.225553

Table 2 Pressure Ratio 1.2

$\frac{p^0}{p_e}$ = 1.5

ANGLE OF ATTACK	0		28		39		46	
Type of grid	U	S	U	S	U	S	U	S
Mass flow rate (Kg/s)	19.36425	19.44695	21.17554	21.44551	20.68325	20.65574	N/A	N/A
Inlet Pressure (Pa)	130409.8	130185.9	113474	111864.3	92759.53	93276.05	N/A	N/A
Outlet Pressure (Pa)	101325	101325	101325	101325	101325	101325	N/A	N/A
$P_{exit} - P_{inlet}$	-29084.8	-28860.9	-12149	-10539.3	**8565.47**	8048.95	N/A	N/A
Inlet velocity(m/s)	160.6319	161.5113	219.7442	224.8262	281.6465	280.1667	N/A	N/A
Outlet velocity(m/s)	203.1422	202.9201	219.8997	222.2054	218.4798	220.7071	N/A	N/A
$\lvert\Delta V\rvert$	42.5103	41.4088	0.1555	2.6208	63.1667	59.4596	N/A	N/A
Outlet average density (Kg/m^3)	1.262977	1.263275	1.279808	1.282113	1.279441	1.282012	N/A	N/A

Table 3 Pressure Ratio 1.5

5.11 Pressure coefficient (C_p) along the blade.

5.11.1 Present study and the experiment by Sanger and Shreeve.

This results are only made for the pressure ratio of 1.03, and for the angles of attack of 28, 39, and 46.

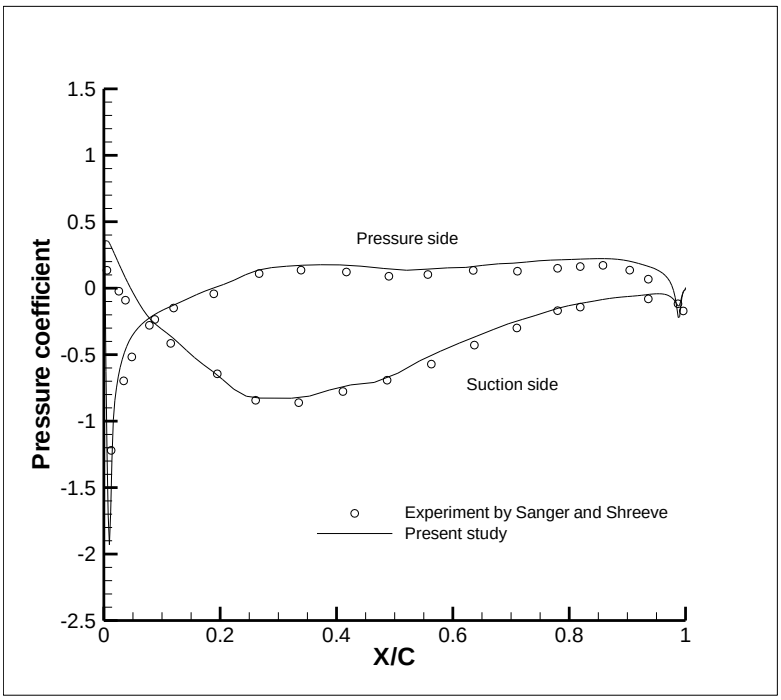

Angle of attack = 28. Structured grid

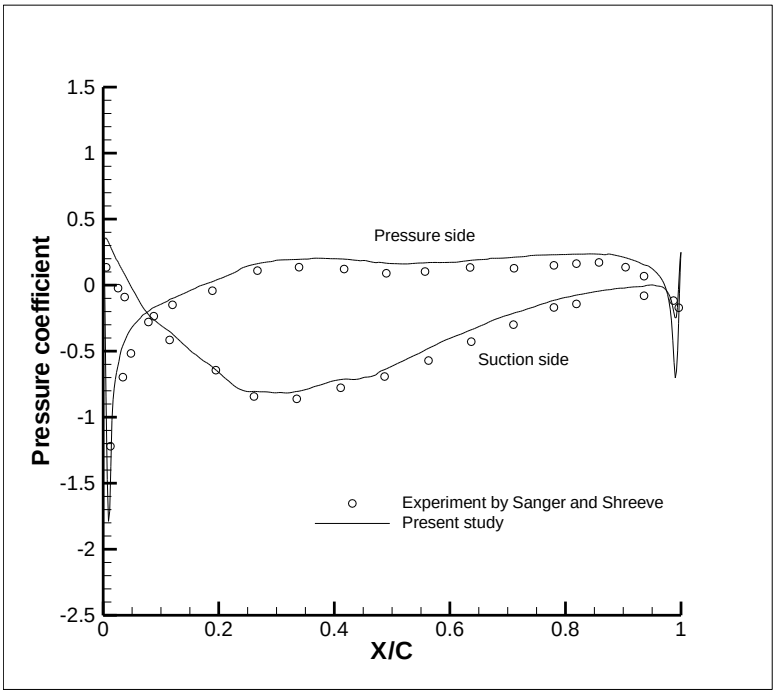

Angle of attack = 28. Unstructured grid

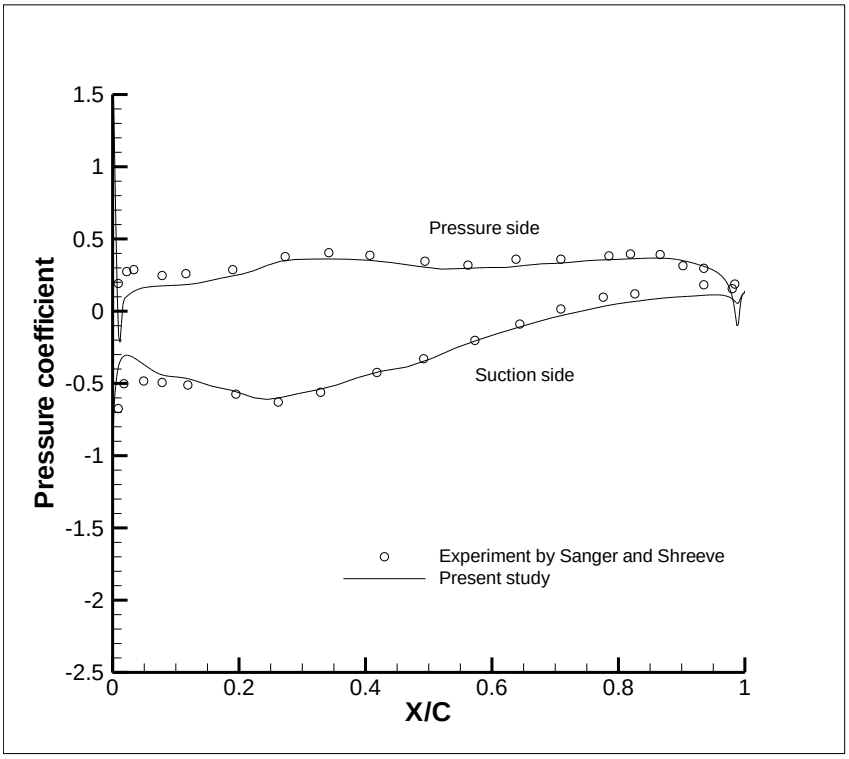

Angle of attack = 39. Structured grid

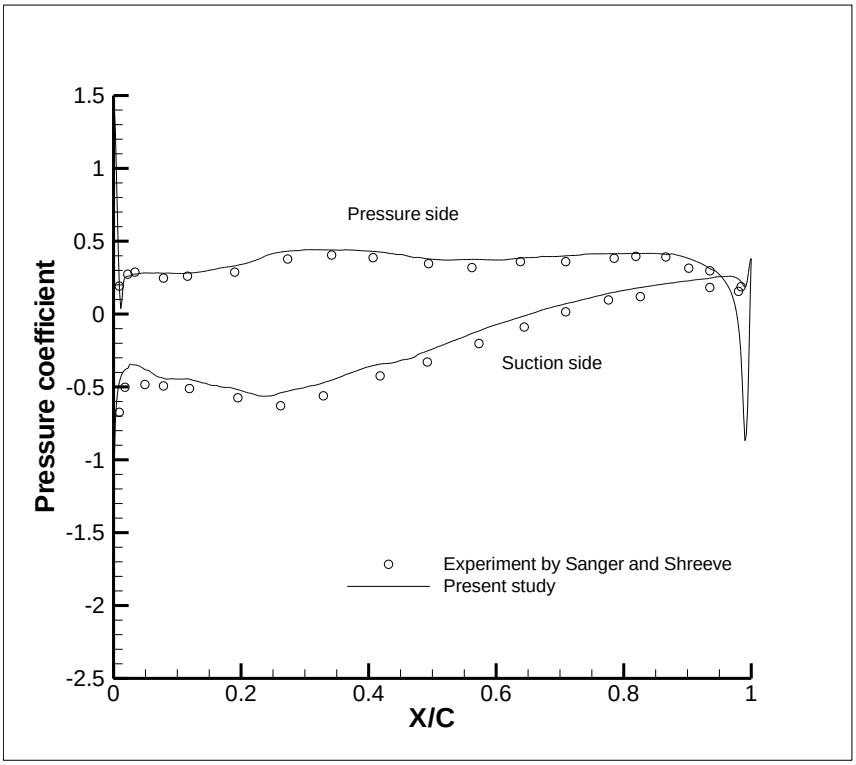

Angle of attack = 39. Unstructured grid

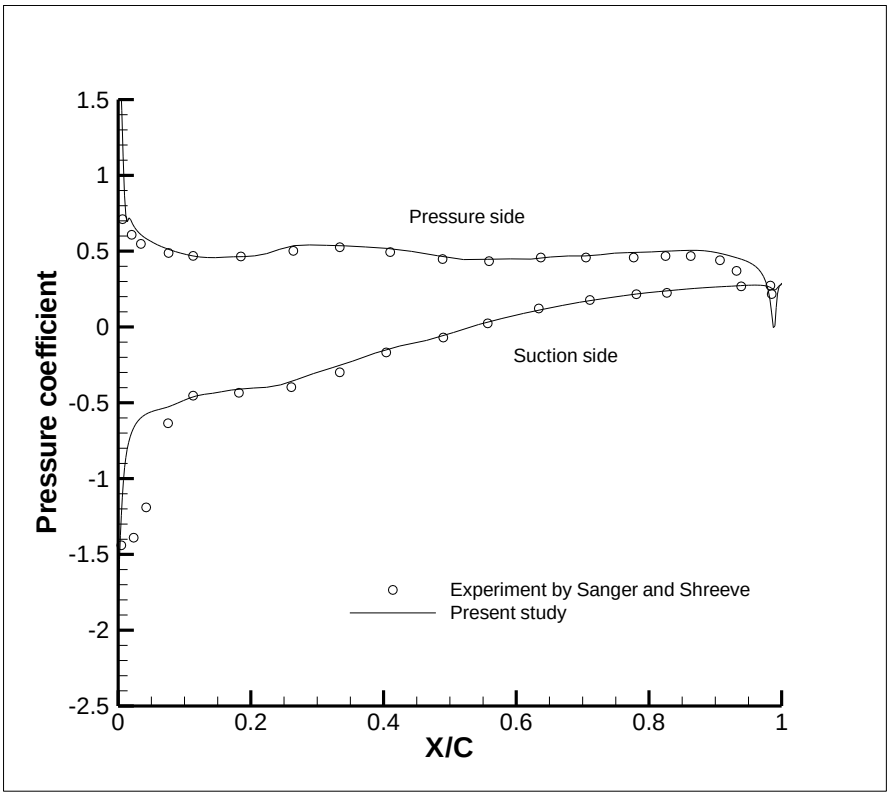

Angle of attack = 46. Structured grid

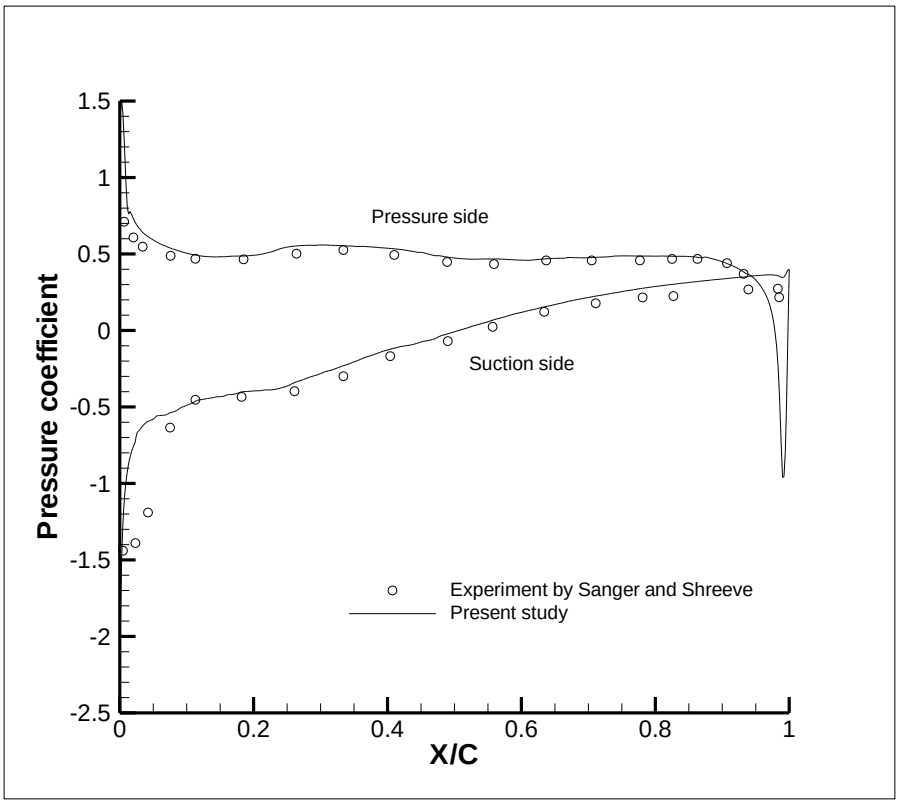

Angle of attack = 46. Unstructured grid

5.11.2 (C_p) graphs according to the pressure ratio.

Pressure ratio of 1.03

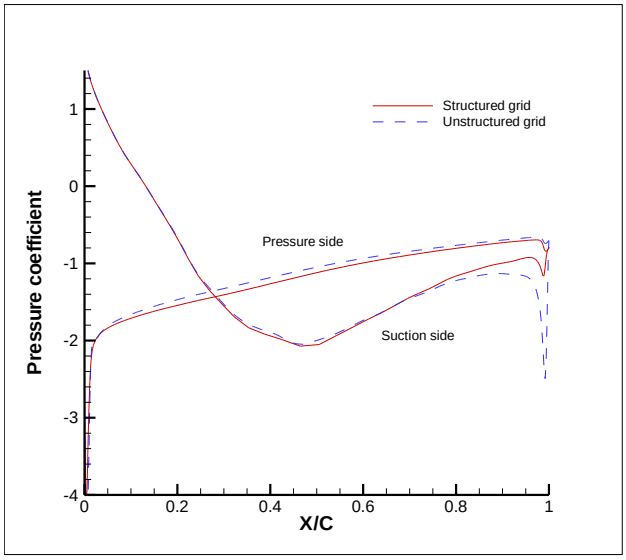

Angle of attack = 0

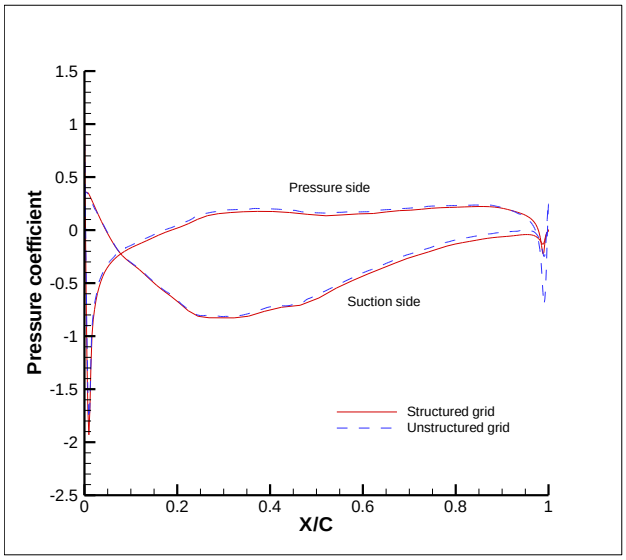

Angle of attack = 28

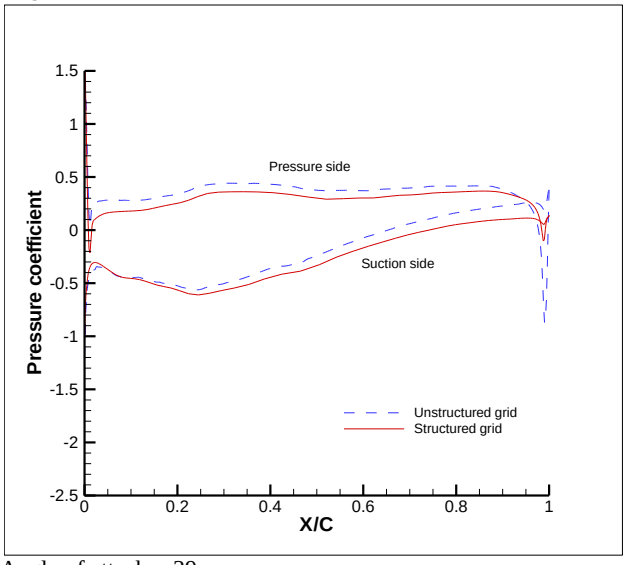

Angle of attack = 39

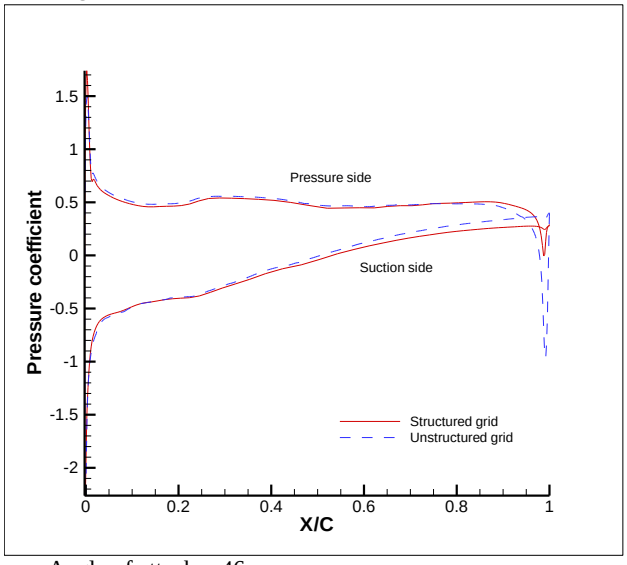

Angle of attack = 46

Pressure ratio of 1.2

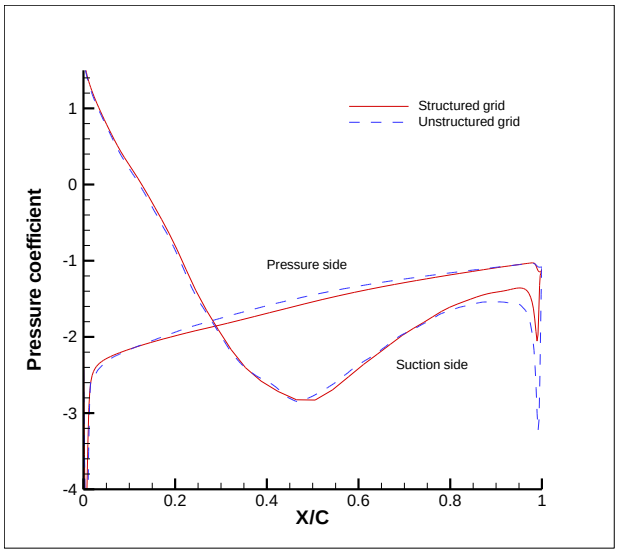

Angle of attack = 0

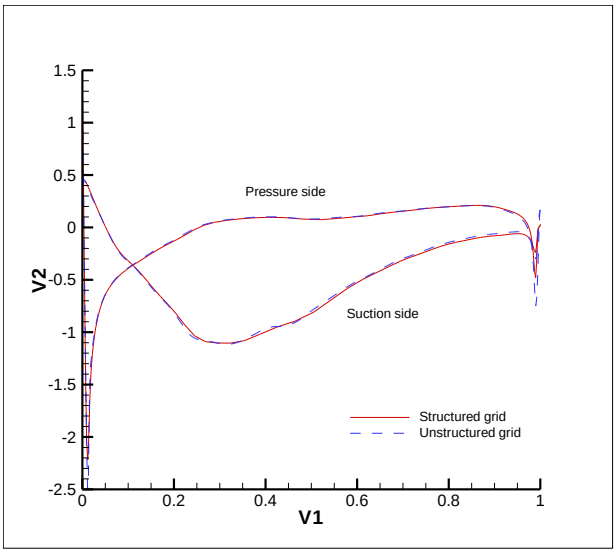

Angle of attack = 28

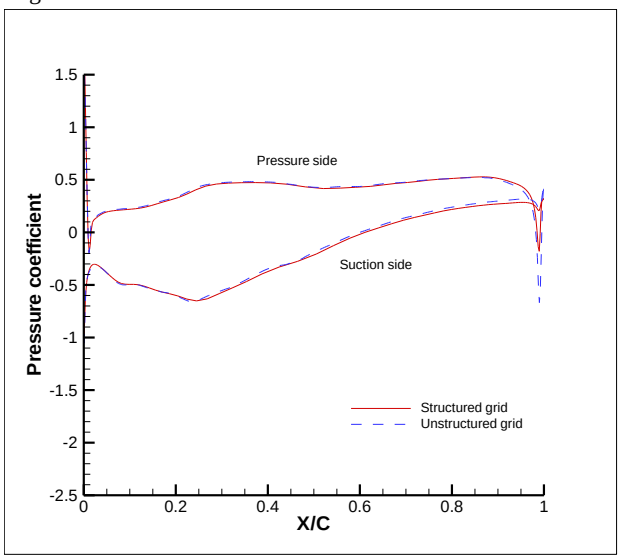

Angle of attack = 39

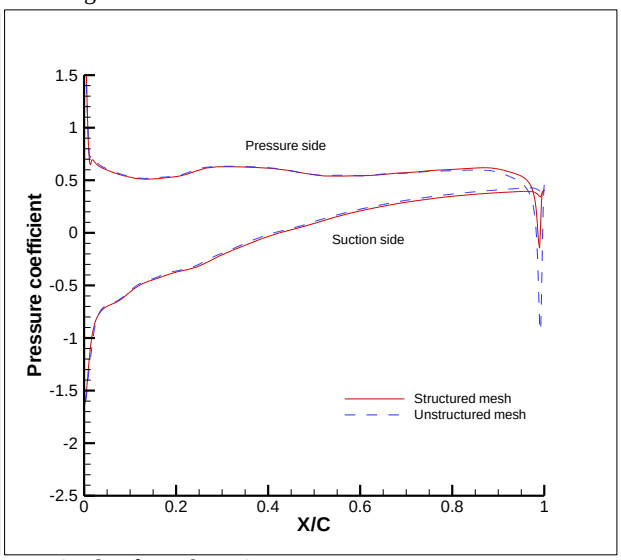

Angle of attack = 46

Pressure ratio of 1.5

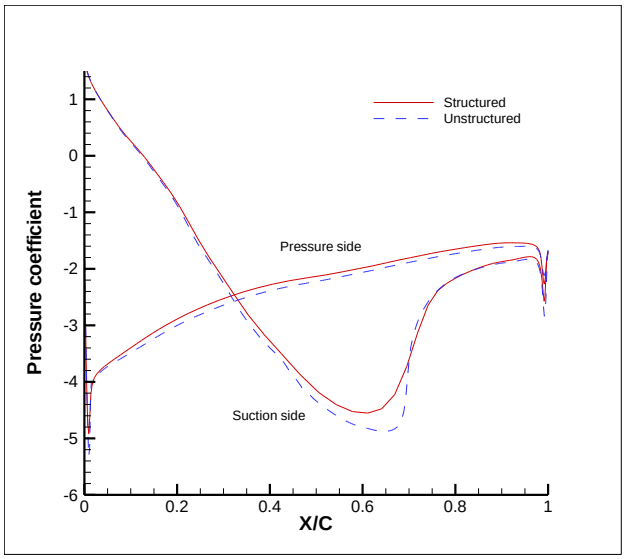

Angle of attack = 0

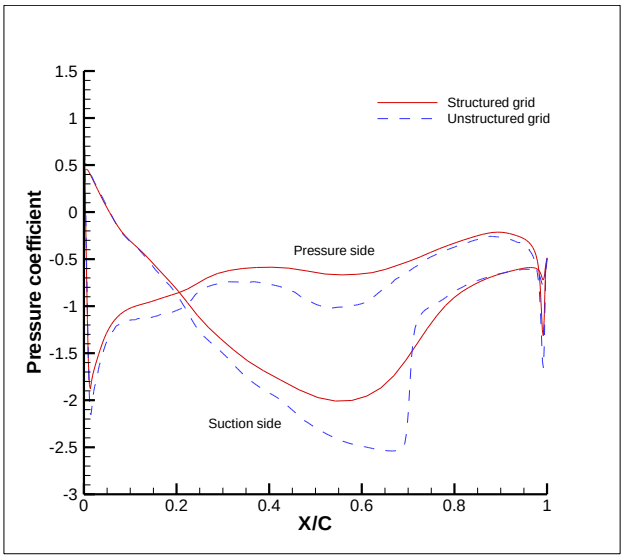

Angle of attack = 28

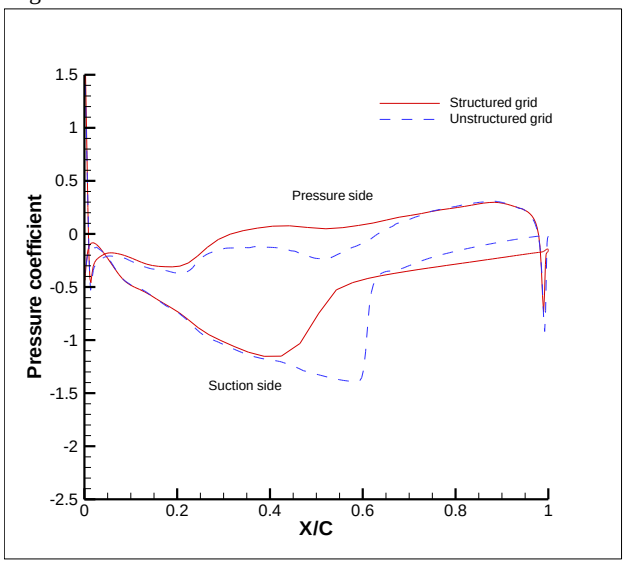

Angle of attack = 39

5.11.3 (C_p) graphs according to the angle of attack.

For this case, this project only analyzes the structured grid, as it is more accurate and the goal of this chapter is to analyze the differences of the different pressure ratios and not the influence of the angle of attack.

Angle of attack = 0

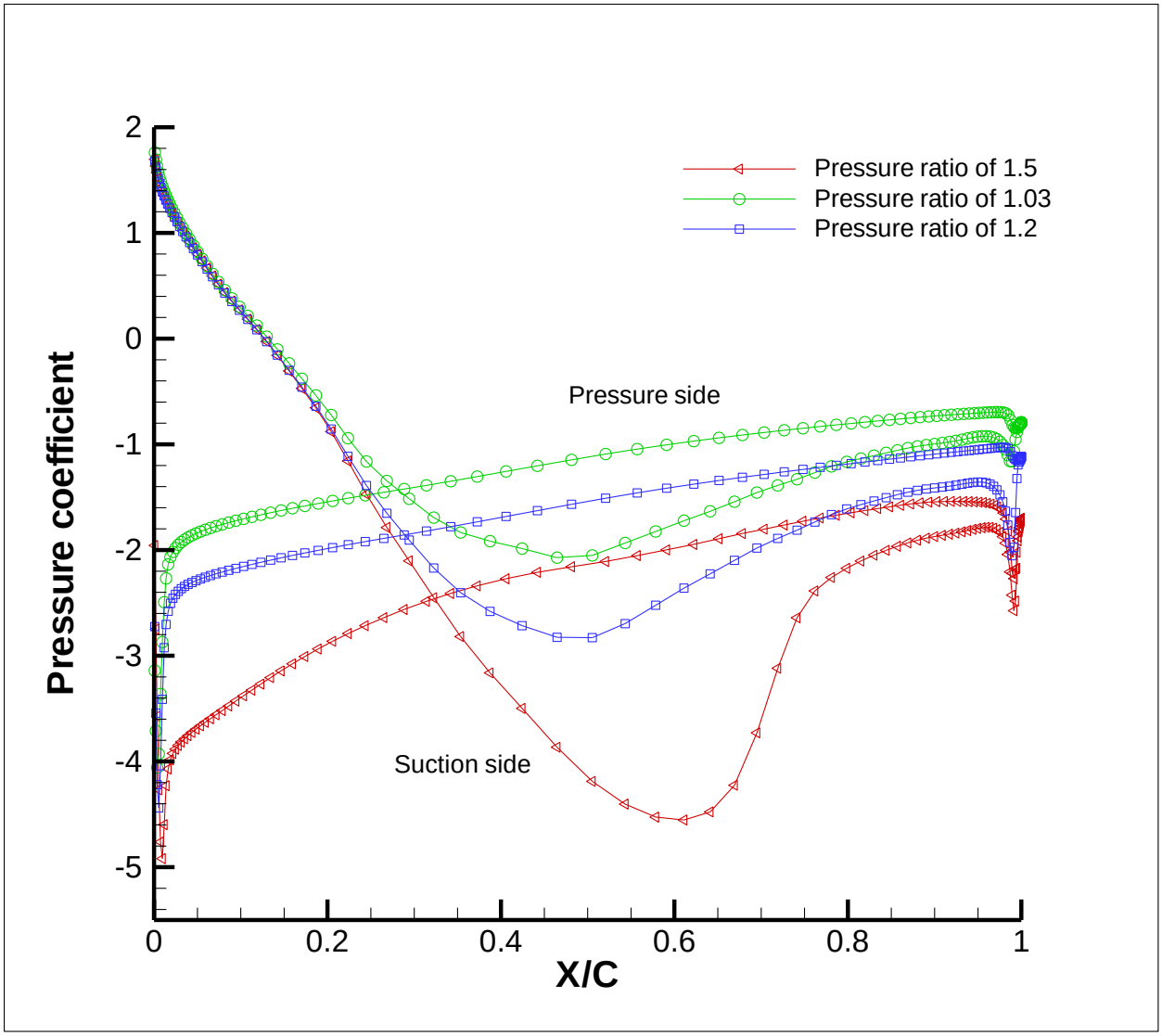

Pressure coefficient along the blade for the angle of attack of 0 degrees

Angle of attack = 28

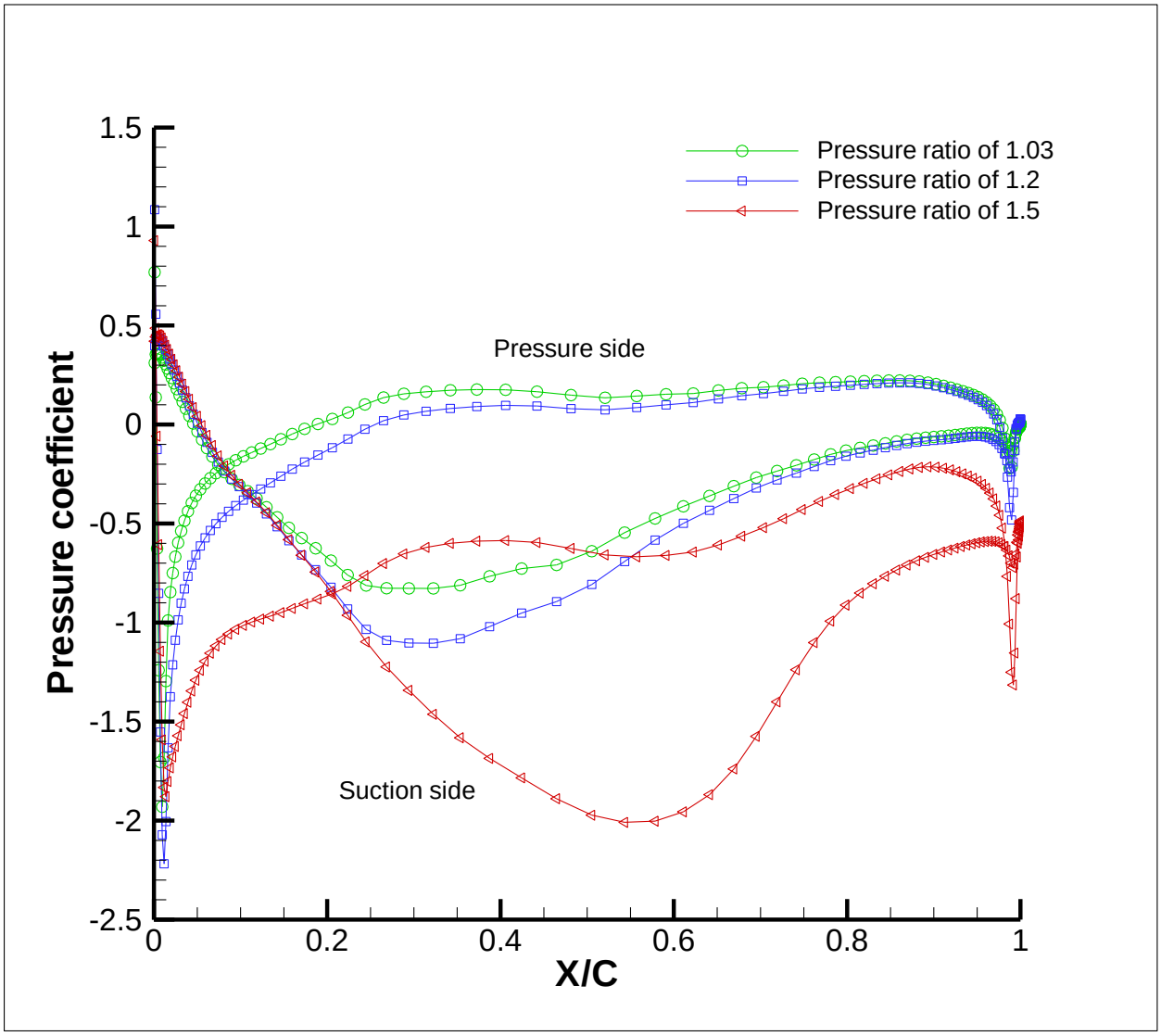

Pressure coefficient along the blade for the angle of attack of 28 degrees

Angle of attack = 39

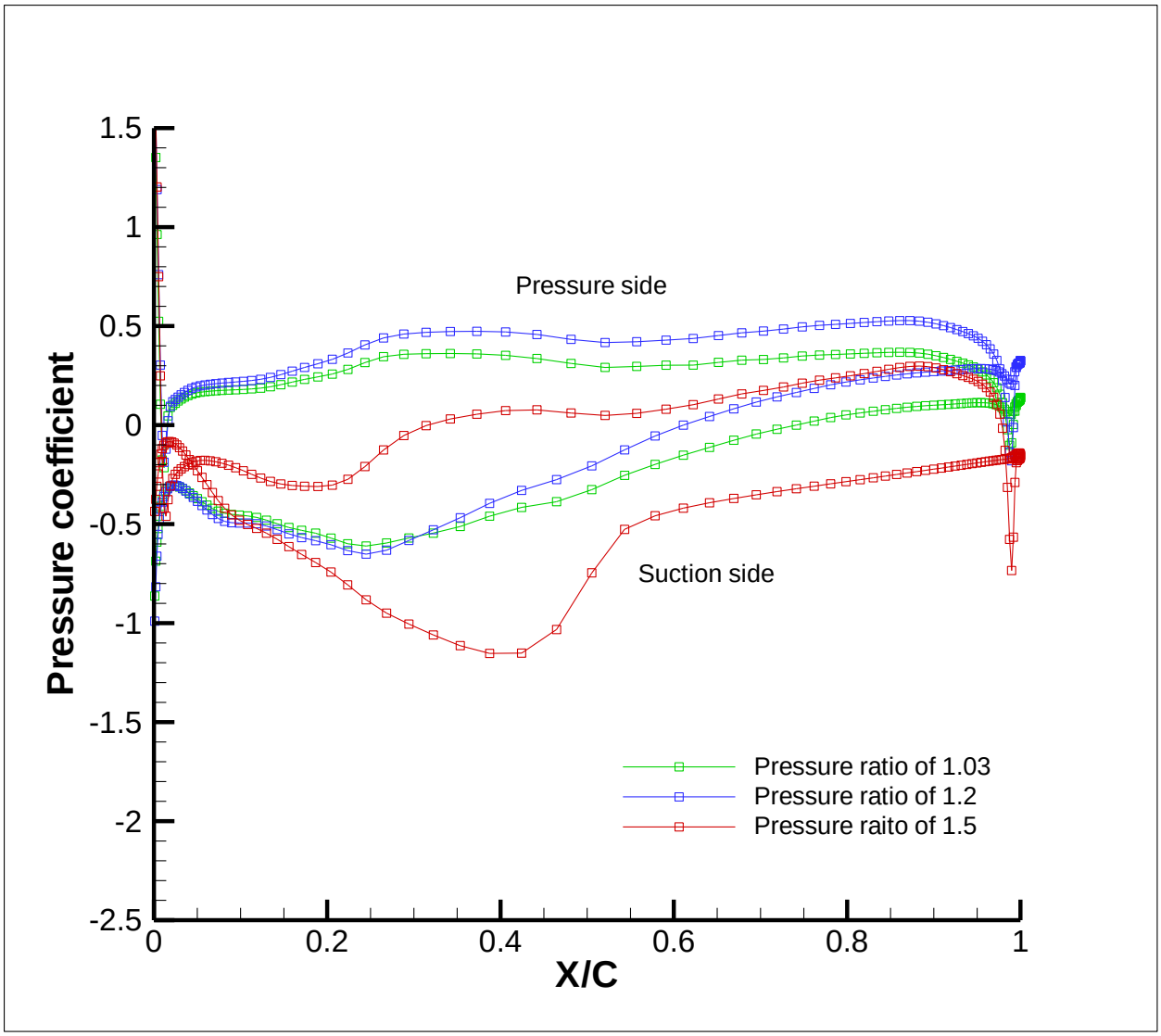

Pressure coefficient along the blade for the angle of attack of 39 degrees

Angle of attack = 46

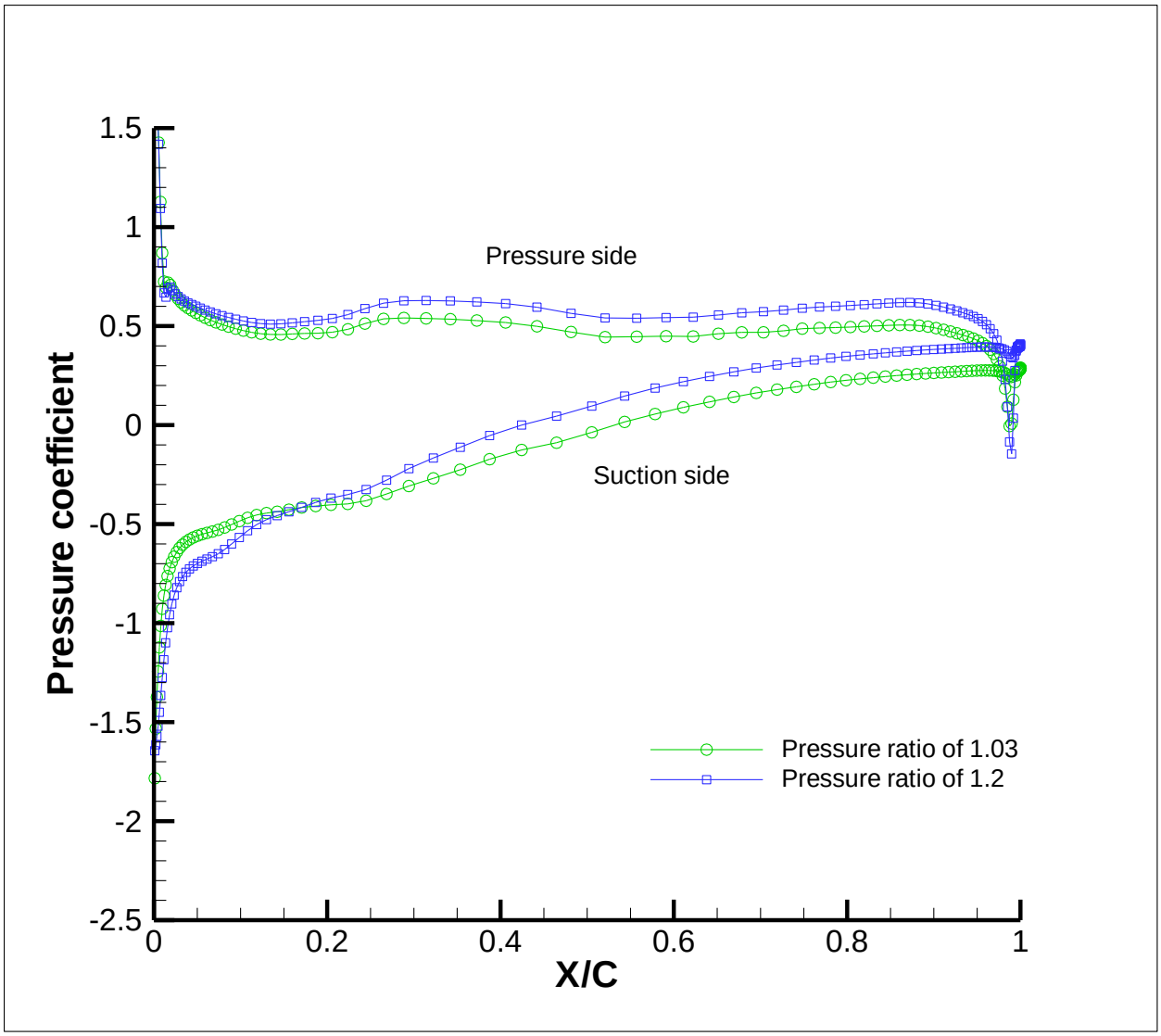

Pressure coefficient along the blade for the angle of attack of 46 degrees

5.12 Graphs with the influence of the angle of attack and the pressure ratio.

In order to analyze the pressure difference between the inlet and the outlet, this project shows these plots. The *x-coordinate* shows the angle of attack while the *y-coordinate* shows the pressure in Pascals.

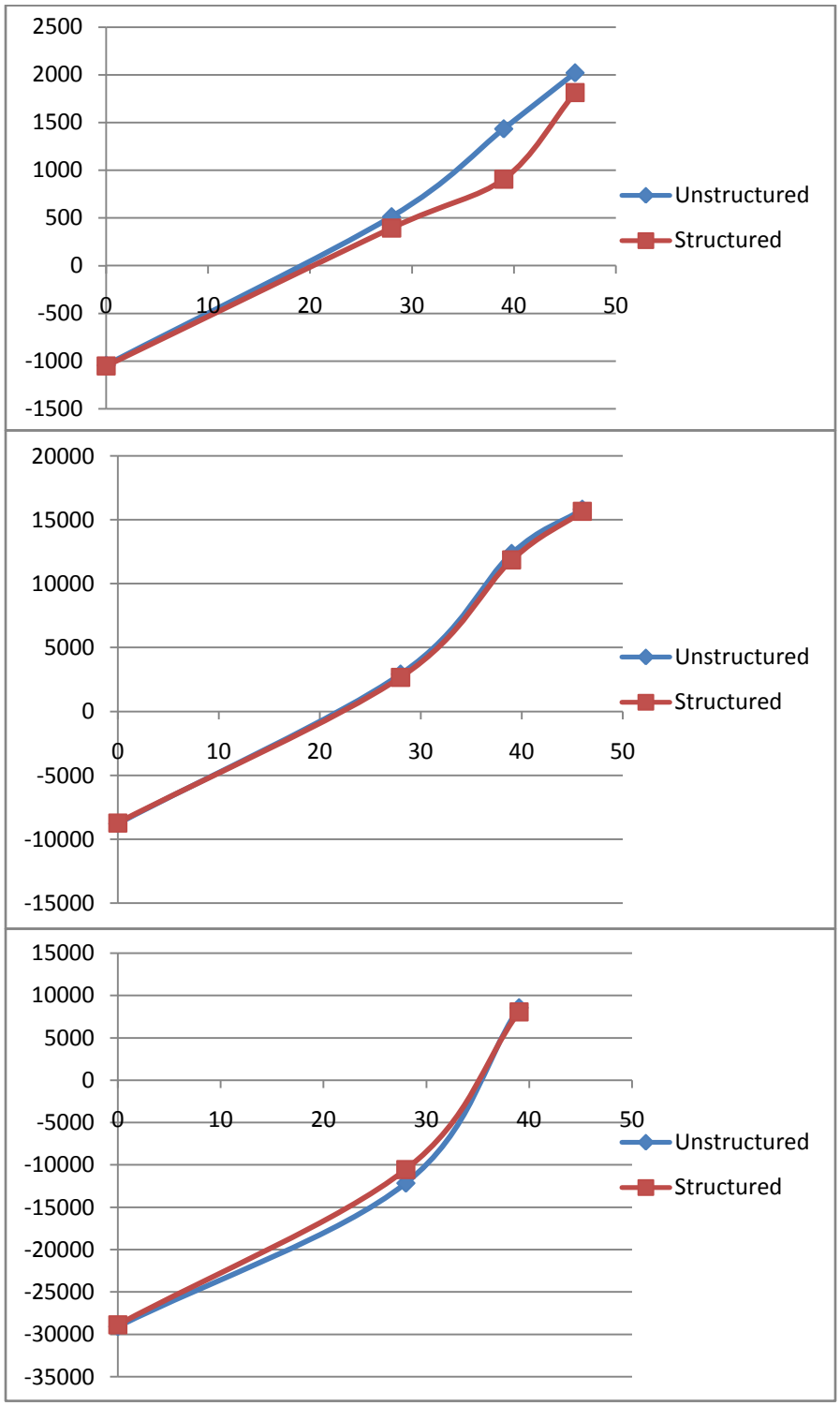

Pressure ratio of 1.03

Pressure ratio of 1.2

Pressure ratio of 1.5

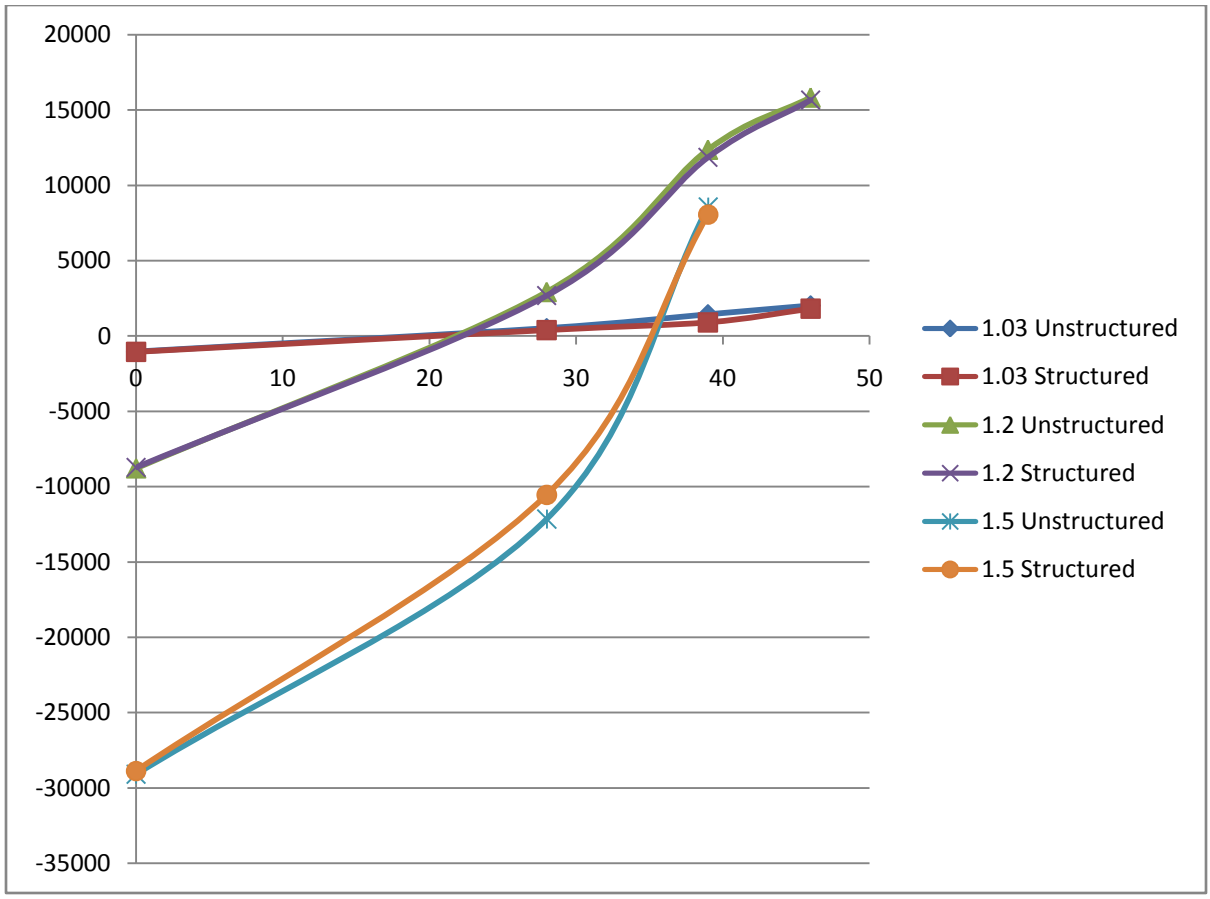

The maximum increase of the pressures comes with the design inlet angle (39 degrees). As we go increasing the pressure ratio, the angle of attack in which we obtain an increase of the pressure keeps increasing.

5.13 Graphs with the influence of the angle of attack and the mass flow rate.

In order to analyze the mass flow rate, this project shows these plots. The *x-coordinate* shows the angle of attack while the *y-coordinate* shows the mass flow rate in $(\frac{Kg}{s})$.

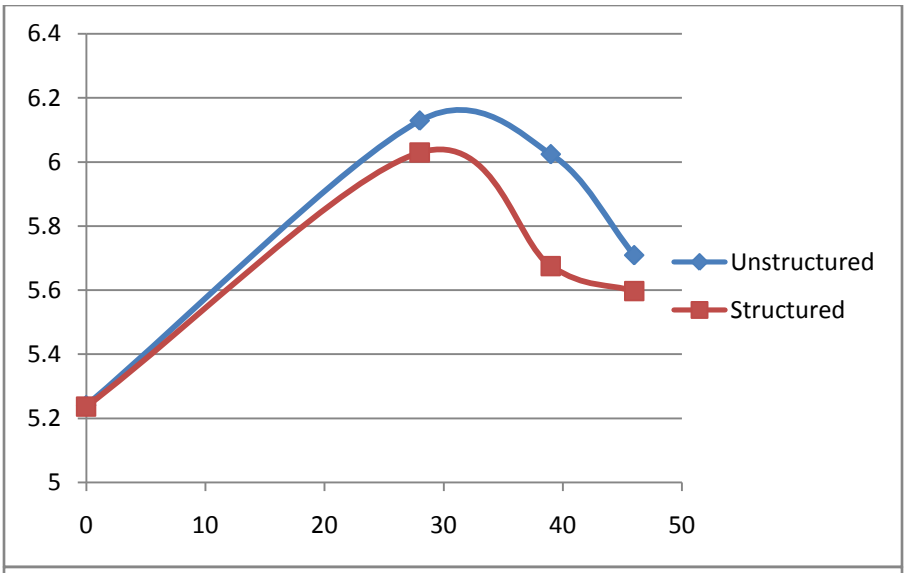

Pressure ratio of 1.03

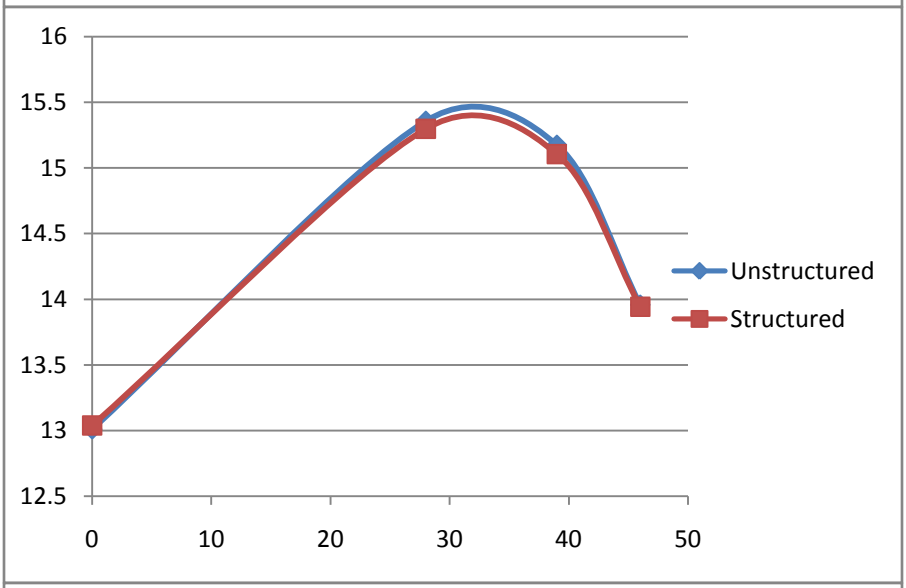

Pressure ratio of 1.2

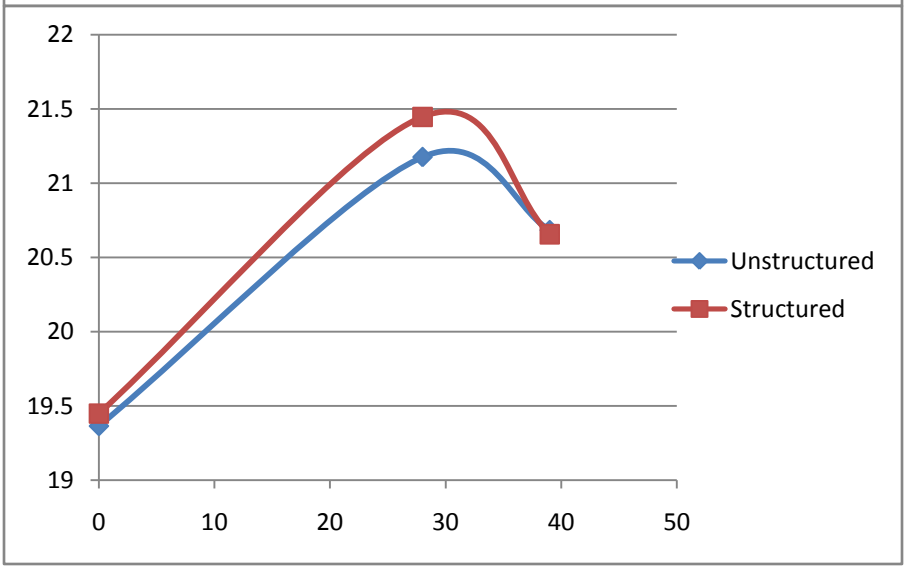

Pressure ratio of 1.5

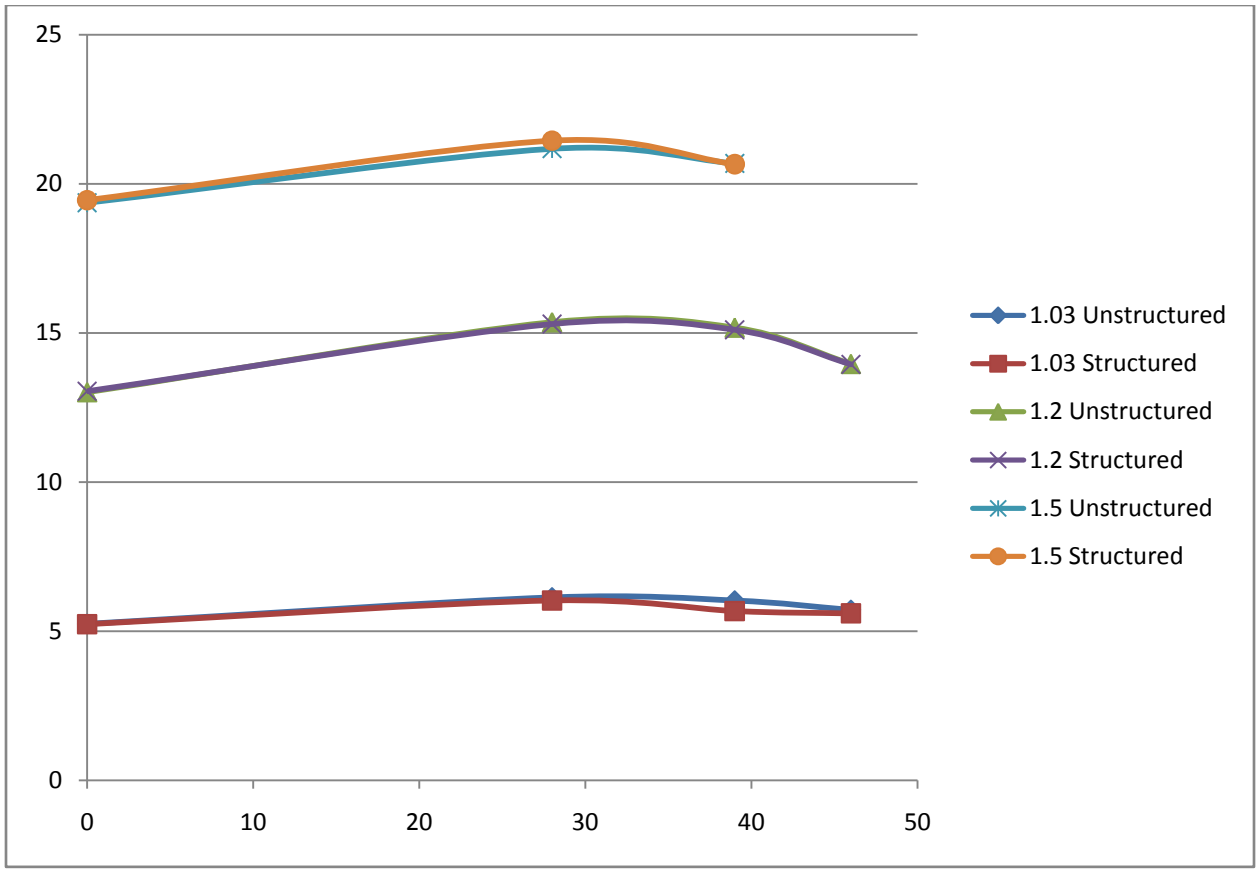

The mass flow rate increases with the pressure ratio. The higher value comes with the angle of attack of 28 degrees because as show in the contours and vectors, the flow goes through the cascade smoothly. The maximum mass flow rate does not come with the design inlet angle (39 degrees) because the flow motion decreases at the outlet in order to increase the pressure.

6. CONCLUSIONS

The analysis of two-dimensional compressor cascade flows is not an easy task. It required heaps of different configurations and many tries for each one of them in order to get an accurate result. As for the grid type, it was easier to build the unstructured grid as it does not have a pattern to follow and therefore the equisize and equiangle skew ended up to be smaller. As for the structured grid, the computational time seems to be a little bit quicker as it follows the flow direction and it does not have to check the nodes around the point of study each time. In order to build the structured grid with desirable values of the equisize and equiangle skew, a higher number of nodes were needed.

As for the attack angle, the best results were reached with the design conditions, in our case of study, for the design inlet angle of 39°. It's been demonstrated that if we modify the angle of attack of the flow from the design inlet angle, the flow becomes more turbulent and in some cases, a separation of the flow from the wall was founded. Also, in some cases, due to the high difference of the angle of attack from the inlet design angle, a drop of the pressure at the outlet was founded due to the abrupt entrance of the flow in between the blades passage, which leaded to a turbulence flow, recirculation, and in some cases, a separation of the flow from the wall ,which ended up being a transient problem.

In conclusion, for a good performance of the compressor, a smooth air flow along the blades is needed, and the angle of attack should be as close as possible to the design inlet angle. In order to improve the performance and efficient of our job, a good mesh with low equisize skew, equiangle skew, aspect ratio and a small number of nodes without compromising the accuracy and validity of the results. is required in order to speed up the computational time.

7. BIBLIOGRAPHY

References:

- *An introduction to COMPUTATIONAL FLUID DYNAMICS, the finite volume method, H K Versteeg, V Malalasekera*
- *Grid generation methods. Vladimir D. Liseikin*
- Fluent documentation: *http://my.fit.edu/itresources/manuals/fluent6.3/help/*
- *The no-slip condition of fluid dynamics. Michael A. Day*
- *Introduction to CFD Basics by Rajesh Bhaskaran Lance Collins*
- *CFD simulations of pressure loss in pipes with different geometries*
- *Flight Simulator Database Population from Wind Tunnel and CFD Analysis of a Homebuilt Aircraft by Robert P. Little*

CFD ANALYSIS OF CENTRIFUGAL COMPRESSOR IMPELLER FLOWS

By

Javier García Unzue

Computational Fluid Dynamics Laboratory
Advisor: Professor Yun-Ho Choi

Ajou School of Engineering

Spring semester of 2011

CONTENTS

ABSTRACT

The following study analyzes the air flows through a high speed centrifugal compressor impeller with the Fluent code. The problem studied is a compressible and steady flow, with a finite volume calculation, a density-based solver, and a two-equation k-ε turbulence model. The flow distributions are presented in six different measurement areas, from the inducer inlet to the impeller discharge. A single rotating reference and an absolute velocity formulation have been used in the Fluent code. The present study is being validated by comparing the results with the measured data of the Eckardt impeller. The main purpose of this study is to compare and analyze the results given by Fluent.

The pre-processing has been carried out with Gambit while the Post processing has been done with Fluent and Tecplot. The use of Matlab and spreadsheets have been required as well.

NOMENCLATURE ----------

A	Area
AVF	Absolute Velocity Frame
b	Meridional impeller channel width
c	Absolute velocity
e	Internal energy
e_t	Relative total internal energy
$\overrightarrow{F_b}$	Body forces
H	Enthalpy
h_{tr}	Total enthalpy
K	Thermal conductivity
$\dot{m}$	Mass flow rate
$\dot{Q}$	Heat generation source term
P	Total pressure
P0	Static Pressure at the inlet (I)
PR	Stagnation pressure ratio
PS	Pressure side
SRF	Single Reference Frame
SS	Suction side
S_m	Meridional shroud contour length
S_ϕ	Source term
T	Stagnation temperature
t	Blade spacing
U	Blade velocity
U_2	Tip speed
$\vec{V}$	Absolute velocity
$\vec{W}$	Relative velocity
x	Coordinate along meridional shroud contour
x/S_m	Relative meridional shroud contour
y/t	Relative blade spacing
z	Coordinate normal to the shroud contour
z/b	Relative meridional channel width
$\vec{\omega}$	Angular velocity
Φ	Scalar variable
Γ	Scalar diffusion coefficient
τ	Shear stress
τ_v	Viscous stress
ρ	Density
μ	Dynamic viscosity
U2	Tip Speed
I,II,III, IIIA,IV, V	Measurament areas

INTRODUCTION

Centrifugal compressors compress the working fluid by radial acceleration of the impeller. The basic aim is to deliver the working fluid with a higher pressure than its original. Compressions are required in many applications such as providing air for combustion (gas turbines), or transporting processes fluid through pipelines for example.

In centrifugal compressors, the working fluid enters axially and exits radially. The working fluid is forced through the impeller by the rotating impeller blades. The kinetic energy from the rotating impeller is converted into pressure energy, partially in the impeller and partially in the stationary diffuser. The diffuser consists of a vaneless space, which converts the velocity head into pressure energy. The impeller is shrouded by a stationary casing which prevents the working fluid from avoiding the blade passages.

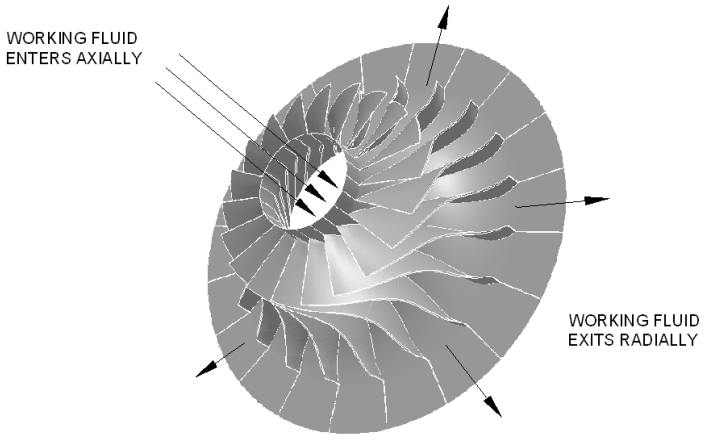

Note: This is a schematic sample of how the impeller works. The flow enters through the inlet (in between the blades), and not through the eye.

The basic principles are,

- *Centrifugal action*: It can be described in terms of energy transfer from the mechanical rotation of the impeller to the motion and pressure of the working fluid. In moderns impellers, most of the energy conversion is due to the outward force that curved impeller blades impart on the working fluid.

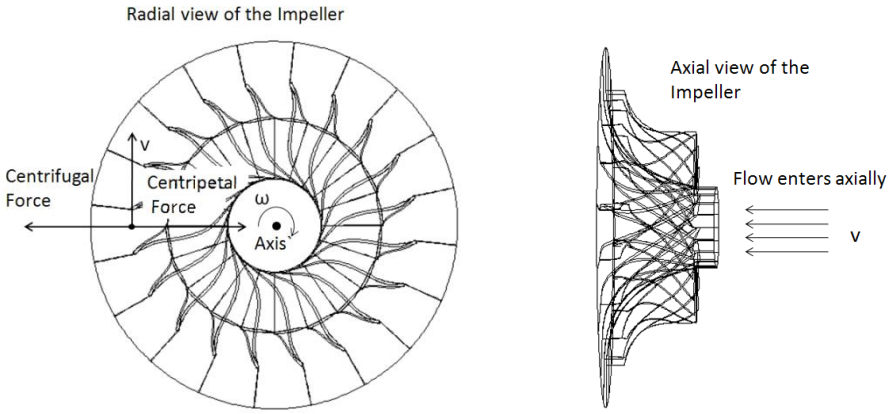

- *Centrifugal stage*: Most of the velocity leaving the impeller is converted into pressure in the vaneless diffuser. If a high pressure ratio is needed, it is common to have several stages (multistage) in a single compressor. The low pressure fluid will enter the inlet and increase the pressure stage by stage respectively.

- *Energy conversion*: When the fluid reaches the impeller outlet, it enters the vaneless diffuser where the velocity of the working fluid drops, and therefore increases the pressure. The pressure, velocity and temperature are different at every point. Due to the fact that compressors operate during long periods of time, it is classified as a steady flow process. Based on ideal gas law, the pressure and temperature for every stage are always higher than before because the volume is decreased for every upcoming stage.

The flow through the impeller is complex due to the growth of boundary layers, flow separations on blades surfaces, formation of secondary flows and formation of jet-wakes areas. Spanwise circulatory secondary flows (vortex flows) due to rotation and passage curvature are observed on the measurement areas. These flows are undesirable as they are responsible for head losses, flow non-uniformity, flow separation, and slip. To minimize this problem, turbomachinery designers often employ flow guiding elements such as splitters (curved) vanes and other hardware modifications. As a result, resulting jet-wake areas are formed which affects the efficiency of the impeller and the efficiency of the vaneless diffuser. To improve the aerodynamic performance of centrifugal compressor it is necessary to suppress the separation and wake formation maintaining high level of diffusion within the impeller. It is essential to understand the flow structure to achieve these objectives within the passages. The complexity of the flow in a centrifugal impeller impacts the performance of the impeller and makes it difficult to predict the flow field correctly.

In order to simplify this study, we avoid the tip clearance geometry on our geometry and we do not have in count the blade thickness.

The tested impeller used in the Eckardt experiment is an unshrouded one with a tip clearance. Slight differences on the results may apply because of these, but it does not cancel the validity of the present calculation.

FLUENT CODE

Basics

The commercial code Fluent, solves the well-known Navier-Stokes equations. The Fluent calculations are based on the finite volume method :

- The domain is divided onto a finite set of controls volumes (cells).
- The general transport (conservation) equations for mass, momentum, energy etc. are solved in these set of control volumes.
- The partial differential equations are discretized into a system of algebraic equations.
- All algebraic equations are then solved numerically to render the solution field.

$$\underbrace{\frac{\partial}{\partial t}\int_V \rho \emptyset \mathrm{dV}}_{\text{Unsteady}} + \underbrace{\int_A \rho \emptyset \mathrm{V} \cdot \mathrm{dA}}_{\text{Convection}} = \underbrace{\int_A \Gamma \nabla \emptyset \cdot dA}_{\text{Diffusion}} + \underbrace{\int_V S_\emptyset dV}_{\text{Generation}}$$

Applying the fundamental laws of mechanics to a fluid yields the governing equations for a fluid.

- Conservation of mass:

$$\frac{\partial \rho}{\partial t} + \nabla \cdot \left(\rho \vec{V} = 0\right)$$

- Conservation of momentum:

$$\rho \frac{\partial \vec{V}}{\partial t} + \rho\left(\vec{V} \cdot \nabla\right)\vec{V} = -\nabla p + \rho \vec{g} + \nabla \cdot \tau_{ij}$$

These equations along with the conservation of energy equation, form a set of coupled, non-linear partial differential equations. It is not possible to solve these equations analytically for most engineering problems. However, it is possible to obtain approximate computer-based solutions to the governing equations for a variety of engineering problems.

There are two kinds of velocity formulations, relative and absolute. Nonetheless, for the density-based solver, we have only the absolute formulation.

Single reference frame

Many problems permit the entire computational domain to be referred to as a single rotating reference frame (hence the name SRF modeling). In such cases, the equations

$$\overrightarrow{v_r} = \vec{v} - \overrightarrow{u_r}$$

where

$$\overrightarrow{u_r} = \vec{\omega} \times \vec{r}$$

are solved in all fluid cell zones. Steady-state solutions are possible in SRF models if provided suitable boundary conditions are prescribed. In particular, wall boundaries must adhere to the following requirements:

- Any walls which are moving with the reference frame can assume any shape. An example would be the blade surfaces associated with a pump impeller. The no slip condition is defined in the relative frame such that the relative velocity is zero on the moving walls.
- Walls can be defined which are non-moving with respect to the stationary coordinate system, but these walls must be surfaces of revolution about the axis of rotation. Here the no slip condition is defined such that the absolute velocity is zero on the walls. An example of this type of boundary would be a cylindrical wind tunnel wall which surrounds a rotating propeller.

Rotationally periodic boundaries may also be used, but the surface must be periodic about the axis of rotation. As an example, it is very common to model flow through a blade row on a turbomachine by assuming the flow to be rotationally periodic and using a periodic domain about a single blade. This permits good resolution of the flow around the blade without the expense of modeling all blades in the blade row

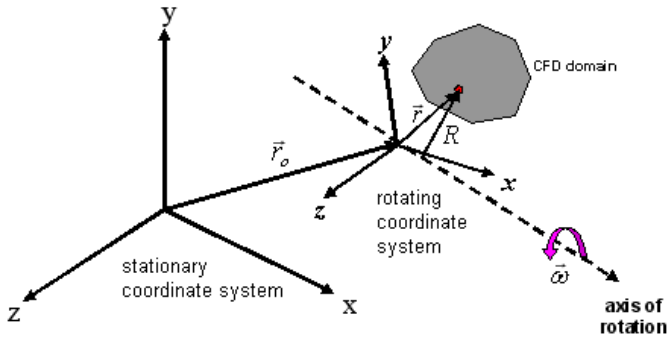

We use a rotating reference frame because:

- A flow field which is unsteady with respect to the stationary frame becomes steady with respect to the rotating frame.
- Steady-state problems are easier to solve:
    1. Simpler boundary conditions
    2. Lower computational cost
    3. Easier to postprocess and analyze

The moving frame is associated with a single fluid zone and the domain rotates with a constant, prescribed rotational speed about a specified axis of rotation. There is no translation considered and no acceleration frame of reference, although we can implement this through user defined functions.

The relationship between the absolute and relative velocities is given by

$$\vec{V} = \vec{W} + \vec{U} \text{ where}$$

$\vec{V}$=Absolute velocity $\quad \vec{W}$ = Relative velocity $\quad \vec{U} = \vec{\omega} \times \vec{r}$

For our study, this relationship can be illustrated using the law of vector addition. This is also known as the velocity triangle.

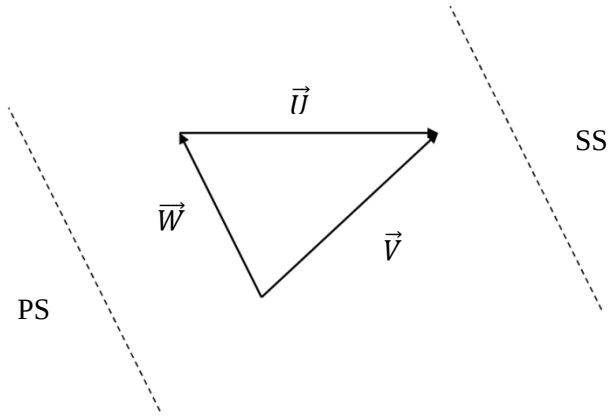

The absolute velocity formulation is derived from the relative velocity formulation. It uses the absolute velocity as the dependent variable in the momentum equations. It also uses the absolute total internal energy as the dependent variable in the energy equation.

The absolute velocity formulation uses the following equations:

- $\frac{\partial \rho}{\partial t} + \nabla \cdot \rho \vec{W} = 0$ (Continuity)
- $\frac{\partial \rho \vec{V}}{\partial t} + \nabla \cdot \left(\rho \vec{W} \otimes \vec{V}\right) + \rho\left(\vec{\omega} \times \vec{V}\right) = -\nabla p + \nabla \cdot \bar{\bar{\tau}} + \overrightarrow{F_b}$ (Momentum)
- $\frac{\partial \rho e_t}{\partial t} + \nabla \cdot \left(\rho \vec{W} h_t\right) = \nabla \cdot \left(k \nabla T - p\vec{U} + \bar{\bar{\tau}} \cdot \vec{V}\right) + \overrightarrow{F_b} \cdot \vec{V} + \dot{Q}$ (Energy)

- $e_t = e + \frac{1}{2}V^2$ (Relative total internal energy)
- $\bar{\bar{\tau}}_v = \mu\left[\nabla\vec{V} + \left(\nabla\vec{V}\right)^T - \frac{2}{3}\left(\nabla\vec{V}\right)\bar{\bar{I}}\right]$ (Viscous stress)
- $h_{tr} = e + \frac{p}{\rho} + \frac{V^2}{2}$ (Total enthalpy)

In the absolute velocity formulation, accelerations due to rotating frame are as follow. The coriolis and centrifugal acceleration are reduced to a single term:

$$\vec{\omega} \times \vec{W} + \vec{\omega} \times (\vec{\omega} \times \vec{r}) = \vec{\omega} \times \vec{V}$$

Coriolis acceleration

Centripetal acceleration

The scalar transport equation in a moving reference frame is:

$$\frac{\partial \rho \phi}{\partial t} + \nabla \cdot \left(\rho \vec{W} \phi\right) = \nabla \cdot (\Gamma \nabla \phi) + S_\phi$$

IMPELLER GEOMETRY

The impeller's geometry was built in Gambit. A set of data points (*71x31x31*) from a single passage were obtained from the previous work of *Yun-ho Choi & Hyung-Taek Kim* and a tedious work was done in order to create the geometry. Tecplot was needed to extract all the outer points of the geometry. Due to the noticeable improvement of PCUs nowadays, a bigger grid was developed in order to assure grid independence. An initial grid of *105x46x46* was built and initialed studied (streamwise, spanwise and shroud to hub respectively). More grids with an increase 50% and 80% of nodes in the $\vec{\imath}$ direction were tested to prove the grid independence, 158x46x46 and 189x46x46 respectively. However, a final mesh of 158x69x46 with an increase of 50% in the $\vec{\jmath}$ direction was finally proven to give better results on the spanwise (blade to blade) direction.

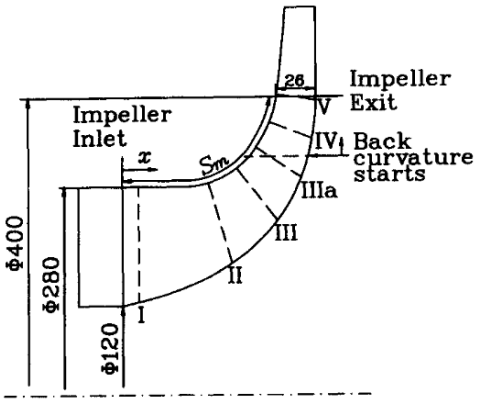

FIGURE 1: Meridional cross-section of the centrifugal impeller with measurement plane locations. Dimensions in mm.

The impeller has 20 blades and the main camber line has an elliptic shape in cylindric sections. The outlet was extended due to computational issues as well as the inlet. The impeller's backward curvature of the blades commences at $R/R_2=0.8$ and terminates at the blade exit with a backward sweep angle of 30°. A meridional sketch of the impeller can be seen in figure 1.

The following part after the impeller exit is the vaneless diffuser. The outlet domain for the CFD computation is located at a *440 mm* from the axis of rotation.

A section through the impeller axis is called "meridional section". Farther in this study, the meridional component of the velocity is used in order to discuss the flow development throughout the passage, and hence, it needs to be clearly understood.

This geometry is slightly different from the test impeller studied by Eckardt. The test impeller was an unshrouded one, while in the real one there is a tip clearance in between the impeller and the shroud which for computational reasons has been ignored in the present study.

It must be noticed that for impellers with backsweep blades, the direction of the tangential velocity of the relative velocity (*W*), is opposite to the tip speed direction.

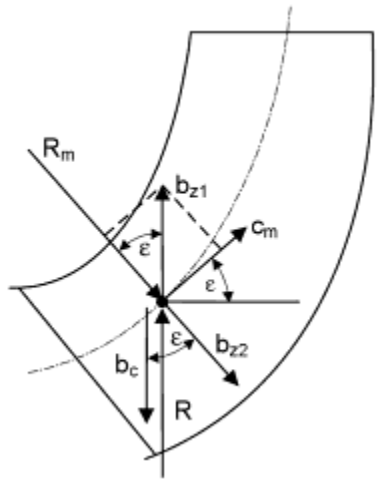

FIGURE 2: Meridional section.

The results are presented on six different measurement areas. A sketch of these areas can be seen in figure 3.

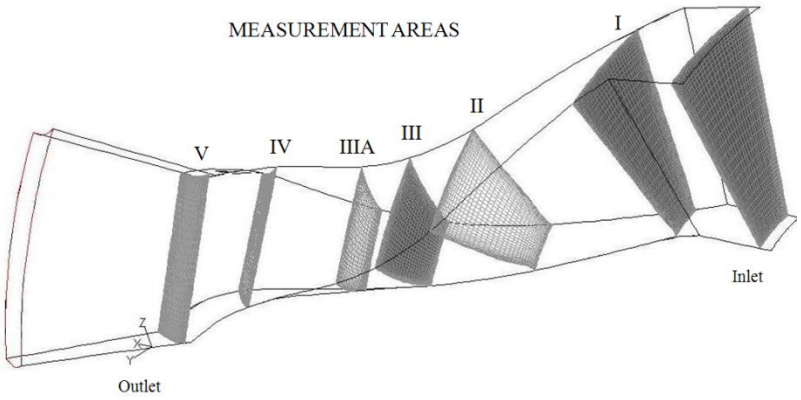

FIGURE.3: Measurement Areas

The position of the measurement areas are defined in Table 1.

Measurement Area	x/S_m
I	0.08
II	0.43
III	0.59
IIIA	0.68
IV	0.87
V	1.01

Table 1 Measurament area locations

Backsweep impeller

For impellers with a backward sweep, the direction of the tangential component of the relative velocity, *W*, is opposite to the tip speed direction. For such impellers, *V* becomes less than *U* and is reduced further by higher impeller backswept angles. However, since the impeller tip speed U2 is several times larger than the total relative velocity at the impeller discharge W2, the relative change in V2 θ due to impeller backsweep is much less than the relative change in radial velocity, caused by impeller backswept. Because the increased backsweep reduces the absolute radial velocity to a much larger extent than the absolute tangential velocity *V2*, another effect of increased impeller discharge blade angle backsweep with constant shroud stream surface diffusion is a reduction in the absolute flow angle α_2 leaving the impeller.

By comparing two different impellers, it can be concluded that an increase in the impeller backsweep reduces the blade to blade normal distance of the discharge normal flow area. That is, the higher backsweep impeller with its attendant reduced blade to blade normal distance, requires a greater impeller discharge blade height, than the other impeller discharge blade height, which is associated with the lower backsweep impeller. If we assume that we want to maintain the relative velocity radio W_2/W_1, where W_2 is the relative impeller discharge velocity and W_1 is the relative impeller inlet shroud velocity, then an increase in impeller backsweep angle will therefore result in an increase in the impeller tip blade height . This relatively wider tip impeller tends to provide stability at low flow conditions since it results in smaller absolute impeller discharge flow angles α_2 which therefore will show smaller angle variations at reduced flow. Consequently, incidence effects will be less to thereby promote stability.

PRE-PROCESSING

As said before, the pre-processing has been carried out with the Gambit software. A data file with all the grid points from the impeller passage was provided, modified by Tecplot, and introduced to Gambit. It must be mentioned that there are several other commercial and private softwares such as, *ICEM CFD, STAR-CD, ANSA*, among others.

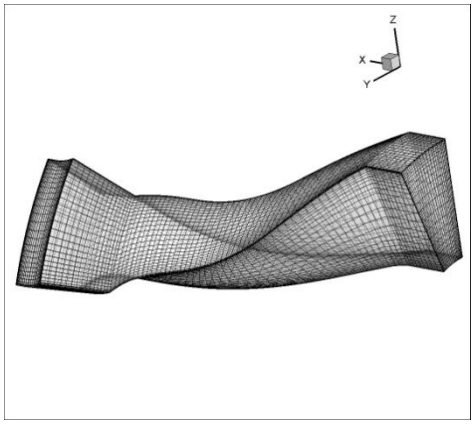

FIGURE 4: Original grid provided

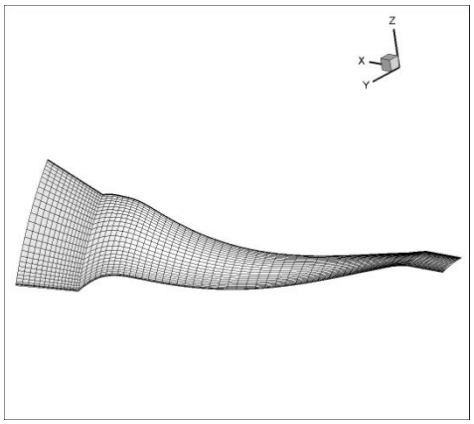

FIGURE 5: Example of an outer face

The starting point of this study was the data file containing the grid information. Such grid can be seen on figure 4. In order to build the geometry, 6 outer faces were extracted using *Tecplot.* These six surfaces were introduced to Gambit and a tedious task began in order to connect the 10726 points of the six outer faces. Once the whole volume was created, the domain was divided into several parts. Each individual part was meshed and studied accordingly.

Due to the high importance of the viscous layer near the walls, a highly-densed grid was needed to be built, and hence, a higher number of nodes were introduced. However, the more close the nodes get to the wall, the higher aspect-ratios and skew values we get, which will lead to convergence problems, and hence, the more nodes we need to overcome this problem. A non-dimensional parameter which measures the distance between the first node and the wall is called *Yplus.* Sadly, it cannot be measured in Gambit, and the case need to be run in order to know the Yplus value. Further details will be provided about this non-dimensional parameter later on.

Finally, figure 6 shows the final grid.

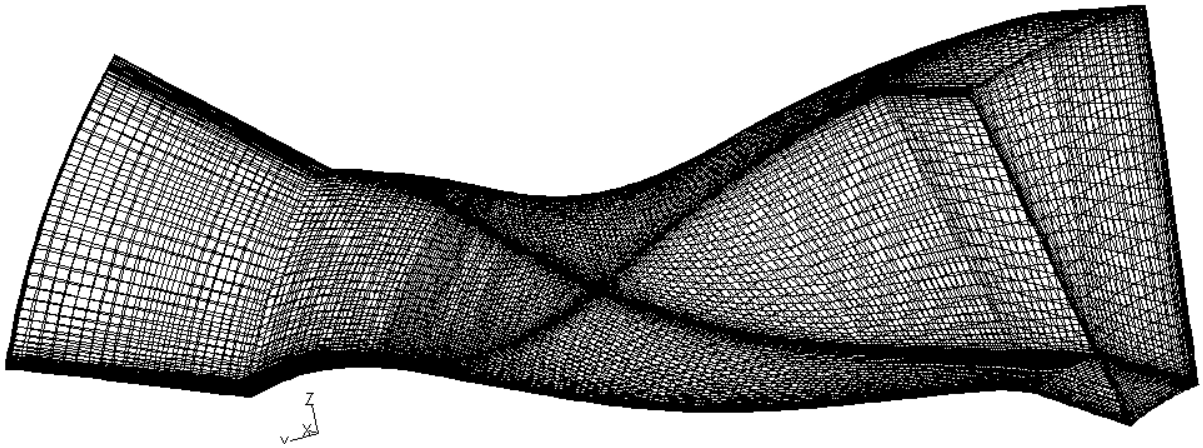

FIGURE 6: Final grid

The quality of the mesh is tested by two parameters, the aspect-ratio, and the skewness.

Property:	Value:
Aspect-ratio	99.8286
Equisize skew	0.886744

Table 2

The equisize skew value comes from:

$$Q_{EVS} = \frac{(V_{eq} - V)}{V_{eq}}$$

where V is the volume (3-D) of the mesh element, and V_{eq} is the maximum volume (3-D) of an equilateral cell the circumscribing radius of which is identical to that of the mesh element.

Q_{EVS}	Quality
$Q_{EVS} = 0$	Equilateral (Perfect)
$0 < Q_{EVS} \leq 0.25$	Excellent
$0.25 < Q_{EVS} \leq 0.5$	Good
$0.5 < Q_{EVS} \leq 0.75$	Fair
$0.75 < Q_{EVS} \leq 0.9$	Poor
$0.9 < Q_{EVS} \leq 1$	Very poor
$Q_{EVS} = 1$	Degenerate

Table 3

The poor quality of the mesh is due to the complex geometry and the need of a densely mesh near the wall.

IMPLEMENTATION OF CFD

Basics.

The solver selected to analyze and solve our problem is Fluent. Fluent is a computational fluid dynamics (CFD) commercial software package to simulate fluid flow problems. It uses the finite-volume method to solve the governing equations for a fluid. It provides the capability to use different physical models such as incompressible or compressible, inviscid or viscous, laminar or turbulent, etc. Geometry and grid generation was done using Gambit which is the preprocessor bundled with Fluent.

For this study, we are using the density-based solver, compressible flow (ideal-gas), k-ε turbulence model with the enhance wall treatment option (only for the last grid), and a single reference frame with a rotational speed of 14.000 rpm. Convergence was slow and hard to find and a previous case with a incompressible flow was needed to run in order to get some acceptable initial values.

Setting up the case.

The next step about setting up a case to run in Fluent is to choose the appropriate models Fluent will run from the "Define-Models" menu. We select the density-based solver type, the steady option under the time menu, and absolute velocity formulation (the only one available for this solver). We use the density-based solver instead of the pressure-based solver because it suits better for high speed compressible flows, where the mach number is above 0.3. Modeling the flows as steady-state allows pertinent flow features to be captured while not placing an excessive computational load on the computer.

We allow the energy equation as we set our material as a compressible ideal gas. Fluent automatically enables the solution of the energy equation when the ideal gas law is used, in case we did not already enable it manually in the energy panel. In order to activate the turbulence model a viscous model is needed to be selected. The viscous model used in this project is the *k-epsilon*, as is the most commonly used and most user-friendly when it comes to convergence. Our problem does not include any special phenomenon such as combustion or supersonic flow etc.

Once all the appropriate models are specified, the user must ensure that the fluid material used by Fluent is air. This is found under the "Define-Materials" menu. The appropriate values for density and viscosity should be entered under the "Material Properties" section of the menu. Unless otherwise stated, these values correspond to standard atmosphere sea level conditions for the CFD runs presented in this project.

The desired pressure ratio (*PR*) and rotational speed for a given case are specified under the "Define-Boundary Conditions" and "Cell Zone Conditions" menu respectively. For the pressure inlet boundary condition specified in Gambit, the pressure magnitude and direction is specified in Fluent. For example, to run a Fluent case of 1 atmosphere as the static pressure in the outlet, the magnitude is specified in the boundary condition menu and we need to be careful as the pressure inputted here is relative to the operating pressure defined in the operating conditions panel. As for the rotational speed, this is specified in the cell zone conditions menu with the *x*- component as the axis of rotation and a rotational speed of 14000 rpm.

Boundary conditions.

In differential equations, a boundary value problem is a differential equation together with a set of additional restraints, called the boundary conditions. A solution to a boundary value problem is a solution to the differential equation which also satisfied the boundary conditions. All CFD problems are defined in terms of initial and boundary conditions. Boundary conditions specify the flow and thermal variables on the boundaries of our physical model. They are, therefore, a critical component of our CFD simulation and it is important that the user specifies these appropriately and understands their role in the numerical algorithm.

In FLUENT, boundary conditions are associated with zones and not with individual cells or faces. Generally, a pressure condition cannot be used at a boundary where velocities are also specified, due to the fact that velocities are influenced by pressure gradients.

The boundary conditions used for the present study are:

- *Pressure inlet*
- *Pressure outlet*
- *Wall*
- *Periodic*

A sketch of the boundaries conditions applied to our study can be seen in figure 7,

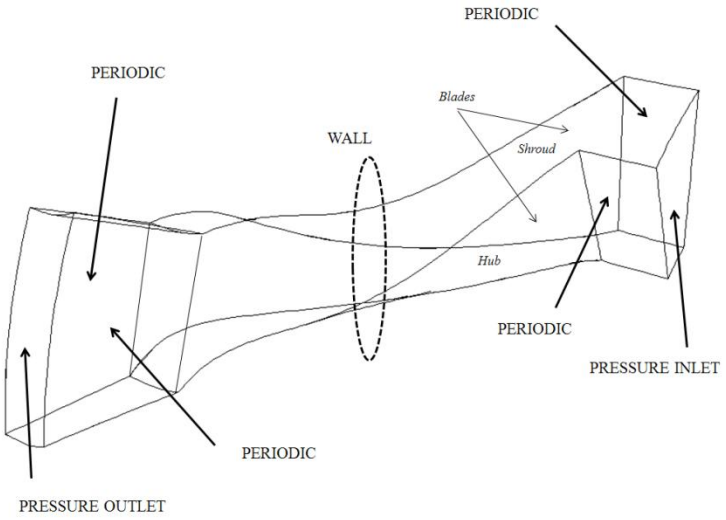

FIGURE 7: Sketch of the boundary conditions

Periodic boundary type cannot be set up through GAMBIT and it has to be specified first as a wall boundary condition and then create it in FLUENT.

PRESSURE INLET:

This boundary condition is used to define the fluid pressure at flow inlets, along with all other scalar properties of the flow. We use this boundary conditions in this problem because we know the inlet pressure and we don't know the velocity or the flow rate.

This paper study the impeller at a near stage optimum point, with *14000 rpm*, a mass flow rate of *4.54 kg/s*, a stagnation pressure ratio of *PR=2.1*, and an isentropic stage efficiency η_{is}*=0.88*. The operating pressure is 101325 Pa.

Thus, the pressure inputted at the inlet was *-25 Pa*. A stagnation temperature of *288.1 K* was also applied. The turbulent kinetic energy and the turbulent dissipation rate were left as default (1).

PRESSURE OUTLET:

This boundary condition requires a static (gauge) pressure at the outlet. This value is only used while the flow is subsonic.

The static pressure given for the outlet was *163300 Pa.* As the pressure outlet in fluent is relative to the operative pressure, the pressure inputted in the pressure outlet panel was *61975 Pa*.

Two methods (Method 1 and Method 2) are available for adjusting the pressure at a pressure-outlet zone in order to meet the desired mass flow rate. Both methods are based on the simple Bernoulli's equation. However, they differ in the internal iteration strategy for obtaining the change in pressure on a pressure-outlet zone. In general, the target mass flow rate is achieved by adjusting the pressure value at the pressure-outlet zone up and down at every iteration. This is done in accordance with one of the two available methods until the desired target mass flow rate is obtained.

The change in pressure based on Bernoulli's equation is given by the following equation:

$$dP = 0.5\rho_{ave}\left(\dot{m}^2 - \dot{m}_{req}^2\right)/(\rho_{ave}A)^2$$

where *dP* is the change in pressure, $\dot{m}$ is the current computed mass flow rate at the pressure-outlet boundary, $\dot{m}_{req}$ is the required mass flow rate, ρ_{ave} is the computed average density at the pressure-outlet boundary, and *A* is the area of the pressure-outlet boundary.

The default method, Method 1, should suffice in obtaining a converged solution on the targeted mass flow rate. However, if convergence difficulties are encountered while using the default method, then the user may want to select the alternate method, Method 2. There are other solution strategies that may be used if convergence difficulties are encountered, which will be discussed at the end of this section.

The target mass flow rate option can be activated from the Pressure Outlet boundary panel by selecting the target mass flow rate button. This option will allow you to specify either a constant value or attach a UDF to set the target mass flow rate.

Ass our mass flow rate for the impeller is *4.54 Kg/s*, and the impeller has 20 blades, we target the mass flow rate as *0.227 Kg/s*, for one impeller passage.

WALL:

This boundary condition is used to bound fluid and solid regions. If we set a viscous model, the no-slip condition would be enforced on the wall by default. It is possible to model a slip wall in a viscous model by using the symmetry boundary type, or specifying a tangential velocity component of the wall boundary or just by specifying shear. The shear stress and heat transfer between the fluid and wall are computed based on the flow details in the local flow field. This study does not include the effect of heat transfer, and therefore, we only focus on the flow motion.

As default, walls are set as stationary wall, and relative to adjacent cell zones in Fluent. That is, all the walls are moving according to the rotating reference frame. However, the shroud does not rotate, and has to be specified as a moving wall, with an absolute speed of 0.

PERIODIC:

As said before, we cannot set the periodic condition through GAMBIT, so we first need to set the boundary condition as wallS and then create the periodic zones in FLUENT.

To create periodic zones in FLUENT we need to write some commands on the console:

1. Press enter to get the command prompt (>)
2. Write and press enter ⟶ Grid ⟶ modify-zones ⟶ make-periodic
3. Write the periodic zone ID
4. Write the shadow zone ID
5. Select translational as this is a two dimensional linear cascade flow
6. Create periodic zones ⟶ Yes
7. Auto detect translation vector ⟶ Yes

The flow is allowed to escape through this boundary type

Convergence.

Finding convergence for this problem was tricky. A high number of iterations such as 14000 were required to reach acceptable levels of convergence. Lower number of iterations could have been done by increasing the Courant number, but the instability of the flow during this calculation didn't allow it. Two different ways were monitored to check the convergence, the residuals, and the mass flow rate at the outlet.

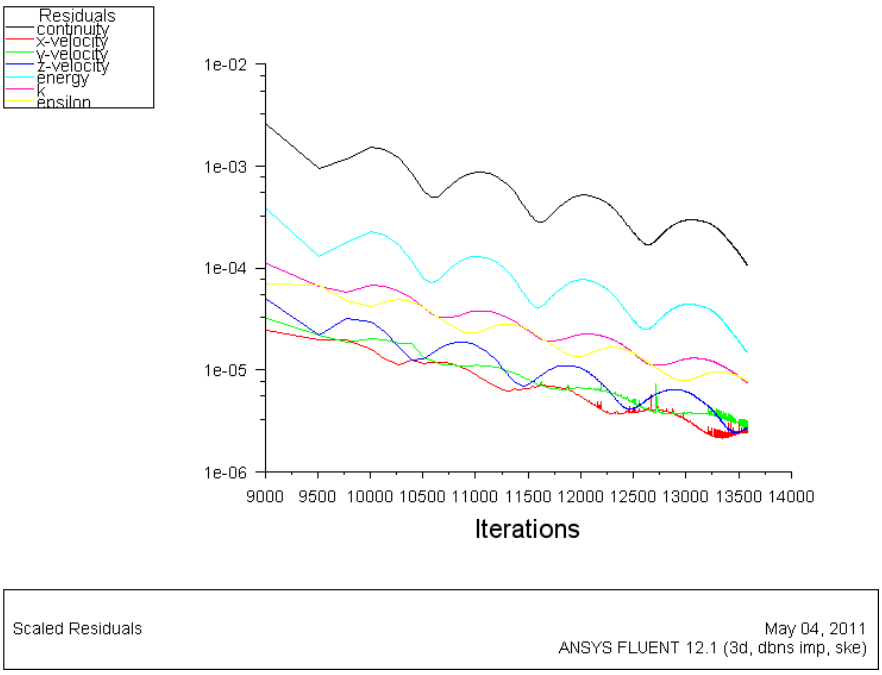

FIGURE 8: Residuals

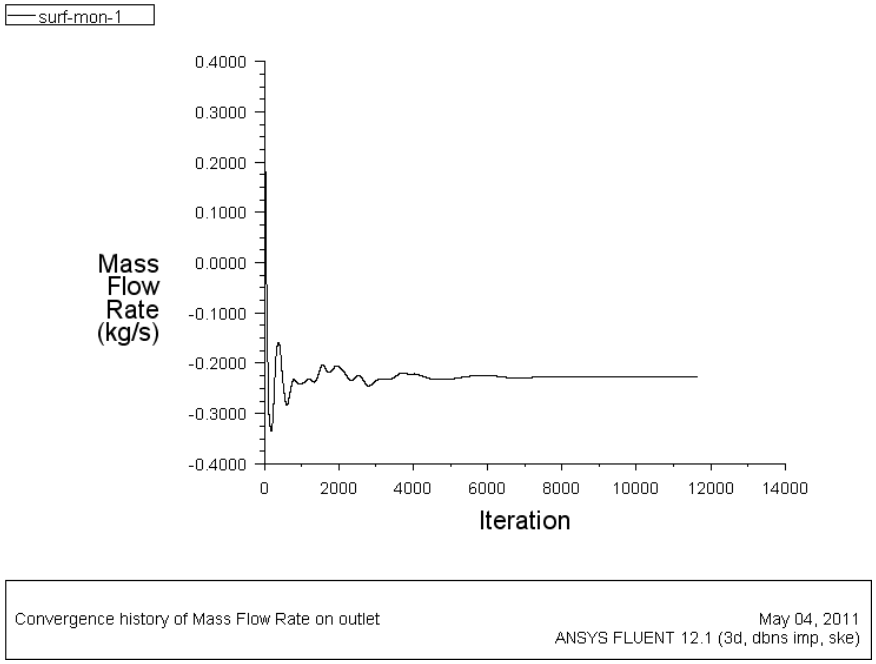

FIGURE 9: Mass flow rate history at the outlet

PRESSURE DISTRIBUTION

The main point of the impeller is to discharge the flow with a higher pressure that its original. The circumferentially averaged static pressure distribution calculated on the shroud, are compared with the experimental results obtained by Eckardt. The pressure continuously increases through the impeller at the design condition. There is a slight increase of the static pressure from the inlet to a value of x/S_m = 0.5. An abrupt increase of the static pressure can be seen after x/S_m = 0.5, due to the backswept curvature of the blade. The variation of static pressure is successfully predicted in this present study.

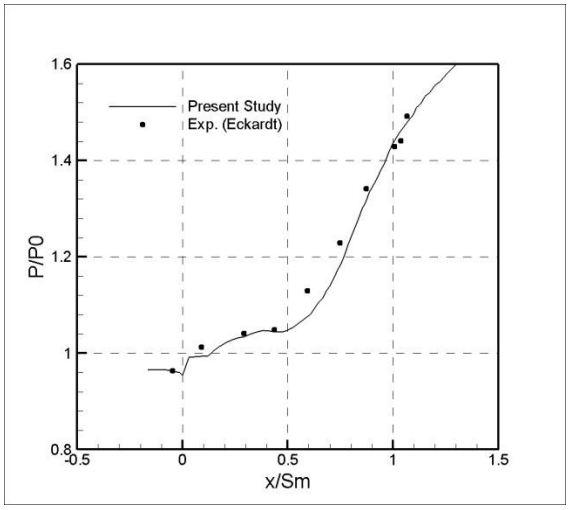

FIGURE 10: Static pressure distribution on the shroud

Figure 8 shows the pressure distribution obtained in our calculation compared with the experimental results from Eckardt. Different set ups regarding the turbulence model, discretization order etc. showed no difference on the static pressure distribution. Grid independence was tested by comparing this graph and relative velocities on the different measurement areas. A graphical sketch with the static pressure along the shroud is showed in figure 9.

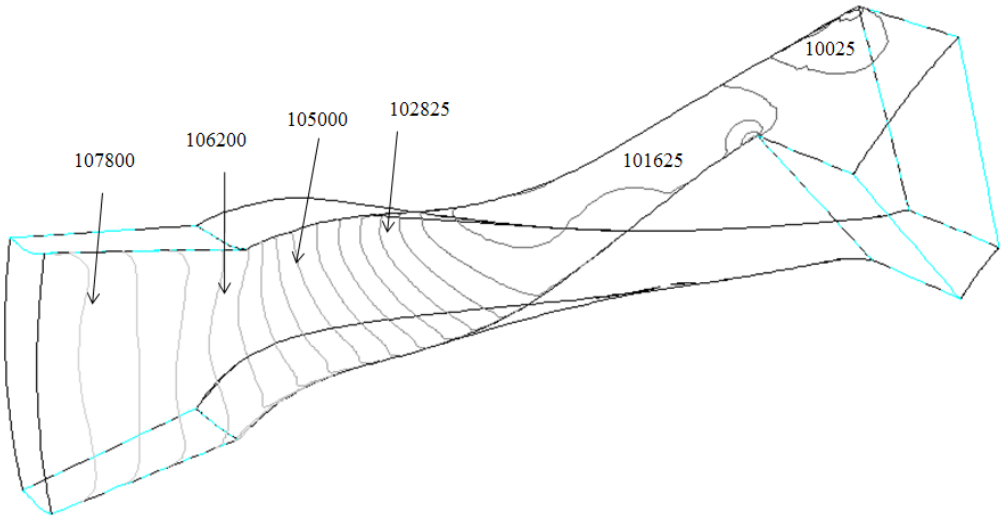

FIGURE 11: Static pressure contours on the shroud

THROUGH-FLOW DEVELOPMENT

The calculated through-flow development of the backsweep impeller is presented in Figure 10 by presenting the results in the five measurement areas. This is also compared with the experimental data obtained by Eckardt. The results show quite similar conclusions and are accepted by this study. The plots show the meridional component of the absolute velocity (C_m) referred to the impeller tip speed (*U2)*.

The measurement areas I and II, are located in the axial region, the areas III and IIIA are in the axial to radial, at the beginning of the backswept curvature, and the areas IV and V are located in the radial regions, close to the impeller exit. In the first two planes, the velocity distribution develops smoothly and regularly due to the lack of curvature. In the axial to radial region, the velocity distribution shows a disturbance near the suction side on the shroud. This flow distortion starts at x/$S_m = 0.59$, in the range of the highest blade area and shows a pronounced velocity dip near the shroud which marks a beginning flow separation. The beginning flow separation in the measurement area III, rapidly enlarges downstream, as shown in the subsequent plots, developing a wake. The wake region can be characterized by:

- A low mass-flow component
- A high fluctuation intensity. Local relative fluctuation $\mathcal{F} > 0.2$
- A steep, relatively stable velocity gradient to the surrounding main flow

Near the impeller exit region, the low-momentum wake region is near the suction side, at the plane IV and V. The wake regions move towards the shroud and suction side due to the secondary flow and this can also be observed on the measurement areas. This study shows a small discrepancy at the measurement area V, where the wake region seems to weaken when it reaches the vaneless diffuser. This can be also seen in figure 11.

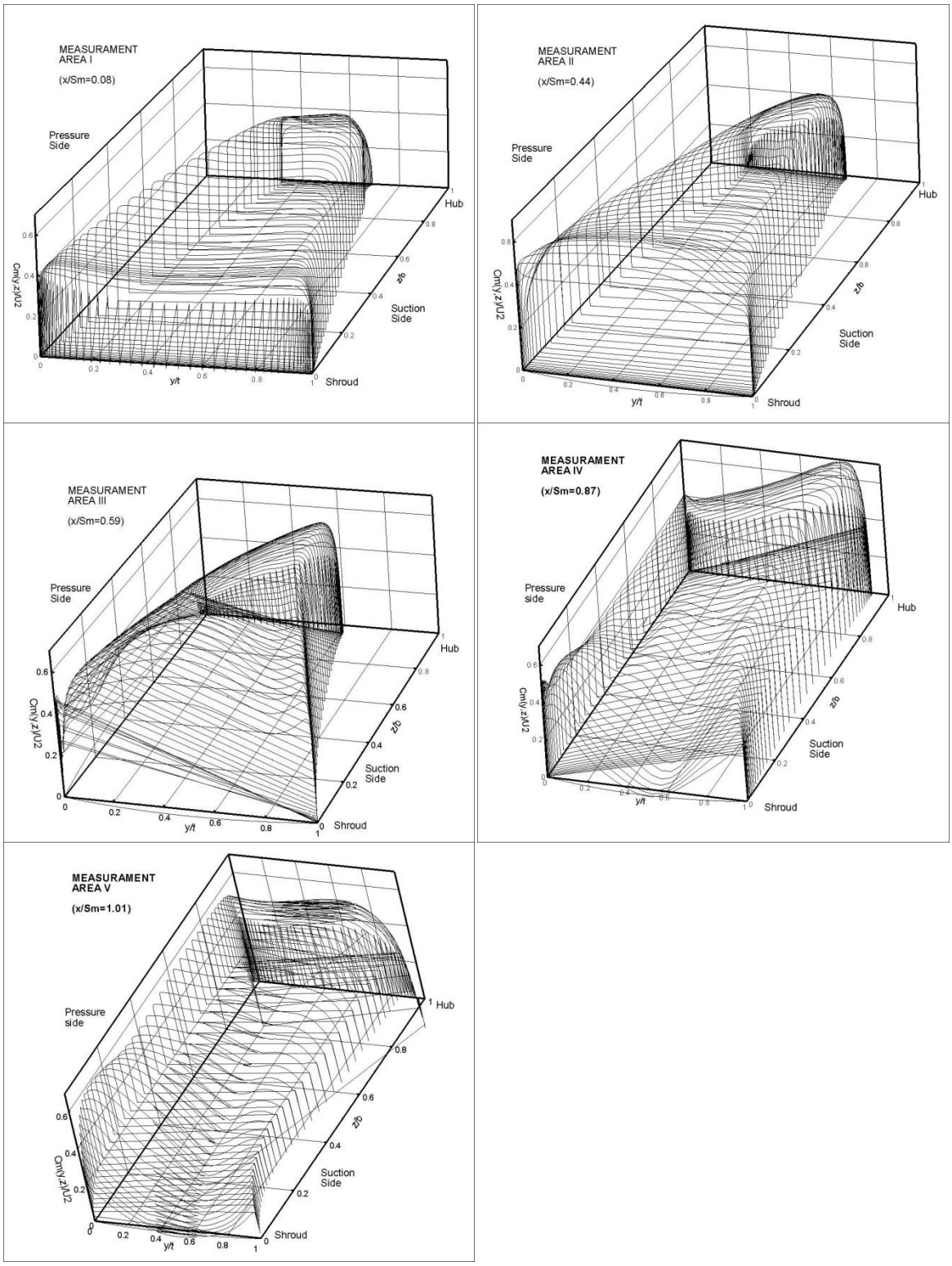

FIGURE 12: Velocity distribution on the measurement areas

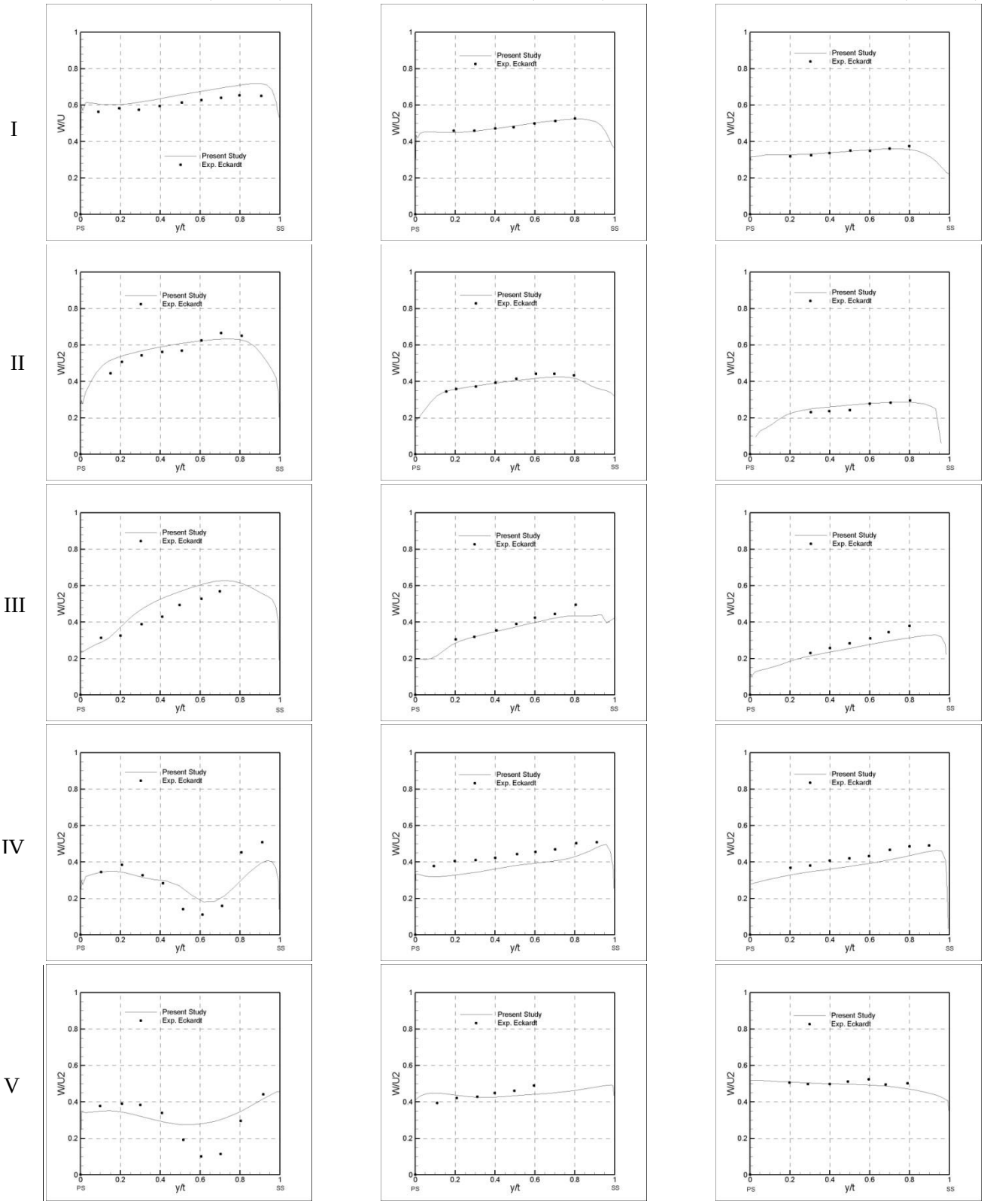

FIGURE 13: Spanwise relative velocity distribution

SECONDARY FLOWS AND JET-WAKE FORMATION

Due to the impeller's rotation and the channel curvature, we should highlight the importance of the secondary flows and the variations in the turbulence structure. Separation onset and jet/wake interaction within the impeller are analyzed in this study.

On the secondary flow velocity vectors, it can be seen the general tendency of the core-flow toward the blade pressure side. Wake areas are appreciated after the backswept curvature of the impeller's blade (after measurement area *III*), which is due to the imperfect guiding of the fluid by the impeller blades. A soft vortex can be seen near the shroud and pressure side in figure 10 & 11. The migration and accumulation of low momentum fluid in the boundary layer and the decadence of the wake region throughout the end of the impeller passage can be appreciated observing the secondary flows on the different measurement areas.

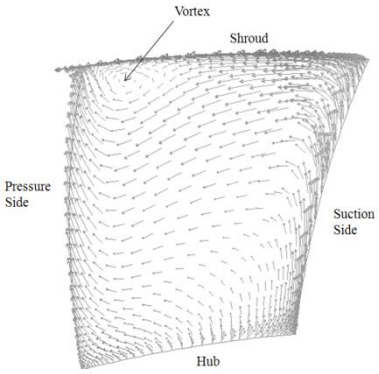

Fig.10 Measurement area IIIA. Secondary flows

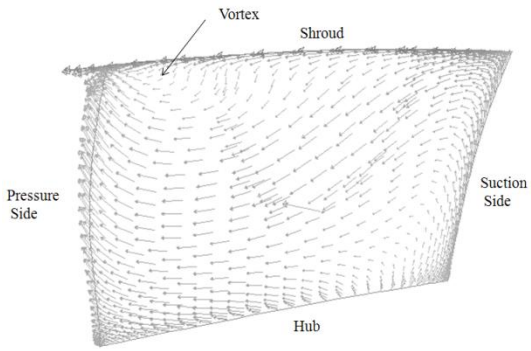

Fig.11 Measurement area IV. Secondary flows

The rapid increase of the wake between the areas III and V, suggests a certain interaction with the secondary flow intensity and, indeed our computational results indicate a comparable intensification of the cross- flow within the radial impeller.

Streamwise vorticity and secondary flows develop when a shear or boundary layer is subjected to centrifugal and Coriolis forces. The relative magnitude of these two contributions is defined by the Rossby number which governs the stable locations of wake flows:

$$R_0 = W/\omega R_n$$

The main secondary flow mechanisms can be analyzed in terms of the Rossby number. Meridional curvature, the effect of rotation, blade forces and axial flow are the reason of the existence of secondary flows in a centrifugal impeller.

The blade curvature induces the secondary flow in the inducer region and the shroud and hub curvature induce secondary flow in the axial to radial bend. Rotation induces the secondary flow in the radial section of the impeller downstream. For the backsweep impeller, the Coriolis-induced secondary flow, is usually opposed by the secondary flow generated by the backsweep blade curvature.

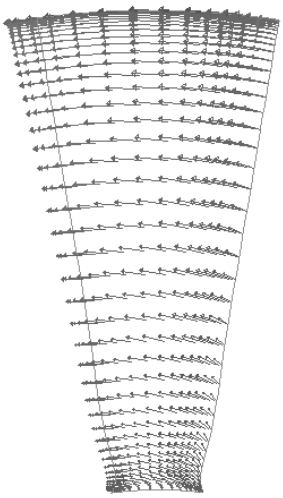

Measurement area I

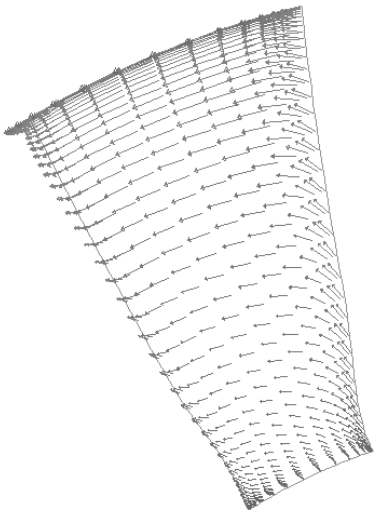

Measurement are II

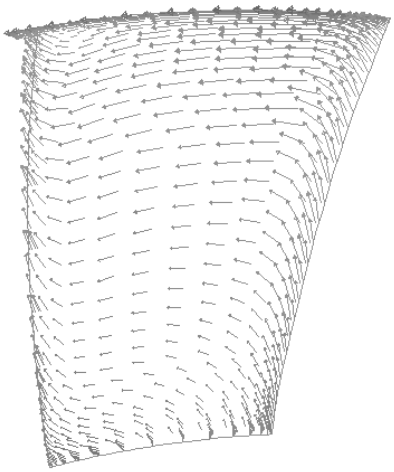

Measurement are III

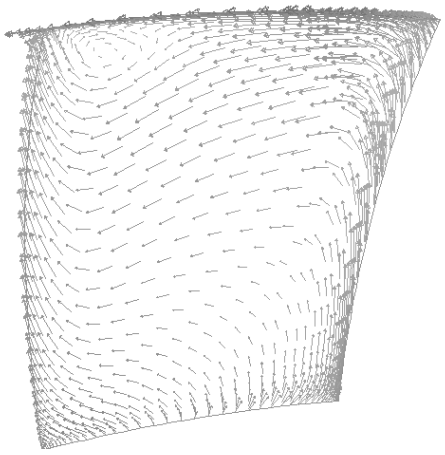

Measurement area IIIA

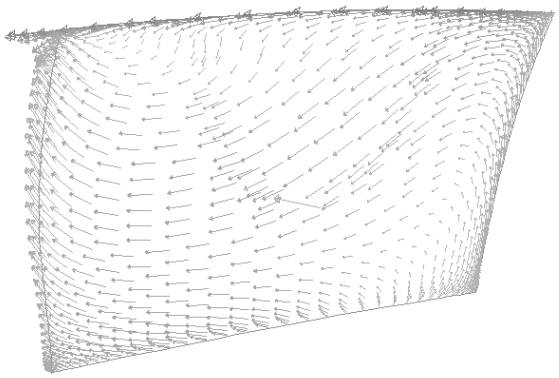

Measurement area IV

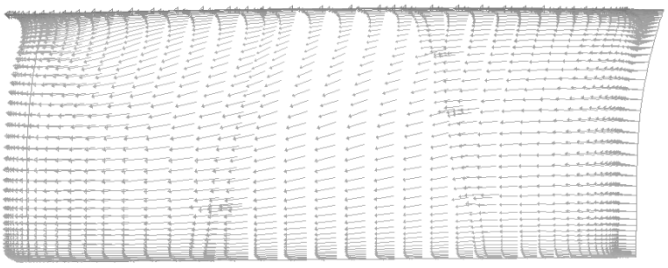

Measurement area V

FIGURE 12: Secondary flow velocity vectors on the different measurement areas along the impeller's passage.

Concluding, secondary flows are always caused by an imbalance between a static pressure field and the kinetic energy in the flow. The strength of the vortex is mostly determined by the starting conditions and the further development of the vortex is determined by the conservation of its angular momentum. In a rotating system the analogy is that the vortex flows are principally generated by the meridional flow field while the centrifugal and Coriolis forces only act to change the vortex vector direction (on the vortex plane).

PATHLINES

It is easy to figure out how the flow develops through the impeller passage, however, it is important to show the results because they may help understand some issues. Relative velocity path lines are shown in figures 13 and 14. Figure 14 shows the pathlines in the impeller passage. The effect of the wall and secondary flows can be seen in this figure by some particle deviations and some particles deceleration.

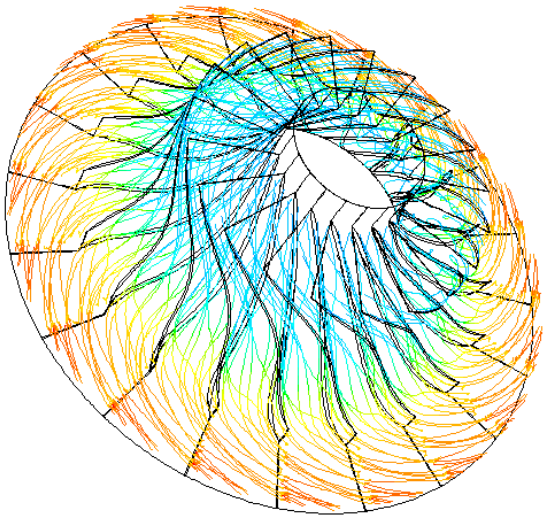

FIGURE 13: Impeller pathlines

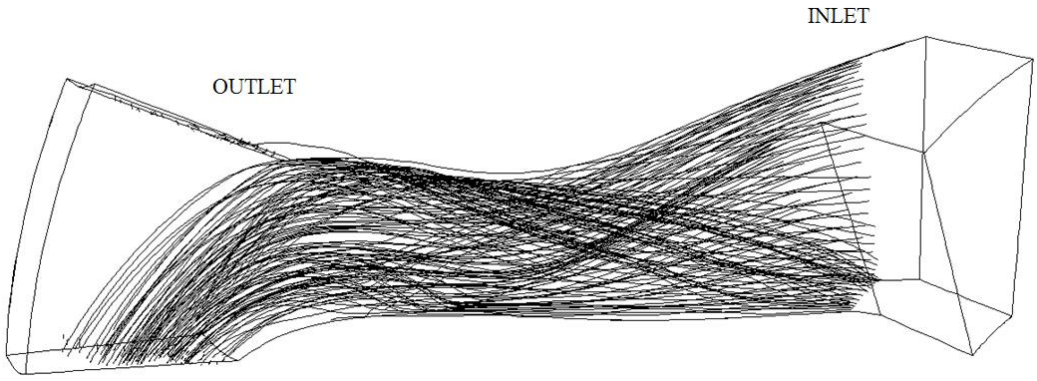

FIGURE 14: Impeller's passage pathlines

CONCLUSION

Centrifugal impeller flows are highly complicated. In order to design it, many factors have to be taken into consideration. Some phenomenon such as flow separation and wake regions, have to be minimized, so the performance of the impeller is not affected. This study shows the tendency of the secondary flow along the passage which affects the jet-wake formation and location. The design of the curvature of the blades must guide the flow smoothly, without any complication which could lead the flow to separate from the wall and affect the impeller's performance. The use of the commercial CFD code Fluent, has been proved to give good results, however, a developed code for predicting the flow through the impeller would be preferred, as the convergence problems reached in this study, didn't allow it to analyze different turbulence models, solution method etc. The present calculation of the backsweep Eckardt impeller, shows overall, good results and coherence with the measured values obtained by Eckardt.

REFERENCES

- D.Eckardt (1976) *Detailed Flow Investigations Within a High-Speed Centrifugal Compressor Impeller*
- Y.S. Choi and S.H. Kang (1998) *Application of Through-Flow Calculation to Design and Performance Prediction of Centrifugal Compressor*.
- Yun-Ho Choi and Hyung-Taek Kim (1998) *Navier-Stokes Code Development for Analysis of Flow inside the Centrifugal Compressor*
- R.A. Tough. *Improving of the microturbine's centrifugal impeller performance by changing the blade angles*
- Muhammad Ridhwan (2010) *Introduction to centrifugal compressors*
- J.Moore, J.G.Moore and M.W. Johnson (1977) *On three-dimensional flow in centrifugal impellers*
- Klaus Brun & Rainer Kurz (2005) *Analysis of secondary flows in centrifugal impellers*
- Rajesh Bhaskaran & Lance Collins. *Introduction to CFD basics*
- S.Ramamurthy, K. Murugesan, D. Prithviraj, and M. Govardhan. *Slip factor for Jet-Wake Flow in a centrifugal impeller*
- J F Gulich (1999) *Impact of three-dimensional phenomena on the design of rotodynamic pumps*
- *http://my.fit.edu/itresources/manuals/fluent6.3/*